INDUCING TRANSITIONS AND QUANTUM TRANSPORT IN TOPOLOGICAL META-MATERIALS

by

AYKUT TEKER

Submitted to the Graduate School of Engineering and Natural Sciences
in partial fulfillment of
the requirements for the degree of
Doctor of Philosophy

Sabancı University
Fall 2018

INDUCING TRANSITIONS AND QUANTUM TRANSPORT IN TOPOLOGICAL META-MATERIALS

APPROVED BY

Assoc. Prof. İnanç Adagideli
(Thesis Supervisor) .....

Prof. Zafer Gedik .....

Assoc. Prof. İbrahim Burç Mısırlıoğlu .....

Assoc. Prof. Levent Subaşı .....

Assoc. Prof. Cem Çelebi .....

DATE OF APPROVAL 07.01.2019

ABSTRACT

INDUCING TRANSITIONS AND QUANTUM TRANSPORT IN TOPOLOGICAL META-MATERIALS

Aykut Teker

Physics, Doctor of Philosophy Thesis, 2019

Thesis Supervisor: Assoc. Prof. Dr. İnanç Adagideli

Keywords: Mesoscopic and nanoscale systems, topological insulators and superconductors, spintronics, quantum thermodynamics

In this Thesis, we propose a novel method that changes the topological order in superconductor wires. We first consider the case of disorder in one dimensional topological superconductors and show how disorder can destroy or create topological order leading to reentrant topological phases. We then consider the effects of a superlattice potential, a zero-average piecewise continuous weak electrostatic potential, on p-wave and s-wave topological superconductor wires. We call such stacked wires leading to weak periodic potential modulation, meta-topological superconductor wires. Topological superconducting wires in their nontrivial phases exhibit Majorana modes as their edge states. We show that by stacking topologically trivial pieces of superconductors, it is possible to induce a topological phase which feature Majorana states at the edges of the superlattice: the meta-topological superconductor. The presence of an electrostatic superlattice allows us to control the topological phase space via the geometry of the electrostatic superlattice. We consider strictly one dimensional meta-topological superconductor wires as well as their quasi-one dimensional multichannel counterparts and show that reentrant topological phases in multichannel meta-topological superconductors occur. Finally, we consider the analogous case of a meta-topological insulator, a quantum anomalous Hall insulator featuring a weak superlattice of magnetic modulation, and show that the transmission can be topologically controlled as a function of energy. The topological protection leads to binary transmission (either transmit or reflect) through the meta-topological quantum anomalous Hall insulator, details of which can be controlled by tuning the properties of the weak superlattice.

ÖZET

TOPOLOJİK META-MATERYALLERDE TOPOLOJİK GEÇİŞLERİN TEŞVİKİ VE KUVANTUM TAŞINIM

Aykut Teker

Doktora Tezi, 2019

Tez Danışmanı: Doç. Dr. İnanç Adagideli

Anahtar kelimeler: Meso ve nanoölçekli sistemler, topolojik yalıtkan ve üstüniletkenler, spintronik, kuantum termodinamiği

Bu tezde, topolojik süperiletken tellerin topolojik durumunu değiştiren yeni bir metod öneriyoruz. Öncelikle bir boyutlu topolojik süperiletkenlerde düzensizliği ele alıp, düzensizliğin topolojik düzeni hem kurabildiğini hem de bozabildiğini ve böylece yeniden girişli topolojik fazlara yol açabildiğini gösteriyoruz. Sonra, sıfır-ortalamalı parçalı sürekli zayıf elektrostatik potansiyelden oluşan süperörgü potansiyellerin p-dalga ve s-dalga süperiletken tellerin üzerindeki etkilerini irdeliyoruz. Böyle birbirlerinin üstüne yığımlı zayıf periyodik potansiyel modülasyonu oluşturan bu sistemleri meta-topolojik süperiletken teller olarak adlandırıyoruz. Sıradışı fazda bulunan topolojik süperiletken teller, kenar durumlarında Majorana modları sergilerler. Topolojik olarak sıradan fazda bulunan süperiletken parçalarını dizerek süperörgünün kenarlarında Majorana durumu bulunduran topolojik faz indüklenmesinin mümkün olduğunu gösteriyor ve bu süperiletkenlere meta-topolojik süperiletken adını veriyoruz. Elekstrostatik süperörgünün geometrisiyle topolojik faz uzayının durumunu kontrol edebiliyoruz. Bir boyutlu ve yarı-bir boyutlu çok-kanallı meta-topolojik süperiletkenlerde yeniden girişli topolojik fazların oluştuğunu gösteriyoruz. En sonunda meta-topolojik sıradışı kuvantum Hall yalıtkanındaki ikicil tipli (yalnız ileten ya da yansıtan) iletimin zayıf manyetik süperörgü ile kontrol edilebileceğini gösteriyoruz.

ACKNOWLEDGEMENTS

The author of this Thesis would like to express his most cordial appreciation and gratitude to his supervisor Dr. İnanç Adagideli. The author would like to thank him for his invaluable and undeterred guidance over the years.

The author would like to thank his friends, colleagues and co-authors. Amongst them, the author would like to especially thank Dr. Barış Pekerten for his support.

The author would also like to thank his family for their support and guidance. The author would like to make a distinction to thank his mother Şengül Teker specifically, even though words cannot express his gratitude.

The author would also like to express his appreciation to The Science Academy (Bilim Akademisi) Turkey and to Feza Gürsey Center for Physics and Mathematics for the use of their facilities. The author also gratefully acknowledges financial support from the Erdal İnönü chair, from Lockheed Martin Corporation Research Grant.

Contents

List of Figures and Tables

Chapter 1

INTRODUCTION

In this Thesis, we investigate effects of regular and irregular scattering on the topological order of p-wave and s-wave topological superconductors. Starting from disordered single channel topological wires, we extend our analysis to multichannel topological wires that are under a piecewise continuous electrostatic potential which we name as *meta-topological insulators*. Meta-topological insulator wires have a weak electrostatic superlattice that does not lead to local changes in the topological order. We show that topological order in p-wave and s-wave meta-topological wires depend on the geometry of the electrostatic potential. We then apply our understanding of piecewise continuous potentials to put a quantum anomalous Hall sample into its topologically nontrivial phase using a magnetic piecewise continuous potential. The main results of this Thesis is reported in Chapters 3, 4, 5 and 6.

This Thesis is organized as follows: In Chapter 2, we briefly summarize developments in topological insulators. After we present the most general classification of topological insulators we concentrate on p-wave and s-wave topological superconductors. We then explain the existence of zero-energy states that are called as Majorana fermions at the ends of a p-wave chain [2] which we use as a sign of topological order in superconducting wires. After defining p-wave and s-wave Hamiltonians, we continue to briefly summarize our numerical tight-binding method to detect Majorana modes at the ends of thin wires to compare with our analytical calculations.

In Chapter 3, we calculate topological numbers for single-channel p-wave and s-wave topological superconducting wires that have zero average Gaussian disorder [3]. We do this by investigating the asymptotic limit of the zero-energy wavefunction. We distinguish accidental solutions from topologically nontrivial Majorana mode wavefunctions in

order to calculate topological indeces that reflects the existence of Majorana modes. We compare our results to our tight-binding simulations and they show significant agreement.

In Chapter 4, we introduce single channel *meta-topological insulator wires* that are topological superconductor wires on which a weak piecewise continuous electrostatic potential is applied. We call such potentials as electrostatic superlattices and we show that they lead to changes in the topological order. We calculate topological indeces for meta-topological insulators using the method of asymptotic behavior of wavefunctions. We also calculate new topological indeces that use the recursive nature of the electrostatic superlattice. We make numerical simulations for single channel wires that shows that our formulations are equivalent.

In Chapter 5, we extend our derivations of topological indeces to multichannel topological superconductor and meta-topological thin-wires. We calculate topological indeces that are compliant with topological classification of multichannel topological insulator wires. We then compare our tight binding simulations with our analytical formulae and they show significant agreement.

In Chapter 6, we discuss piecewise continuous modulation using magnetic superlattices on a quantum anomalous Hall insulator sample. We find binary transmission of the edge state depending on the energy where we show that the details of energy dependence can be controlled by the magnetic superlattice strength. This allows us to realize edge states using superlattices and we consider our method of applying magnetic superlattices opens the way edge state engineering.

Finally; in Chapter 7, we present our conclusions.

Chapter 2

OVERVIEW

Topologically nontrivial phases are exotic states of matter that have an electonic bandgap in their bulk and gapless excitations on their boundaries[4, 5]. Superconductors, being quasiparticle insulators, also feature topological phases with a quasiparticle gap in the bulk and excitations at their edges. For one-dimensional systems, these edge states are fermionic zero-energy modes called Majorana states [6–8]. These states attracted intense attention due to their non-Abelian nature, which led to proposals to use them as topological qubits immune to decoherence [2, 9]. Although predicted to appear in exotic condensed matter systems with unconventional superconducting pairing, [10–15] recent proposals [16–19] involving hybrid structures of more conventional materials have appeared [20–30]. This led to the recent conductance measurements done on a proximity coupled InSb nanowire [31], which showed possible evidence of Majorana end states in the form of zero-bias conductance peaks. Other experiments reported further observations of zero-bias peaks in similar settings [32–34]. Very recently, scanning-tunneling spectroscopy experiments carried out on magnetic adatom chains on a conventional superconductor reported zero-bias peaks at the ends of the chains[35]. While it is compelling to interpret the observation of these zero-bias peaks as signatures of Majorana states, the issue is still under intense discussion [36].

Semiconductor nanowire structures that are proximity coupled to superconductors are technologically attractive platforms for Majorana physics. However, disorder has been prominently present in all such experimental samples to date. This led to a renewed interest in disordered superconducting wires, particularly focusing on the effects of disorder on Majorana states [1, 36–52]. These works focused mostly on disordered p-wave superconducting wires and showed that disorder is detrimental to the spectral gap as well as to the formation of Majorana fermions in both strictly 1D systems [37–40, 53] and in

multichannel wires [36, 43, 44, 54]. We show that disorder need not be detrimental to topological order, and in fact can even create topologically nontrivial topological phases in strictly 1D wires[3]. In this Thesis, we show that disorder is not always detrimental to topological order –it can also change the topological order of s-wave and p-wave semiconductor wires. After analyzing the effects of irregular scattering on topological order, we continue to investigate the cases of regular scattering in order to control topological order. We use electrostatic superlattices in order to drive p-wave and s-wave topological superconductors into and out of their topological phases. The application of the electrostatic superlattice causes the quasiparticle band gap open or close depending on the topological order of the wire [3]. In our investigation we use weak electronic superlattices that does not lead to topological phase transitions along the wire. We also apply our understanding of superlattices to open mini gaps in quantum anomalous Hall spectrum by using weak magnetic superlattices. In this Chapter, we present a brief summary of topological insulators focusing on topological superconductors and Majorana end states.

2.1. Topological Phases of Matter

2.1.1. Quantum Hall Effect and Chern Insulator

The discovery of Quantum Hall Effect by von Klitzing, Dorda and Pepper in 1980 had shown that a 2D material under the effect of strong transverse magnetic field exhibit states that lie on the edges even though there are no states in its bulk at Fermi energy [55–58]. These states are named as *edge states* and exhibit metallic behavior. This experiment showed that conductance of this 2D material is quantized, in units of so-called conductance quantum $G_0 = e^2/h$, to a very high accuracy. This effect is named Quantum Hall Effect. The presence of edge states can be explained using a cartoon picture by the closed circular orbits of the electrons in the bulk under strong magnetic field: The total net current turns out to be zero in the bulk due to these closed circular orbits but, at the edge, the electrons cannot complete a full circle and present metallic behavior. This phenomenon can be further understood in physical terms by using the concept of Landau levels of electrons [59], and the bulk-edge correspondence.

Robust nature of the edge states and their dependence on the bulk band structure implies a topological difference between types of materials since the edge states cannot be created or destroyed with local perturbations. The concept of topology is then applied onto the classification of materials. In mathematics, topological classes are defined for geomet-

ric shapes of objects. The most concrete distinction between shapes that are in different topological classes is the number of holes or handles it has. If a shape can be smoothly deformed into another they are considered to be in the same topological class [5, 7, 60–64]. Here, the notion of smooth deformation is limited by punching holes on a geometrical shape; the number of holes are counted during mathematical topological classification. The number of holes is related to the integral of the Gaussian curvature of the system plus an integral of the curvature along the boundary of the shape [64–66]. We briefly outline how topology enters the picture in gapped systems as follows: The simplest Hamiltonian describing a gapped system is a 2×2 Hamiltonian with levels corresponding to the level just below and just above the gap. Such a Hamiltonian in general could be written as $H(k) = d_0(k)\sigma_0 + \mathbf{d}(k) \cdot \boldsymbol{\sigma}$, where σ_i are the Pauli matrices. One could readjust the zero of the energy level by setting $d_0 = 0$, and rescale the energy by setting $|\mathbf{d}| = 1$. Thus, the vector $\mathbf{d}$ represents a mapping from the Brillouin zone to a unit sphere. It is the topology of this mapping that is considered in the topic of topological insulators. As one scans the Brillouin zone via k, how many times $\mathbf{d}$ winds around a degeneracy point is a topologically protected number. If the band gap closes, the topological index of the material changes. The closing of the band gap can be justified using an argument called *bulk-boundary correspondence* [5, 65]: Consider a topologically nontrivial material in contact with vacuum. The vacuum has zero genus and the topologically nontrivial material has a nonzero genus where both the vacuum and the bulk of the topological material has a band gap since there is no metallic behavior in either of them. The presence of the edge states follows from the required closing of the band gap at the boundary between two materials with different topological indices. At the boundary topological index changes and creates an edge state. This argument can be generalized to materials in different topological classes having different genera to show that the edge states are also present. So a discontinuous change in topological index –which is the direct result of a contact of two topologically different material– leads to the closing of the bulk band gap and leads to metallic states at the edge. Hence, a gapped band structure can be characterized with a topological index. *Topological insulators* are such band insulators whose topological index is different to that of the vacuum. The robustness of the edge states follows from the robustness of these topological invariants; any change that does not change the genus does not change topological behavior of the materials. Smooth deformations like altering "the shape of the material" or the band structure of the material adiabatically do not alter

the genus so we conclude that the edge states are topologically protected.

The importance of the discovery of quantum Hall effect with its robust and edge states is considered to be the first encounter of a topological material. As explained earlier; the application of an external magnetic field is crucial to the existence of the quantum Hall edge state. In presence of a magnetic field, time-reversal symmetry of the material is broken and it cannot be considered to be a smooth deformation of the material with no magnetic field: Thus the symmetry breaking is the reason these materials belong into different topological classes.

The distinction between topological and nontopological materials originates from their Chern numbers [58, 64–66] In order to calculate Chern invariants; we first calculate the Berry phase of a Bloch wavefunction $|u_n(\mathbf{k})\rangle$ that it acquires when it gets transported along a closed loop in the momentum space which is calculated by integrating the momentum space path $\mathcal{A}_n = \langle u_n(\mathbf{k})|\nabla_n|u_n(\mathbf{k})\rangle$. Berry phase is then used to calculate Berry curvature as $\mathcal{F}_n = \nabla \times \mathcal{A}_n$ which is the momentum space field strength. The Chern invariant for a band is

$$c_n = (1/2\pi) \int \mathcal{F}_n d^2\mathbf{k} \tag{2.1}$$

where it accounts for the total Berry flux in the band. Finally, the Chern number for the topological insulator is calculated by summing over all occupied channels $c = \sum_n c_n$ where $c \in \mathbb{Z}$ is invariant unless a topological phase transition closes the band gap.

It has been shown by Thouless *et al.* [57] that Hall conductivity σ_{xy} is a Chern number multiplied by half a quantum conductance $G_0 = 2e^2/h$ and is coined as the Thouless-Kohmoto-Nightingale-den Nijs invariant [58]. Connecting Chern number to Hall conductivity explained the precision behind the conductance quantization in quantum Hall effect since it cannot be altered with smooth alterations on the material.

2.1.2. Quantum Spin Hall Effect and $\mathbb{Z}_2$ Topological Insulator

In 2005, Kane and Mele [67] suggested that there exists a different type of topological insulator in which time-reversal symmetry remains intact, *i.e.* when there's no applied magnetic field. This type of topological insulators owe their topological characteristics

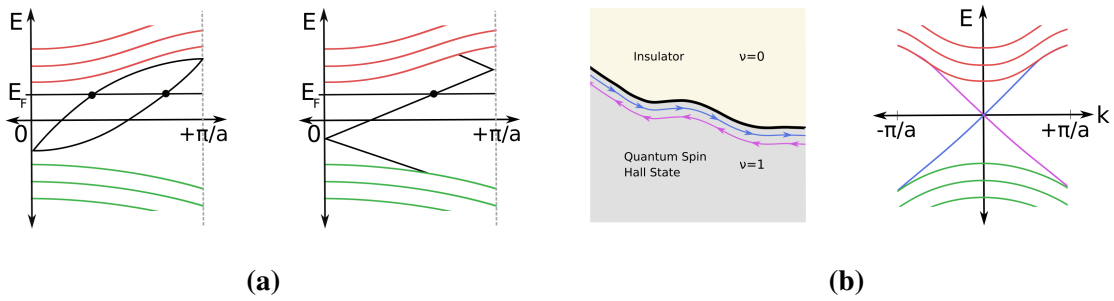

(a) **(b)**

Figure 2.1: Zero-energy crossing of the bands within the band-gap at Fermi energy E_F (Fig. 2.1a) for a $\mathbb{Z}_2$ topological insulator. Between Γ_a and Γ_b an even number of crossings occurs for a trivial state. These crossings can be smoothly deformed to a bulk bandgap and are not topologically protected. Odd number of crossings (Fig. 2.1b), on the other hand, cannot be adiabatically transformed to a gapped band structure and thus are topologically protected, resulting in chiral edge-states.

due to their intrinsic spin-orbit coupling and they also exhibit topological edge states [67, 68]. In such systems Thouless-Kohmoto-Nightingale-den Nijs invariant vanishes and new topological invariants needs to be considered [5, 65, 69].

We understand these type of topological insulators by examining the effects of time-reversal symmetry on spin-1/2 particles. The spin-1/2 time-reversal symmetry operator Θ is defined as $\Theta = exp(i\pi S_y/\hbar)K$ where S_y is spin along the y-axis and K is complex conjugation [70]. Since the time-reversal symmetry operator is antiunitary, we have $\Theta^2 = -1$. This feature requires time-reversal invariant Hamiltonians to have degenerate pairs known as Kramer's pairs. In the band structure of time-reversal invariant Hamiltonians the consequence of this invariance is a symmetrical band structure around $k_x = 0$ in the first Brillouin zone $-\pi/a < k_x < \pi/a$ [70]. There's also another degeneracy built in to the band structure that owes its existence to Kramer's pairs: The electronic states at $\Gamma_a = 0$ and $\Gamma_b = \pi/a$ are also degenerate [70]. This degeneracy allows two types of connection between Kramer's pairs. The spin-orbit coupling plays a crucial role when degenerate eigenstates start to split apart in energy between $\Gamma_a = 0$ and $\Gamma_b = \pi/a$ points. If these states split pairwise as depicted in Fig. 2.1a, edge states can be pushed out of the band gap because of spin-orbit coupling so there would be no topological protection. However; if a Kramers pair does not split pairwise, these states cannot be canceled by spin-orbit coupling and thus we would have topological protection. This logic is implemented to define a new topological invariant known as $\mathbb{Z}_2$ by counting number of crossings for states whose Fermi energy lies within the band gap [67]. Hence an even number of Fermi energy crossings at either half of the Brillouin zone will result in gapped states whereas if the there's an odd number of crossings, spin-orbit coupling would not be able to push the

last remaining state out of the band gap and hence an edge state will be present. Using this logic; $\mathbb{Z}_2$ topological invariant is defined as $N = \nu(mod2)$ where ν is the total number of crossings at the Fermi energy in the band gap.

2.1.3. Topological Superconductors

Since superconductors also harbor a bulk quasiparticle gap [4, 7, 69], they also have a topological index [71, 72]. The Bardeen-Cooper-Schriffer Theory allows a mean field description of superconductors in terms of a Bogoliubov-de Gennes Hamiltonian [13]. For spinless fermions, this reads:

$$H = \frac{1}{2}\sum_{\mathbf{k}} \begin{bmatrix} c_{\mathbf{k}}^{\dagger} & c_{\text{-}\mathbf{k}} \end{bmatrix} \mathcal{H}_{\text{BdG}} \begin{bmatrix} c_{\mathbf{k}} \\ c_{\text{-}\mathbf{k}}^{\dagger} \end{bmatrix}, \tag{2.2}$$

where $c_{\mathbf{k}}^{\dagger}$ is electron creation operator and $\mathcal{H}_{\text{BdG}}$ is a 2×2 block Hamiltonian which is defined as

$$\mathcal{H}_{\text{BdG}} = \mathcal{H}_0\tau_z + \mathbf{\Delta} \cdot \tau \tag{2.3}$$

Here, $\mathcal{H}_0 = \hbar^2|\mathbf{k}|^2/2m$ is kinetic term of quasiparticles, Pauli matrices τ_i $(i = x, y, z)$ designate particle-hole space and $\mathbf{\Delta} = \Delta_x + i\Delta_y$ is the superconducting pair potential which also is responsible for the superconducting energy gap. By its construction, particle-hole symmetry is intrinsic in Bogoliubov-de Gennes Hamiltonian, *i.e.* $\Xi\mathcal{H}^*_{\text{BdG}}(\mathbf{k})\Xi^{-1} = -\mathcal{H}_{\text{BdG}}(-\mathbf{k})$ and particle-hole symmetry operator for spin-1/2 particles is defined as $\Xi = \tau_x K$ where it is antiunitary with $\Xi^2 = +1$. For a superconducting eigenstate at energy $+\epsilon$ there exists a complimentary solution at the opposite energy $(-\epsilon)$ because of the particle-hole invariance built into the Bogoliubov-de Gennes Hamiltonian. These complementary solutions of opposite energies represent antiparticles of each other, and are degenerate at $\epsilon = 0$. If, at zero energy, the antiparticle of such a fermionic state is itself, they are called Majorana states, which are the main focus of this thesis. Just as in the case of quantum spin Hall effect where a time reversal protected topological state exists, there are other phases where the topological state is protected by a combination of time reversal and particle-hole symmetry. In the next section, we focus on the classification of these phases.

Symmetry				Dimension							
A-Z	Θ	Ξ	Π	1	2	3	4	5	6	7	8
A	0	0	0	0	$\mathbb{Z}$	0	$\mathbb{Z}$	0	$\mathbb{Z}$	0	$\mathbb{Z}$
AIII	0	0	1	$\mathbb{Z}$	0	$\mathbb{Z}$	0	$\mathbb{Z}$	0	$\mathbb{Z}$	0
AI	1	0	0	0	0	0	$\mathbb{Z}$	0	$\mathbb{Z}_2$	$\mathbb{Z}_2$	$\mathbb{Z}_2$
BDI	1	1	1	$\mathbb{Z}$	0	0	0	$\mathbb{Z}$	0	$\mathbb{Z}_2$	$\mathbb{Z}_2$
D	0	1	0	$\mathbb{Z}_2$	$\mathbb{Z}$	0	0	0	$\mathbb{Z}$	0	$\mathbb{Z}_2$
DIII	-1	1	1	$\mathbb{Z}_2$	$\mathbb{Z}_2$	$\mathbb{Z}$	0	0	0	$\mathbb{Z}$	0
AII	-1	0	0	0	$\mathbb{Z}_2$	$\mathbb{Z}_2$	$\mathbb{Z}$	0	0	0	$\mathbb{Z}$
CII	-1	-1	-1	$\mathbb{Z}$	0	$\mathbb{Z}_2$	$\mathbb{Z}_2$	$\mathbb{Z}$	0	0	0
C	0	-1	0	0	$\mathbb{Z}$	0	$\mathbb{Z}_2$	$\mathbb{Z}_2$	$\mathbb{Z}$	0	0
CI	1	-1	1	0	0	$\mathbb{Z}$	0	$\mathbb{Z}_2$	$\mathbb{Z}_2$	$\mathbb{Z}$	0

Table 2.2: Classification of topological materials with different symmetries and in different dimensions. The 0 entries show topologically trivial configurations and ± 1 values on the left pane are values of Ξ^2, Θ^2 and Π^2 when the material is topologically nontrivial and a zero value denotes the absence of the corresponding symmetry.

2.1.4. Topological Classification of Materials

In this section we present the most general topological classification of materials. The original work on the classification of random Hermitian matrices by Wigner and Dyson [71–74] was expanded by Altland and Zirnbauer in 1972 to include superconductivity. Along with different dimensionalities, these symmetry classes are classified using three distinct symmetries: time-reversal symmetry with operator with Θ, particle-hole symmetry with operator Ξ and chiral symmetry $\Pi = \Xi\Theta$. The zero values signify the absence of the corresponding symmetry in material configurations, and ± 1 values specify the eigenvalues of Ξ^2, Θ^2 and Π^2.

Classification of topological materials with different symmetries and in different dimensions. The 0 entries show topologically trivial configurations and ± 1 values on the left pane are values of Ξ^2, Θ^2 and Π^2 when the material is topologically nontrivial and a zero value denotes the absence of the corresponding symmetry.

For example, the quantum Hall insulator which has no symmetries ($\Theta = \Xi = \Pi = 0$) is referred to as a class A topological insulator and has a $\mathbb{Z}$ topological invariant in 2D. Quantum spin-Hall insulator that has time reversal symmetry with $\Theta^2 = -1$ belongs to the class AII with a topological invariant $\mathbb{Z}_2$ invariant in 2D and 3D. The particle-hole symmetric topological superconductors with $\Xi^2 = 1$ belong to the topological class D with topological invariants $\mathbb{Z}_2$ in 1D and $\mathbb{Z}$ in 2D. We present the most general topological classification scheme in Table 2.2; we now focus on the physical systems considered in this Thesis.

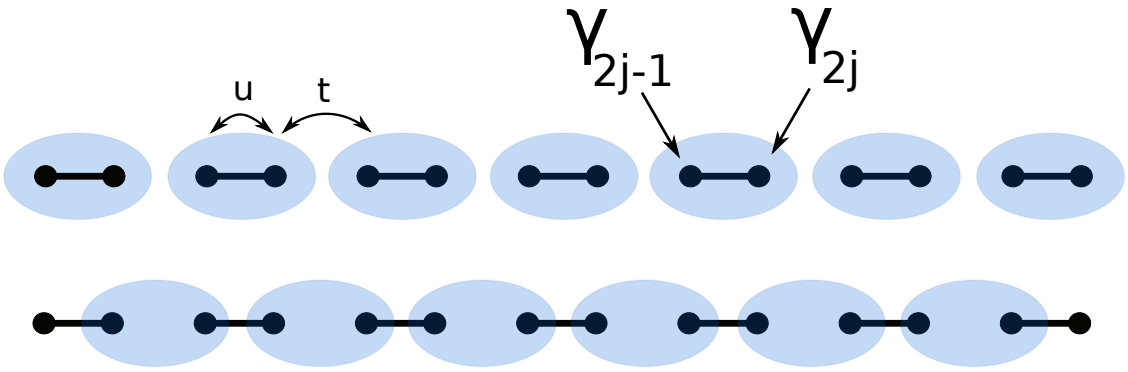

Figure 2.3: An illustration of of the Kitaev chain. a) Electrons at a given site j can be divided into a real and an imaginary part, each of which is a Majorana fermion. b) The diagonalized Hamiltonian (for a certain range of parameters) relates Majorana fermions at consecutive sites, leaving one Majorana fermion free at each end of the chain. If this state is occupied, the system is in a topologically nontrivial phase.

2.2. Topological Superconductor Wires

In this section we begin to explore topological superconducting wires which are the physical systems that we concern ourselves in this Thesis. We first start with the Kitaev model which demonstrates Majorana edge states in a p-wave topological superconductors.

In 2001, Kitaev introduced a toy-model [15] of a 1D p-wave paired topological superconductor wire that exhibits topologically nontrivial states at its ends. In order to show that a spinless chain of p-wave topological superconductor can topologically only exist in two states, a tight-binding approach is implemented and a simple particle transformation showed that the topologically nontrivial edge states are actually Majorana fermions which can be loosely interpreted as half electrons. In tight-binding formulation, the Hamiltonian of a 1D p-wave topological superconductor can be written as

$$H = -\sum_{j} uc_j^\dagger c_j + t(c_j^\dagger c_{j+1} c_{j+1}^\dagger) - \Delta(c_j c_{j+1} + c_{j+1}^\dagger c_j^\dagger) \tag{2.4}$$

where $c_j^\dagger$ operator that creates an electron at site j, u is the chemical potential, t is the hopping term between nearest-neighbor sites and Δ is the superconducting pair-potential which normally opens a gap in the electronic spectrum. We set $\Delta \geq 0$ to insure the opening of the bulk we require a positive pair potential. With the existence of a certain insulating gap, we continue to make a simple particle transformation that transforms the Hamiltonian to a different basis that is the *Majorana basis*. These newly introduced Majorana operators will signify the real and complex parts of the electronic operators

(see Fig. 2.3). We define Majorana operators in terms of electronic operators as

$$c_j = \gamma_{2j-1} + i\gamma_{2j}$$

which corresponds to doubling of sites in the chain. The new operators are defined with the following relations

$$\begin{aligned} [\gamma_i, \gamma_j]_+ &= 2\delta_{ij} \\ \gamma_j^2 &= 1 \\ \gamma_j^\dagger &= \gamma_j. \end{aligned}$$

So the Hamiltonian can be cast into this new basis as

$$H = -\frac{i}{2}\sum_{j=1}^{N} u\gamma_{2j-1}\gamma_{2j} + (\Delta + t)\gamma_{2j}\gamma_{2j+1} + (\Delta - t)\gamma_{2j-1}\gamma_{2j+2}. \tag{2.5}$$

We consider two special limiting cases and set $\Delta = t$ for simplicity. If the hopping term is set to zero and chemical potential is assumed to be zero the system turns out to be collection of noninteracting electrons with no hopping between them. The other limiting case occurs when $t \neq 0, u = 0$ and the Hamiltonian gives a tally of coupling between successive sites. This time, there is $N - 1$ terms in the Hamiltonian where γ_1 and γ_{2N} do not show up in Eq. 2.5. These are the Majorana states manifesting themselves at the ends of the wire separated from each other. In the more general case, Majorana states have localized wavefunctions that exponentially decay through the wire over a length scale set by superconducting coherence length $\xi \propto 1/\Delta$. Majorana states are at zero energy because of the intrinsic particle-hole symmetry built into the superconducting Hamiltonian. More strikingly, Majorana states are their own antiparticles since $\gamma_1^\dagger = \gamma_1$ and $\gamma_{2N}^\dagger = \gamma_{2N}$; however, two Majorana states hybridize when their wavefunctions overlap to generate a finite energy fermion state ($\gamma_1 \pm i\gamma_{2N}$). Next we investigate possible physical realizations of p-wave topological superconductors.

The model p-wave topological insulators we consider above needs spinless electrons, which do not exist in nature. Nevertheless, there are theoretical proposals to find material examples that approximates this physics. First proposal involved a proximity coupling an ordinary superconductor to a quantum spin Hall insulator [67, 75]. As mentioned above, a quantum spin Hall insulator harbors edge states that are chiral counterparts of each other

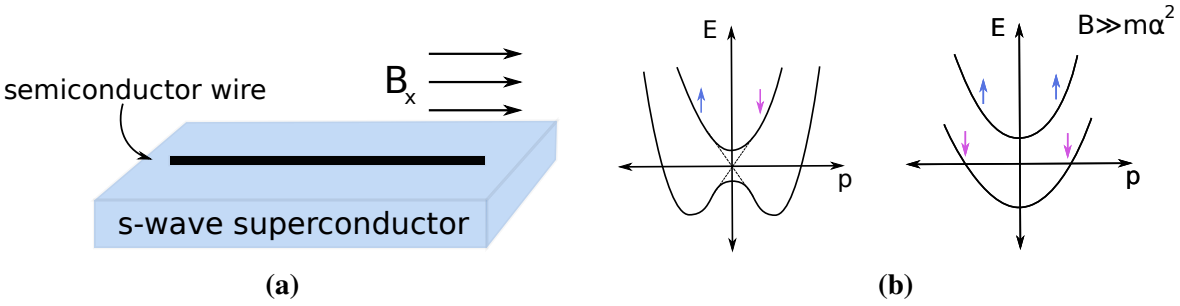

Figure 2.4: An experimental proposal to realize topological superconductors (Fig. 2.4a). A semiconductor wire is placed in proximity of an s-wave superconductor that creates an induced coupling in the electron-hole bands of the semiconductor. The application of a magnetic field breaks time-reversal symmetry that leads to topologically nontrivial states. In Fig. 2.4b, the effects of magnetic field on the semiconductor wires is illustrated. When spin-orbit coupling is larger than the magnetic field, both spin-bands of the semiconductor merge to create nontrivial states. The application of high magnetic fields leads to spin polarization so spin bands do separate from each other: Bands of opposite spin move away from each other. The lower energy band then features spinless (spin-polarized) p-wave topological superconductivity.

so that it can be coupled to an ordinary s-wave superconductor since chiral edge states carry opposite spins. However, proximity is not sufficient for topological superconductor edge states to form because time-reversal symmetry still remains intact so a magnetic field is applied onto it to break time-reversal symmetry. When the time reversal symmetry is broken, the existence of edge modes simply lie in between a configuration between the gapped phase and the magnetic field. When $\Delta = 0$ and $B \neq 0$ there will not be any edge states since the band structure is gapless; and the edge states still cannot exist at the other extreme ($\Delta \neq 0$ and $B = 0$) since the system is time-reversal invariant. Hence we conclude that an edge state can be present if we are dealing with a system with an energy gap and an external magnetic field. Promising as this construction sounds, it requires the existence of an already topological material which may complicate experimental realizations since quantum spin Hall effect is not a very common phenomenon in materials and materials that feature quantum spin Hall effect has not been available very widely. This obstacle is overcome with the proposal and application of employing a semiconductor wires instead of a quantum spin Hall insulators [17, 19, 31, 32, 34, 76]: When a semiconductor wire with a strong spin-orbit coupling is put on top of a conventional s-wave superconductor slab, the induced superconductivity exhibits Majorana states provided that time-reversal symmetry is broken with an external magnetic field. The magnetic field destroys spin degeneracy and the spin-orbit coupling tilts the polarization direction so that these bands get coupled by an s-wave pairing potential Δ, which provides a band gap in

which edge states can be present.

The existence of zero energy edge Majorana modes have been demonstrated using Kitaev's chain, so we now define the corresponding continuum model Hamiltonian for spinless p-wave topological superconductor [4, 5]

$$\begin{aligned} H &= \int d^2\mathbf{r} \begin{bmatrix} \psi^\dagger & \psi \end{bmatrix} H_{\text{BdG}}^{(\text{p})} \begin{bmatrix} \psi \\ \psi^\dagger \end{bmatrix} \\ &= \int d^2\mathbf{r} \Psi^\dagger \left[\left(\frac{\mathbf{p}^2}{2m} - \mu \right) \tau_z + \Delta_{\text{eff}} \mathbf{p} \cdot \tau \right] \Psi, \end{aligned} \tag{2.6}$$

where $\psi^\dagger$ is the electronic creation operator, Ψ is the Nambu spinor, τ_i $(i = x, y, z)$ are Pauli matrices that denote electron-hole space and Δ_{eff} is the effective superconducting pair potential. The Bogoliubov-de Gennes Hamiltonian has particle-hole symmetry so $\Xi H_{\text{BdG}}^{(\text{p})} \Xi^{-1} = -H_{\text{BdG}}^{(\text{p})}$ and each state with energy E should have a counterpart at the same magnitude but negative energy $-E$. At zero-energy this pairing leads to two spatially separated Majorana states which are their own antiparticles.

Adding spin to the spinless p-wave topological superconductor Hamiltonian may seem like a straightforward step since it would not change the zero energy modes; however, this would place two electrons at each site in Kitaev's chain which would mean that there would *always* be two Majorana fermions at both ends of the chain. Since the two could always hybridize, we would never get an isolated Majorana mode. Adding spin to a p-wave topological superconductor wire does not lead to Majorana mode, so is the central reason why we need the spinful s-wave topological superconductor whose Hamiltonian is defined as

$$\begin{aligned} H &= \int d^2\mathbf{r} \begin{bmatrix} \psi_\uparrow^\dagger & \psi_\downarrow^\dagger & \psi_\downarrow & -\psi_\uparrow \end{bmatrix} H_{\text{BdG}}^{(\text{s})} \begin{bmatrix} \psi_\uparrow \\ \psi_\downarrow \\ \psi_\downarrow^\dagger \\ -\psi_\uparrow^\dagger \end{bmatrix} \\ &= \int d^2\mathbf{r} \Psi^\dagger \left[\left(\frac{\mathbf{p}^2}{2m} - \mu \right) \tau_z + \alpha(\mathbf{p} \times \sigma)\tau_z + B\sigma_x + \Delta\tau_x \right] \Psi, \end{aligned} \tag{2.7}$$

where the Nambu spinors now also include the spin degree of freedom which are denoted with $\sigma_i \mid (i = x, y, z)$. The energy spectrum of the s-wave topological superconductor is

found by analyzing the expectation value of $\langle {H^{(s)}_{\rm BdG}}^2 \rangle$ which is

$$E^2_{\pm} = \epsilon^2 + B^2 + \Delta^2 + \alpha^2|\mathbf{p}|^2 \pm 2\sqrt{B^2(\epsilon^2+\Delta^2) + \alpha^2|\mathbf{p}|^2\epsilon^2}.$$

In the above equation $\epsilon = |\mathbf{p}|^2/2m - \mu$ and $E^2_{\pm}$ exhibits two gaps one of which is corresponds to Fermi momentum with $\mathbf{p} = \sqrt{2\mu m}$ and the other at low momentum at $\mathbf{p} = 0$ [16]. The gap function near $\mathbf{p} = 0$ is $B - \sqrt{\mu^2 + \Delta^2}$ which is dominated by the magnetic field. The gap near the low energy momentum can change its sign causing the band gap to close and reopen; so we set gap function to positive values in agreement with our earlier assumption $\Delta \geq 0$. Therefore we conclude that when $B^2 > \mu^2 + \Delta^2$ the band gap is open and the s-wave topological superconductor is in its nontrivial topological phase so that it exhibits Majorana modes and when $B^2 = \mu^2 + \Delta^2$ the s-wave topological superconductor makes a topological transition since the band gap is now closed [16], to the topologically trivial state for $B^2 < \mu^2 + \Delta^2$.

We confine ourselves to thin-wire geometry, in which $W \ll \xi$, where W is the width of the wire and ξ is the superconducting coherence length. For p-wave wires, this superconducting coherence length takes the form $\xi_{\rm p} = \hbar/m\Delta$ and for s-wave wires $\xi_{\rm s} = \hbar\sqrt{B^2 - \Delta^2}/m\alpha\Delta$ [42]. In the case of the Fermi wavelength becoming larger than the width $\xi \gg \lambda_F \sim W$, we can further simplify the Hamiltonian by replacing the momentum in y-direction by its expectation value. Employing the fact that the transverse momentum is inversely proportional to width as $\langle p_y \rangle \sim \hbar/W$; we can estimate the contributions coming from the p_y term in terms of coherence lengths as

$$\langle \Delta_{\rm eff} p_y \rangle \sim \frac{\hbar^2}{m\xi_{\rm p} W} = \frac{\hbar^2}{mW^2}\frac{W}{\xi_{\rm p}} \qquad \langle \alpha p_y \rangle \sim \frac{\hbar^2\sqrt{B^2-\Delta^2}}{m\xi_{\rm s}\Delta W} = \frac{\hbar^2\sqrt{B^2-\Delta^2}}{m\Delta W^2}\frac{W}{\xi_{\rm s}}. \quad (2.8)$$

where $\Delta_{\rm eff}$ is the effective spin orbit coupling strength in p-wave wires and α is the spin orbit coupling strength in s-wave wires. The above equations ensures the diminishing of p_y contribution to the Hamiltonian since $\xi \gg W$. After we show that p_y contributions to the Hamiltonian can be neglected for very-thin wires; the quadratic transverse momentum term p_y^2 solutions can be found by treating the y-degree of freedom as a perturbation that is confined on the lateral edge. These solutions are in the form of periodic functions which has quantized momenta as $\langle p_y^2 \rangle \propto \hbar^2 n^2 \pi^2/W^2$, where $n = 1, 2, \ldots$ are the transverse occupational numbers. The cancellation of the p_y-term when $\xi \gg W$ also has a very important consequence: The multichannel topological superconductor thin-wires behave

like the collection of topological superconductor wires. We can say that *clean* topological superconductor thin wires with even number of transverse confinement channels can not harbor Majorana modes due to hybridization unless it is forbidden due to symmetry; so they enter into their topologically trivial phase. On the contrary; if the number of channels is odd, we still have a single Majorana mode at the ends making the topological superconductor thin wire topologically nontrivial [77]. When the wire gets thicker as $\xi \simeq W$, the linear p_y contribution cannot be canceled from the Hamiltonian and the y-degree of freedom cannot be treated as a perturbation. The ability to neglect p_y-term contribution in thin wires changes restores chiral symmetry of the Hamiltonians in Eqs. 2.6 and 2.7 which belong to the symmetry class D. Topological superconductors only possess particle-hole symmetry with $\Xi^2 = 1$. As we show; the thin wire condition ($\xi \gg W$) allows us to neglect p_y contribution to the Hamiltonians and makes them chirally symmetric; hence as a direct consequence of restoration of chiral symmetry, the Hamiltonians also become time-reversal invariant since the chiral symmetry operator is defined as a product of time-reversal and particle-hole symmetry operators as $\Pi^2 = 1$ since $\Pi = \Xi\Theta$. The presence of all three symmetries with positive eigenvalues $\Theta^2 = \Xi^2 = \Pi^2 = 1$ makes topological superconductors to *implicitly* belong to the class BDI [72].

We briefly outline the deductions made concerning topological superconductor wires because they are central to the results of this Thesis: The Kitaev model demonstrates the existence of zero-energy modes that are called Majorana fermions at the ends of a p-wave topological superconductor chain by splitting the electronic operators into two parts. That's why Majorana fermions are sometimes loosely called as *half electrons* in literature. We then briefly discussed theoretical proposals for Majorana fermion realization. In order to add spin degree of freedom to the p-wave wire, the s-wave wire is introduced, since merely doubling the p-wave wire would never exhibit Majorana fermions by construction. After the introduction p-wave and s-wave wire Hamiltonians we confined our problem to very-thin wires ($\xi \gg W$) and showed that the time-reversal symmetry breaking linear transverse momentum term can be omitted in thin-wires. After that we have quantized the remaining quadratic transverse momentum term and showed that clean multichannel wires behave as a collection of topological chains. We have also explained that with the recovery of the time-reversal symmetry, the very-thin wires become also chirally symmetric which allow them to behave in class BDI with topological index $\mathbb{Z}$ –where according to

the Table. 2.2, topological superconductors are classified in class D with topological index $\mathbb{Z}_2$. Finally we mentioned that an s-wave topological superconductor wire can be thought as a collection of two p-wave topological superconductor wires since at high magnetic fields compared to the spin-orbit coupling ($B \gg m\alpha^2$), s-wave spin degrees of freedom polarized and behave as two spinless p-wave wires.

2.3. Numerical Methods for Majorana Systems

In this Thesis, we use numerical tight-binding calculations to check the validity of our analytical results using KWANT Library [78]. For spinful s-wave topological superconductors, the tight binding Hamiltonian for a finite lattice site a is given by [3, 17, 19, 43, 79]

$$\begin{aligned}\mathcal{H}_{\text{s}}^{\text{TB}} = &[(4t + V(x,y) - \mu(x,y))\ \tau_z + B\,\sigma_z \\ &+\ \Delta(x,y)\,\tau_x]\ |x,y\rangle\,\langle x,y| \\ &+\ \left[-t\,\tau_z - \frac{i}{2}\alpha_{\text{SO}}(x,y)\,\tau_z\,\sigma_y\right]\ |x+a,y\rangle\,\langle x,y| \\ &+\ \left[-t\,\tau_z + \frac{i}{2}\alpha_{\text{SO}}(x,y)\,\tau_z\,\sigma_x\right]\ |x,y+a\rangle\,\langle x,y| \\ &+ \text{h.c.}.\end{aligned}$$

For p-wave topological superconductors, the tight-binding Hamiltonian is

$$\begin{aligned}\mathcal{H}_{\text{p}}^{\text{TB}} = &[4t + V(x,y) - \mu(x,y)]\ \tau_z\ |x,y\rangle\,\langle x,y| \\ &+\ \left[-t\,\tau_z - \frac{i}{2}\Delta_{\text{eff}}(x,y)\,\tau_x\right]\ |x+a,y\rangle\,\langle x,y| \\ &+\ \left[-t\,\tau_z - \frac{i}{2}\Delta_{\text{eff}}(x,y)\,\tau_y\right]\ |x,y+a\rangle\,\langle x,y| \\ &+ \text{h.c.}\end{aligned}$$

In the above formulation, $t = \hbar^2/2ma^2$ is the hopping parameter, $V(x,y)$ is the electrostatic potential, $\mu(x,y)$ is the potential of the leads, B_z is Zeeman field strength, $\Delta(x,y)$ is the superconducting proximity-induced coupling constant, α_{SO} is the spin-orbit coupling constant and $\Delta_{\text{eff}} = \Delta\alpha_{\text{SO}}/\sqrt{B^2 - \Delta^2}$ is the effective spin-orbit coupling term for p-wave topological superconductors. In our calculations, we take $V(x,y)$, B_z, $\Delta(x,y)$, Δ_{eff} and α_{SO} to be nonzero in the scattering region and we take leads to be metallic so all these terms are taken to be zero in the leads.

We use KWANT Library [78] to calculate the scattering matrix (S-matrix) of the topological superconductor wires [80]. The existence of Majorana modes, and thus the topoogical order can be checked by calculating $\mathbb{Q}_{\mathrm{D}} = \mathrm{sgn}(\mathrm{Det}(r))$ for a system with metallic leads [1].

Chapter 3

DISORDER EFFECTS IN TOPOLOGICAL SUPERCONDUCTOR CHAINS AND SINGLE-CHANNEL NANOWIRES

In this chapter, we investigate the effects of disorder on the topological phases of p-wave and s-wave topological 1D superconductor wires [3]. Previous works [38, 42, 43, 45, 46, 77, 81–83] show that disorder is detrimental to the topological phases of topological superconductors; here, we show otherwise by deriving analytical formulae for the topological indices and obtain the topological phase diagram for p-wave and s-wave single channel topological superconductor wires in presence of Gaussian disorder. We also perform numerical tight-binding calculations of the topological index using a scattering matrix approach [1]. Our analytical results show significant agreement with the the tight-binding calculations.

Topological superconductors we are interested in belong to Altland-Zirnbauer topological symmetry class-D so we use subscripts D that signify our topological index formulae. Our topological index formula is a binary number in $\mathbb{Z}_2$ [72] in agreement with the topological classification in Table 2.2.

We start with spinless p-wave wire in Section 3.1 since it is easier to follow our analysis, then we extend our calculation to s-wave wires in Section 3.2. Since we deal with a strictly one dimensional construction here; the zero-energy states at the ends of the wire are Majorana bound-states.

3.1. Topological Index Calculation for Disordered p-wave Wires

We compute a topological index for p-wave topological superconductor wires by imposing a boundary condition at the origin and investigating the asymptotic behavior of its wavefunction as the wire extends. We assume a semi-infinite geometry which has an ordinary insulator and topological superconductor wire interface at the origin, where the wire

extending to infinity as $x \to +\infty$ and the other side ($x < 0$) is where the ordinary insulator resides. Projecting the p-wave Bogoliubov-de Gennes Hamiltonian in Eq. 2.6 [49, 84] into a single dimension along x-direction; we obtain the one-dimensional Hamiltonian for a spinless p-wave wire as

$$H = h(p,x)\tau_z + \Delta_{\text{eff}} p \tau_x, \tag{3.1}$$

where $h(p,x) = p^2/2m - \mu$ is the single-particle Hamiltonian, p is the momentum operator, m is effective electron mass, μ is the chemical potential and Δ_{eff} is effective spin-orbit coupling constant. Here, Pauli matrices τ_i $(i = x, y, z)$ denote electron-hole space. Hamiltonian in Eq. 3.1 is chiral because of the absence of chiral symmetry breaking term proportional to p_y. Chiral symmetry allows us to off-diagonalize the Hamiltonian by a unitary transformation with $\mathcal{U} = exp(i\tau_x \pi/4)$. Similar method is used to study zero-energy modes in d-wave superconductors [35] Using the off-diagonalized Hamiltonian; zero-energy Majorana wavefunctions can be written in chiral pairs as $\chi_+ = \begin{bmatrix} \phi_+ \\ 0 \end{bmatrix}$ and $\chi_- = \begin{bmatrix} 0 \\ \phi_- \end{bmatrix}$ –for both block-Hamiltonians $(h(p,x) \pm i\Delta_{\text{eff}} p)\, \phi_\pm = 0$. Next, we apply an imaginary gauge transformation $\phi_\pm = e^{\pm\kappa x}\psi \mid \kappa = m\Delta_{\text{eff}}/\hbar$ in order to remove the linear momentum term. We choose the exponential factor of this gauge transformation as the inverse coherence length of the p-wave wire ($\kappa \equiv \xi_{\text{p}}^{-1}$). We then solve the block-Hamiltonians for zero-energy as

$$\left(-\frac{\hbar^2}{2m}\partial_x^2 - \bar{\mu}\right)\psi = 0, \tag{3.2}$$

where we define an effective chemical potential $\bar{\mu} = \mu + \hbar^2\kappa^2/2m$ in order to absorb the factor coming from the gauge transformation. For physical results; solutions $\phi_\pm$ should be normalizable as the wire extends into infinity, rather than ψ itself. Hence a diverging solution ψ as $x \to \pm\infty$ is permissible as long as the divergence is not faster than $e^{\mp\kappa x}$. We construct the zero-energy wavefunction at the topological superconductor-ordinary insulator interface as follows: For a normalizable wavefunction; we require that $\chi_\pm \to 0$ fast enough as $x \to \infty$. Assuming f and g are local solutions of the normal state equation in Eq. 3.2, we construct a general solution as $\psi = Af(x) + Bg(x)$ and after the imposition of the boundary condition; the solution can be rewritten as $\psi = g(0)f(x) - f(0)g(x)$. The generalized form of these solutions are $\psi \sim e^{\Lambda x}a(x)$ with $a(x)$ being a nondivergent

function and $\Lambda(\bar{\mu})$ being the Lyapunov exponent that can be calculated using a transfer matrix of the normal solutions [41]. Therefore, the asymptotic behavior of the zero-energy wavefunction has a general form of $\chi_{\pm} \sim e^{\pm\kappa x} e^{\Lambda x} a(x)$ We now continue to analyze the three cases of the asymptotic behavior of these exponents as follows:

(i) $\Lambda < -\kappa$: ψ becomes a bound state solution that contains two exponentially decaying zero mode solutions χ_+ and two exponentially diverging zero mode solutions χ_-. However, these states only exist because of an accidental fulfillment of the boundary condition and thus these states are not topologically protected. Such states do arise from the particle-hole symmetry of the Hamiltonian in Eq. 3.1: In presence of a small perturbation, two zero-energy states get away from the zero-energy in pairs with a positive and a negative energy. These double crossings of the band gap are not topologically protected and a small perturbation can destroy them. When this happens, we obtain an accidental satisfaction of the boundary condition for a zero-energy solutions which are not topologically protected. In Section. 4 we explicitly focus on this accidental satisfaction of the boundary condition in more detail.

(ii) $|\Lambda| < \kappa$: For each block-Hamiltonian; we get a zero-energy solution χ_- that decays exponentially in one block and another one χ_+ that diverges in the other block as the wire extends to infinity. Since no local perturbation can change the asymptotic behavior, this state remains invariant under local perturbations.

(iii) $\Lambda > \kappa$: The wavefunctions $\chi_{\pm}$ cannot be normalized as it gives exponentially diverging solutions, there cannot be zero modes so there are no zero-energy states in this configuration.

We thus relate the existence of Majorana modes to the asymptotic nature of the zero-energy block-Hamiltonian solutions in terms of the exponential factors in these solutions. We obtain the topological charge $\mathbb{Q}_{\mathrm{D}}^{(\mathrm{p})}$ as

$$\mathbb{Q}_{\mathrm{D}}^{(\mathrm{p})} = \mathrm{sgn}\left(|\Lambda| - \frac{1}{\xi_{\mathrm{p}}}\right), \tag{3.3}$$

where we express the topological charge in terms of the coherence length $\xi_{\mathrm{p}} \equiv \kappa^{-1}$, which depend on microscopic constants of the Hamiltonian in Eq. 3.1. The subscript D in Eq. 3.3 stands for the topological class and $\mathbb{Q}_{\mathrm{D}}^{(\mathrm{p})} \in \mathbb{Z}_2$ in 1D which gives -1 when a Majorana mode is present and $+1$ when it is topologically trivial. As we mention above our

results are obtained by comparing the exponent of the normal state equation solutions. $\psi \sim e^{\Lambda x}$ in Eq. 3.2 with the exponent that arises from the imaginary gauge transformation (*i.e.* $e^{\pm x/\xi_{\rm p}}$). Our solution is topologically robust unless infinite, no local perturbation can change the asymptotic nature of Majorana mode wavefunctions. Therefore, the topological charge in Eq. 3.3 is indifferent to local perturbations.

We now continue to analyze the topological phase transitions in a disordered wire in order to draw a boundary where a topological phase transition occurs [41]. For longer wires the Lyapunov exponent is a self averaging quantity, *i.e.* $\Lambda(L) \to \bar{\Lambda}$, as $L \to \infty$, where $\bar{\Lambda}$ is the average Lyapunov exponent [3, 85] that is calculated by solving the differential equation in Eq. 3.2 in presence of disorder. For a wire with Gaussian disorder $\langle V(x)V(y)\rangle = \gamma\delta(x-y)$ at energy ϵ, it can be obtained in closed form [41, 85]:

$$\begin{aligned} \bar{\Lambda}(\epsilon) &= \frac{m^{1/2}}{\hbar\lambda} F\big(\lambda^2\epsilon\big), \quad \lambda = \left(\frac{\hbar}{\gamma m^{1/2}}\right)^{1/3}, \\ F(x) &= -\frac{1}{2}\frac{d\ln\left(\mathrm{Ai}(-2^{1/3}x)^2 + \mathrm{Bi}(-2^{1/3}x)^2\right)}{dx}. \end{aligned} \tag{3.4a}$$

The topological transition condition in Eq. 3.3 becomes $|\bar{\Lambda}| = \xi_{\rm p}$ valid for the entire range of μ, u, γ as long as the system remains within the superconducting band gap. We now move on to compare our results to a tight-binding-calculation for a single disorder configuration.

In Fig. 3.1, we present short- and long-wire topological charge calculations we make for a single disorder realization where we calculate the topological charge as a function of chemical potential (μ) and disorder strength (γ). The blue and grey areas are the results of a tight-binding calculation made using $\mathbb{Q}_{\rm D}^{(\rm p)} = \mathrm{sgn}(\det(r))$ formulation where r is the reflection matrix of the scattering matrix [41]. We calculate the solid red lines using our topological charge calculation in Eq. 3.3 where we obtain Λ from the normal state conductance for short wires and red dashed lines are the phase space boundaries we plot using Eqs. 3.4 and Eq. 3.3 valid for long wires. Our results and tight-binding calculations complement each other well. We explain the difference between topological phases of short- and long-wires as follows: The topological phase depends on the nature of the Lyapunov exponent because it fluctuates more strongly in short wires, making a short p-wave wire harder to remain in its topologically nontrivial phase. For long wires, the two type of red lines converge since we use Eq. 3.4 when calculating Eq. 3.3 assuming that

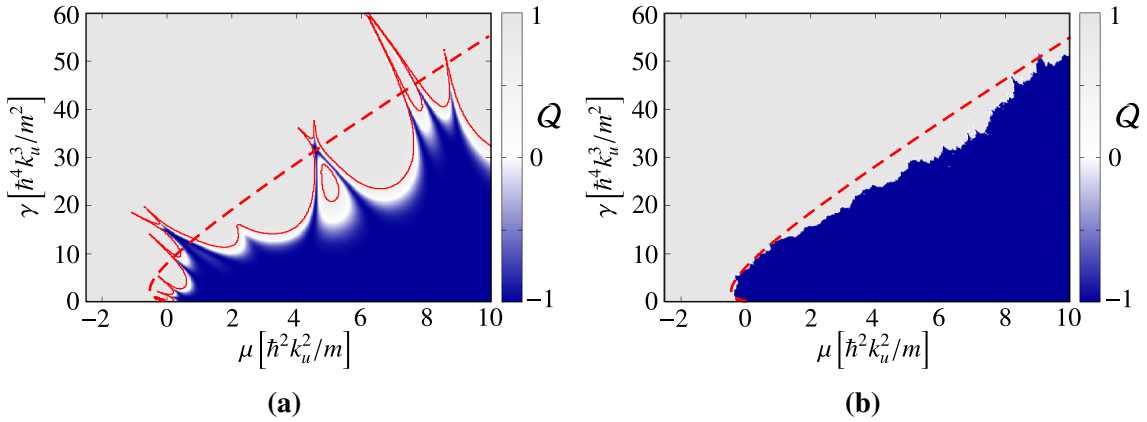

Figure 3.1: Topological charge of disordered p-wave wires as a function of chemical potential μ and disorder strength γ for a single disorder configuration for a short wire $L = 100a$ (a) and long wire $L = 10000a$ (b). White and blue areas are tight-binding simulation results with $k_u = 10a^{-1}$ and a chemical potential of the leads $\mu_{\text{lead}} = 0.5\hbar^2/2ma^2$. Red solid lines are calculated using Eq. 3.3 and red dashed lines are phase boundaries calculated using normal state conductance with Eq. 3.4. The short wire has a smaller topologically nontrivial area compared to a long wire since Lyapunov exponents in short wires fluctuates more rapidly. Disorder damages the topological nontrivial phase but does not completely destroy it. In the short wire, there exists topologically nontrivial configurations beyond the red dashed phase boundary because of disorder.

we have a very long wire. Our calculations show that disorder is not *always* detrimental to topological order as it is expected [37, 38], but it drives p-wave wires out of their topological phases. Also, topological phase space for short-wires exhibit spikes as seen in Fig. 3.1 that shows a topologically nontrivial phase beyond the phase boundary where it actually should be topologically trivial. We conclude that disorder can induce topological phase in a short disordered p-wave wire where it should be nontopological. We revisit this interesting feature in more detail Chapter 5.

We now proceed to apply our calculation to s-wave wires and derive a topological index similar to Eq. 3.3.

3.2. Topological Index Calculation for Disordered s-wave Wires

In this section, we derive a topological charge formula for 1D s-wave topological superconducting wires and compare it with tight-binding calculations of the topological phase space. We start by projecting the Hamiltonian in Eq. 2.7 [17, 19] to a single dimension along x-direction as

$$H = h(p, x)\tau_z + \alpha p \sigma_y \tau_z + B\sigma_x + \Delta\tau_x \tag{3.5}$$

where $h(p,x) = p^2/2m + V(x) - \mu$ is the single-particle operator, α is the spin-orbit coupling strength, B is the Zeeman field strength, and Δ is the superconducting pair potential. Pauli matrices $\sigma_i \mid (i = x, y, z)$ are in spin-space and $\tau_i \mid (i = x, y, z)$ denote electron-hole space. We employ the same method we use for the p-wave wire so we first off-diagonalize the Hamiltonian [35]. Without the chiral symmetry breaking p_y-contribution, Hamiltonian in Eq. 3.5 possesses chiral symmetry, so it can also be off-diagonalized. However, off-diagonalization is more intricate for s-wave wires than it is for p-wave wires. In order to achieve this, we note that Hamiltonian anticommutes with operator $\sigma_y\tau_y$; so the basis that diagonalizes $\sigma_y\tau_y$ into degenerate blocks, will also off-diagonalize the Hamiltonian into degenerate blocks. We find that operator $\mathcal{U} = (1 + i\sigma_x)(1 + i\tau_x)\left((1 + \sigma_z)(1 - \sigma_z)\right)/4$ anticommutes with $\sigma_y\tau_z$ so a unitary transformation $\mathcal{U}^{-1}H\mathcal{U}$ casts the s-wave Hamiltonian into an off-diagonal form as

$$H = h(p,x)\sigma_z\tau_y - \alpha p\tau_y + B\sigma_x\tau_x + \Delta\tau_x$$

with zero energy of solutions of the form $\chi_+ = \begin{bmatrix} \phi_+ \\ 0 \end{bmatrix}$ and $\chi_- = \begin{bmatrix} 0 \\ \phi_- \end{bmatrix}$ for each block-Hamiltonian. Different from p-wave case, $\phi_\pm$ are now solutions of a non-Hermitian eigenvalue problem with zero eigenvalue which reads as

$$\left(\mp ih(p,x)\sigma_z \pm i\alpha p + B\sigma_x + \Delta\right)\chi_\pm = 0.$$

We now find the solutions of the block-solutions as follows: A rotation by $+\pi/2$ in spin space around x-axis and premultiplying with $\pm\sigma_x$ get rid of factors in front of the kinetic term so we rewrite the block-solutions of the off-diagonalized Hamiltonian as

$$\left(h(p,x)\sigma_z - i\alpha p\sigma_x \mp B \mp \Delta\sigma_x\right)\chi_\pm = 0. \tag{3.6}$$

Next, we apply an imaginary gauge transformation $\chi_\pm \rightarrow e^{\mp\kappa_\alpha x}\phi_\pm$ that renormalizes momenta as $p \rightarrow p \pm i\hbar\kappa_\alpha$ by absorbing the linear momentum term; here, $\kappa_\alpha \propto \alpha$ and we determine it very shortly in a way that allows us to construct zero-energy block-solutions. We split each block Hamiltonian into two parts by collecting terms of order α and the remaining terms in order to treat α-terms perturbatively with $H = H_0 + H_1$, where

$$\begin{aligned} H_0 &= h(p,x)\sigma_z \mp B \mp \Delta\sigma_x \\ H_1 &= -i\alpha p\sigma_x + i\frac{\hbar\kappa_\alpha p}{m} + \hbar\kappa_\alpha\alpha\sigma_x - \frac{\hbar^2\kappa_\alpha^2}{2m}\sigma_z. \end{aligned}$$

We absorb the last two terms of H_1 into H_0 by redefining μ and Δ. Here; local solutions of H_0 are of the form $\eta_\pm(\epsilon)\psi(x;\epsilon)$ where the scalar wavefunctions $\psi(x;\epsilon)$ are eigenfunctions of $h(p,x)\psi(x;\pm\epsilon) = \pm\epsilon\psi(x;\pm\epsilon)$ with eigenvalues $\epsilon = \sqrt{B^2-\Delta^2}$. Solving the eigenequation $(\epsilon\sigma_z \mp \Delta\sigma_x)\eta_\pm(\epsilon) = \pm\sqrt{\epsilon^2+\Delta^2}\eta_\pm(\epsilon)$ gives us the spinors as $\eta_\pm(\epsilon)$. So we construct zero-energy solutions $\psi(x;\pm\epsilon)$ as a linear combination of asymptotically decaying and diverging functions as $Af(x;\pm\epsilon) + Bg(x;\pm\epsilon)$. At this point, we choose the gauge transformation parameter κ_α to be $\kappa_\alpha \equiv \xi_{\rm s}^{-1} = m\alpha\Delta/\hbar\epsilon$ so that H_1 anticommutes with $(\epsilon\sigma_z \mp \Delta\sigma_x)$. This choice of κ_α makes H_1 off-diagonal in the $\eta_\pm(x;\epsilon)$ basis and therefore contribution of H_1 vanishes to first order in perturbation theory. Therefore, we write the zero-energy wavefunctions up to the second order of the spin-orbit coupling term as follows:

$$\begin{aligned}\chi_\pm = \eta_\pm(\epsilon)e^{\pm\kappa_\alpha x}\left(Af(x;+\epsilon) + Bg(x;-\epsilon)\right)\\ + \eta_\pm(-\epsilon)e^{\mp\kappa_\alpha x}\left(Cf(x;-\epsilon) + Dg(x;+\epsilon)\right)\end{aligned} \tag{3.7}$$

where $\kappa_\alpha = m\alpha\Delta/\hbar\epsilon$ and $\epsilon = \sqrt{B^2-\Delta^2}$. Also, $f(x;\pm\epsilon)$ and $g(x;\pm\epsilon)$ are linearly independent decaying and increasing solutions of $h(p,x)\psi = \epsilon\psi$. A zero-energy mode is present if this wavefunction decays and becomes normalizable along the wire so we continue to its construction by imposing a boundary condition at the origin. A semi-infinite geometry is again assumed here: $x<0$ is an ordinary insulator and $x>0$ is an s-wave topological superconductor wire. The zero-energy solutions should then satisfy the boundary condition $\phi_\pm\Big|_{x=0} = 0$. Next, we analyze the asymptotic behavior of the zero-energy wavefunctions in Eq. 5.8 using the Lyapunov exponents of the $f(x;\pm\epsilon)$ and $g(x;\pm\epsilon)$ which we define as $\Lambda(\mu\pm\epsilon)$. The wavefunctions $\phi_\pm$ should not diverge as the wire extends to infinity, their convergence supplies us with physical solutions since they become normalizable and do not extend to the other end of the wire. So we check for the overall asymptotic behavior of $\phi_\pm$ –where it depends on the interplay between κ_α and the Lyapunov exponents of the local solutions $\Lambda(\mu\pm\epsilon)$. We list the three possibilities as follows:

(i) $B>\Delta$ and $|\Lambda(\mu\pm\epsilon)| < |\kappa_\alpha|$ or $|\Lambda(\mu\pm\epsilon)| > |\kappa_\alpha|$: Each block-Hamiltonian have two diverging and two converging solutions and the boundary condition can only be satisfied accidentally if both decaying solutions are inherently zero at $x=0$, *i.e.* $f(0;\pm\epsilon) = 0$ or $g(0;\pm\epsilon) = 0$. These states arise from the particle-hole symmetric nature of the Hamiltonian and any perturbation higher than $\mathcal{O}(\alpha^2)$ drives these

states away from zero-energy in pairs. Such transitions away from the zero-energy are double-crossings in the band gap and thus are not topologically protected. So this configuration in the parameter space are topologically trivial zero-energy states therefore are not Majorana modes.

(ii) $B < \Delta$: There again exist two decaying and two diverging solutions for each block but accidental satisfaction of the boundary condition cannot happen for this parameter configuration: For $B < \Delta$, ϵ becomes imaginary implying that Hermitian matrix $h(p, x)$ has solutions f with imaginary eigenvalues; since this cannot be true, zero-energy modes are again *not* present in this parameter space.

(iii) $B > \Delta$ and $|\Lambda(\mu \pm \epsilon)| < |\kappa_\alpha| < |\Lambda(\mu \mp \epsilon)|$: There exists three decaying and one diverging solution in one block-Hamiltonian along with three diverging and one decaying solution for the other block complimenting the particle-hole symmetry. The boundary condition is satisfied in order to write a Majorana wavefunction that has three zero-energy solutions from the corresponding block. Such solutions corresponds to single crossings in the insulating band gap and thus are topologically protected.

Thus we have to be in the parameter range (iii) to be in the topological region and have a Majorana wavefunction. We define a topological quantum charge utilizing the interplay between κ_α and the Lyapunov exponents of the local wavefunction solutions $\Lambda(\mu \pm \epsilon)$ where the existence of the Majorana mode depends on the convergence of the wavefunction as the wire extends into infinity. Different from the p-wave case, there exists two Lyapunov exponents to take into account therefore we use two signum functions for the topological condition as follows

$$\mathbb{Q}_{\mathrm{D}}^{(\mathrm{s})} = \mathrm{sgn}\left(|\Lambda(\mu+\epsilon)| - \frac{1}{\xi_{\mathrm{s}}}\right) \mathrm{sgn}\left(|\Lambda(\mu-\epsilon)| - \frac{1}{\xi_{\mathrm{s}}}\right) \tag{3.8}$$

where we use s-wave superconducting coherence length $\xi_{\mathrm{s}} = \hbar\sqrt{B^2 - \Delta^2}/m\alpha\Delta$ instead of $\kappa_\alpha \equiv \xi_{\mathrm{s}}^{-1}$. Our result in Eq. 3.8 gives out -1 when there exists a Majorana mode and $+1$ when the wire is its topologically trivial phase: Obeying the topological classification in Tab. 2.2 where $\mathbb{Q}_{\mathrm{D}}^{(\mathrm{s})} \in \mathbb{Z}_2$. Our solution is topologically robust just as in the p-wave case since it does not include zero-energy solutions coming from accidental satisfaction of the boundary condition.

The application of large magnetic fields to s-wave wires leads to spin polarization [86] and when these magnetic fields are very large compared to the spin orbit field ($B \gg m\alpha^2$) s-wave wires can be considered to constitute of two p-wave wires that have opposite spins in each wire [16]. The large magnetic field separates the s-wave spin-up and -down bands away from in such a manner that these two bands act as if they are independent of each other so that an s-wave wire can be loosely interpreted as a collection of two p-wave wires. Indeed, comparing our p-wave formula in Eq. 3.3 to our s-wave result in Eq. 3.8, we see that the s-wave wire system behaves as if it is comprised of two p-wave wires that are at different chemical energies $\mu \pm \sqrt{B^2 - \Delta^2}$. This is our central formula for the s-wave case. The first term in Eq. 3.8 reduces to Eq. 3.3 in the large B limit (*i.e.*, only the spin-down band is contributing), recovering the p-wave result, while the second term is due to the presence of the spin-up band and introduces new physics Noting that $\bar{\Lambda}$ is a monotonous function of energy, we get:

$$\mu_{\pm} = F^{-1}(m^{1/2}\lambda\alpha\Delta/\sqrt{B^2 - \Delta^2})/\lambda^2 \pm \sqrt{B^2 - \Delta^2} \tag{3.9}$$

In the weak disorder limit, $\lambda \to \infty$, we recover the clean wire result: $\mu_{\pm} = \pm\sqrt{B^2 - \Delta^2}$. We also find that the topological region is not destroyed by disorder but merely shifted to higher chemical potentials. In fact the chemical potential (or gate) range where the wire is topological, $\mu_+ - \mu_- = 2\sqrt{B^2 - \Delta^2}$, is *independent* of the disorder strength, while the total area of the topological region in the (B, μ) plane is conserved. We stress that this result is valid to all orders in disorder strength.

In Fig. 3.2, we show our results for short- and long-wire topological phase space for a single disorder realization. The blue and gray refer to $\text{sgn}(\det(r)) = -1$ (blue) and $+1$ (gray) that are the results of the tight-binding calculations made using $\mathbb{Q}_{\text{D}}^{(\text{s})} = \text{sgn}(\det(r))$ where r is the reflection matrix. The red lines are calculated using Eq. 3.8 and the blue dashed line shows the topological boundary for clean wires which reads as $\sqrt{B^2 - \Delta^2}$. Our results show significant agreement in defining the topological phases, compared to the tight-binding results Investigating the topologically nontrivial clean limit ($B^2 > \sqrt{\mu^2 + \Delta^2}$), we see that disorder drives the s-wave topological superconductor wire out of its topological phase. What is more interesting is that for both realizations in Fig. 3.2, disorder leads to topologically nontrivial material phases for they should not exist ($B^2 < \sqrt{\mu^2 - \Delta^2}$). This feature is a direct consequence of scattering within the wire that

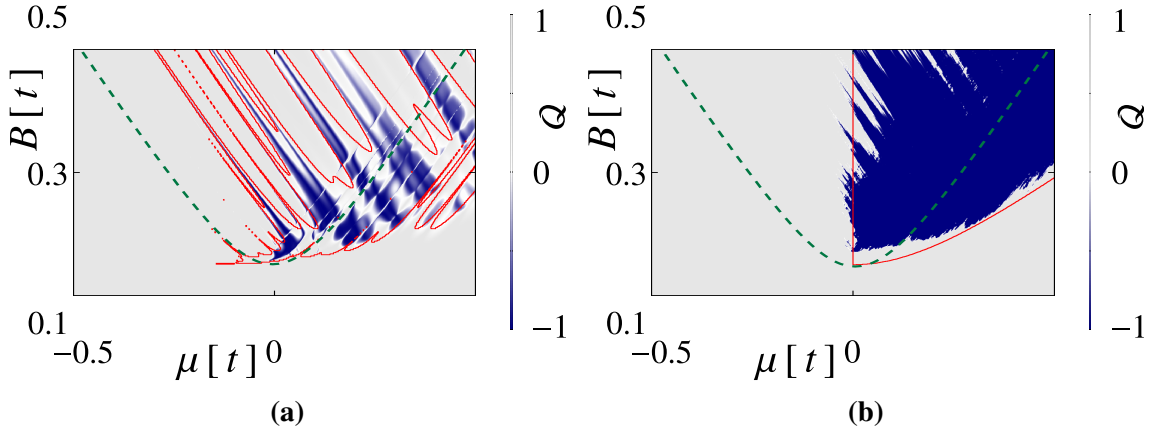

Figure 3.2: Topological phase space of a short ($L = 100a$, a) and long ($L = 4000a$, b) s-wave wire is plotted as a function chemical potential μ and applied magnetic field B. (a is the lattice constant.) Red lines are calculated using Eq. 3.8 and green dashed line is the phase boundary calculated at $B^2 = \mu^2 + \Delta^2$. The remaining tight-binding parameters are $k_{\mathrm{SO}} = 0.05a^{-1}$, $\Delta = 0.15t$ and $\gamma = 0.06t^2$ where $t = \hbar^2/2ma^2$. Short wire has less topologically nontrivial area compared to a long wire where both have topologically nontrivial phases beyond the phase transition line.

leads to the locking s-wave wires into their topologically nontrivial phase by localizing one Kramers partner beyond coherence length. Utilizing the effects of scattering in s-wave wires that locks them in or out of their topological phases can be an experimentally very usable feature –so we continue to investigate these effects in presence of regular scattering in the next chapter.

3.3. Conclusion

In this chapter, we analytically derive new topological quantum numbers $\mathbb{Q}_{\mathrm{D}}^{(\mathrm{p})}$ and $\mathbb{Q}_{\mathrm{D}}^{(\mathrm{s})}$ for both types of topological superconducting wires using asymptotic wavefunction analysis in terms of Lyapunov exponents Λ and superconducting coherence length ξ_{s}. Our topological index formula returns a $\mathbb{Z}_2$ in agreement with the topological classification of topological superconductors. We also calculate topological phase boundaries for the case of irregular scattering using the self-averaging nature of the Lyapunov exponent in long wires. We show that longer wires are more robust against disorder next to shorter wires because of Lyapunov exponent's strong fluctuations in shorter wires. We compare our analytical results (Eqs.3.3, 3.4, 3.8 and 3.9) with a tight-binding topological superconductor model calculated using $\mathbb{Q}_{\mathrm{D}} = \mathrm{sgn}(\mathrm{Det}(r))$ where numerical and analytical results show a strong agreement. From our plots, we infer that scattering leads to the destruction of nontrivial topological phase near the depleted side, but it also locks a topologically trivial realization into a nontrivial one for longer wires. The ability to tune topological

superconductors into topological phases is very useful for experiments so we continue the investigate the effects of regular scattering in topological superconductor wires for a more controllable topological phase tuning. Our results were published in Ref. [3].

Chapter 4

SINGLE CHANNEL META-TOPOLOGICAL INSULATOR WIRES

We now start to investigate topological phases of 1D topological superconductor wires in case of regular scattering as opposed to irregular scattering caused by disorder, by using an electrostatic piecewise continuous potential. As we show in the previous Chapter, irregular scattering caused by Gaussian disorder can drive a topological superconductor *in and out* of its topological phase [3]. We want to utilize this as a means to devise a more controllable approach to these phase transitions with electrostatic superlattices. Making use of the repetitive nature of the electrostatic superlattice, we show that topological order in superconductor wires can be controlled: Hence it is possible to tune into the desired phase, trivial or nontrivial. Similar approaches were proposed in literature [87–90] but those require at least some segment of the wire to be topologically nontrivial –our method differs by employing a weak electrostatic superlattice that does not require a change in topological order along the wire. These proposals [87–90] lead to phase transitions that transforms a topological superconductor into a successive collection of topologically trivial and nontrivial segments that are placed one after another. Such constructions works with creation of Majorana modes at each trivial and nontrivial interface which in turn hybridize at short lengths. In our method, the superconductor wires with a periodic electrostatic modulation remain locally in same region in the topological phase space as a whole, so we name these *meta-topological Insulators*.

We derive new formulae for the topological indices for both types of meta-topological insulator wires that depend on the repetitive construction of these electrostatic modulations. Our approach uses transfer-matrices and we show here that the repetitive nature of the electrostatic superlattice allows us to control topological order of the meta-topological wire. Following our wavefunction analysis in the previous chapter; we inspect the asymptotic nature of zero-energy solutions and derive topological indices that solely depend on dimensions of the superlattice. Our topological formulae also exclude zero-energy wave-

functions from accidental zero-energy modes that are not topologically protected. Once the details of the electrostatic superlattice are set, we derive new expressions for the topological indices using transfer matrices that only require the calculation of transfer matrix of a single superlattice unit-cell.

4.1. Electrostatic Superlattice

In this section, we show how a zero-energy wavefunction for p- and s-wave wires that are under piecewise-constant electrostatic potential can be constructed. For the calculation of the zero-energy wavefunction; we use the transfer-matrix method [85] where the repetitive nature of the superlattice plays a central role. After we construct the transfer matrix, we show how the superlattice allows us to construct a zero-energy wavefunction, which we use to show the existence of Majorana modes. We do this by imposing a boundary condition at the origin ($x = 0$) and constructing the zero-energy wavefunction using selected amplitudes that ensure the asymptotic decay as the wire extends. Using the Hamiltonian off-diagonalization method [3, 35] that we described in the previous Chapter, we show that we can count out zero-energy modes and distinguish that are not topologically protected which arise from the accidental satisfaction of the boundary condition. After we construct the Majorana wavefunction, we continue to derive new topological indices that uses transfer-matrix elements of the superlattice unit cell rather than the transfer-matrix of the whole superlattice.

First, we define the superlattice and choose a superlattice constant that is small compared to the length of the topological superconductor in order to achieve multiple reflections over its unit cells. The combination of backscattering amplitudes in each cell creates Majorana modes in configurations where no such modes can be attained [3].

We assume that the superlattice exhibits multiple potential barriers along x-direction but it is constant along the transverse direction in order to only affect longitudinal modes of the wavefunction. So we define a piecewise continuous superlattice function with period d as

$$V_{\text{SL}}(x) = \begin{cases} V_0, & \text{for } 0 \leq x \,(\text{mod}\, d) < \frac{d}{2} \\ -V_0, & \text{for } \frac{d}{2} \leq x \,(\text{mod}\, d) < d \end{cases}$$

with a zero average $\langle V_{\text{SL}}(x, y)\rangle = 0$ that does not change chemical potential of the topological superconductor wire that may lead to local topological transitions. Generalization

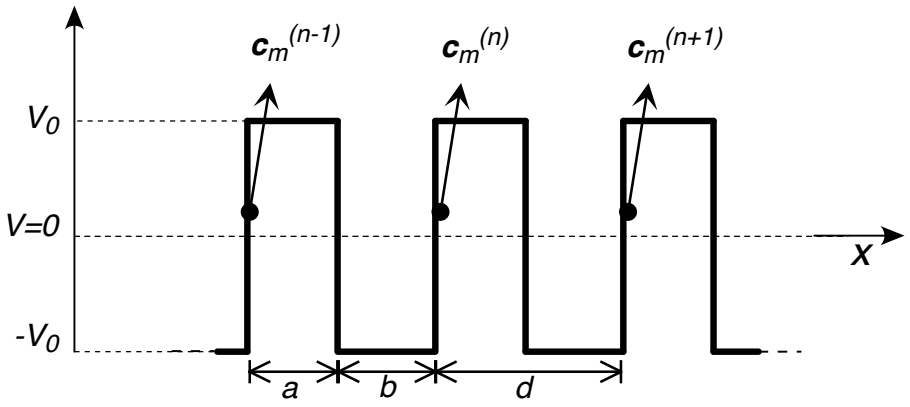

Figure 4.1: A sketch of the electrostatic superlattice along the x-direction of a meta-topological insulator. Here, $a + b = d$ is the period of the superlattice with $a = b = d/2$ and V_0 is the size of the modulation. $\mathbf{c}^{(n)}$ is the amplitude vector in the n^{th} cell.

to other lattices are straightforward in this construction, we only concern with values of V_{SL} that is not large enough to cause a topological transitions locally. Note that the topological order directly depends on chemical potential –we observe topological nontrivial phases when $\mu < |V_{\text{SL}}|$ in p-wave wires and $B^2 < (\mu + V_{\text{SL}})^2 + \Delta^2$ in s-wave wires [16] where the wire is thought to be in its trivial phase.

After defining the nature of the superlattice that we show Fig. 4.1, we continue to calculate its transfer-matrix so that we can construct zero-energy wavefunctions.

4.1.1. Transfer-matrix calculations

For a superlattice that comprises of N unit cells with period d, we compute the full transfer matrix renaming left and right segment of the unit cell as a and b for clearer understanding –here a is the length of left segment of the unit cell with V_0 and b is that of the right with potential value $-V_0$ (see Fig. 4.1). We do this substitution to be able to keep track of wavefunctions in both segments within each cell and we reinstitute d at the end of our unit cell transfer matrix calculations.

We start the calculation of the full transfer matrix by calculating individual transfer matrices of each cell, and later we combine them to get the full transfer matrix of the superlattice to make use of the recursive nature of it. To set the convention, we define the vector $\underline{\mathbf{c}}^{(n)}$ to be the amplitude vector in the n^{th} unit cell. The wavefunctions in the n^{th} unit cell are local solutions of the Hamiltonians in Eqs. 3.1 and 3.5. We define them as follows:

$$\psi^{(n)}_{1,\ldots,N_d/2}(x) = \underline{\chi}^{(n)}_{1,\ldots,N_d/2} exp\left(+\beta^{(n)}_{1,\ldots,N_d/2}x\right)$$
$$\psi^{(n)}_{(N_d/2)+1,\ldots,N_d}(x) = \underline{\chi}^{(n)}_{(N_d/2)+1,\ldots,N_d} exp\left(-\beta^{(n)}_{(N_d/2)+1,\ldots,N_d}x\right),$$

where $\underline{\chi}_m$ are eigenvectors with $1 \times N_d/2$ dimensions and wavenumbers $\beta^{(n)}_m \in \mathbb{C}$ in order to include both nondivergent and exponential features of the solutions as we explain in the previous chapter –here; we calculate wavenumbers $\beta^{(n)}_m$ at the beginning of the n^{th} unit-cell. Also we define the index $m = 1, \ldots, N_d \mid N_d = 4$ for a p-wave meta-topological insulator wire and $N_d = 8$ for an s-wave meta-topological insulator wire. After setting our convention, we proceed to write the most general wavefunction in the n_{th} cell as

$$\Psi^{(n)}(x) = \sum_{m=1}^{N_d} c^{(n)}_m \underline{\psi}^{(n)}_m(x), \tag{4.1}$$

in which the individual amplitudes $c^{(n)}_m$ are used to construct an amplitude vector as $\underline{\mathbf{c}}^{(n)}$. Next we set boundary conditions that reflects the continuity of the wavefunction and its velocity across the interface that separates the $n-1^{\text{th}}$ cell and n^{th} cell along with another boundary condition that is in the middle of the superlattice [70]. We express the boundary conditions down as follows:

- Between $n-1^{\text{th}}$ and n^{th} cells:

$$\Psi^{(n-1)}(x)\Big|_{x\to(n(a+b))_-} = \Psi^{(n)}(x)\Big|_{x\to(n(a+b))_+} \tag{4.2}$$
$$\partial_x\Psi^{(n-1)}(x)\Big|_{x\to(n(a+b))_-} = \partial_x\Psi^{(n)}(x)\Big|_{x\to(n(a+b))_+} \tag{4.3}$$

- In the middle of the n^{th} unit cell where the electrostatic potential changes its sign

$$\Psi^{(n)}(x)\Big|_{x\to(n(a+b)+a)_-} = \Psi^{(n)}(x)\Big|_{x\to(n(a+b)+a)_+} \tag{4.4}$$
$$\partial_x\Psi^{(n)}(x)\Big|_{x\to(n(a+b)+a)_-} = \partial_x\Psi^{(n)}(x)\Big|_{x\to(n(a+b)+a)_+} \tag{4.5}$$

where the subscripts $-$ and $+$ of the x-coordinate signify the direction of approach to the interface from the left and right directions; respectively. We continue to calculate unit cell transfer matrix starting with constructing matrices between $n-1^{\text{th}}$ and n^{th} cells using the boundary conditions in Eq. 4.2 as $\underline{\underline{\mathcal{M}}}_1(x)\Big|_{x\to(n(a+b))_-} \cdot \underline{\mathbf{c}}^{(n-1)}\Big|_{x\to(n(a+b))_-} = \underline{\underline{\mathcal{M}}}_2(x)\Big|_{x\to(n(a+b))_+} \cdot \underline{\mathbf{c}}^{(n)}\Big|_{x\to(n(a+b))_+}$ where

$$\underline{\underline{\mathcal{M}}}_1(x)\Big|_{x\to(n(a+b))_-} =$$

$$\begin{bmatrix} \chi_{1,1}^{(n-1)} exp(+\beta_1^{(n-1)}x) & \cdots & \chi_{N_d,1}^{(n-1)} exp(-\beta_{N_d}^{(n-1)}x) \\ \vdots & & \vdots \\ \chi_{1,(N_d/2)}^{(n-1)} exp(+\beta_1^{(n-1)}x) & \cdots & \chi_{N_d,(N_d/2)}^{(n-1)} exp(-\beta_{N_d}^{(n-1)}x) \\ \beta_1^{(n-1)}\chi_{1,1}^{(n-1)} exp(+\beta_1^{(n-1)}x) & \cdots & -\beta_{N_d}^{(n-1)}\chi_{N_d,1}^{(n-1)} exp(-\beta_{N_d}^{(n-1)}x) \\ \vdots & & \vdots \\ \beta_1^{(n-1)}\chi_{1,(N_d/2)}^{(n-1)} exp(+\beta_1^{(n-1)}x) & \cdots & -\beta_{N_d}^{(n-1)}\chi_{N_d,(N_d/2)}^{(n-1)} exp(-\beta_{N_d}^{(n-1)}x) \end{bmatrix}$$

$$\underline{\underline{\mathcal{M}}}_2(x)\Big|_{x\to(n(a+b))_+} =$$

$$\begin{bmatrix} \chi_{1,1}^{'(n)} exp(+\beta_1^{'(n)}x) & \cdots & \chi_{N_d,1}^{'(n)} exp(-\beta_{N_d}^{'(n)}x) \\ \vdots & & \vdots \\ \chi_{1,(N_d/2)}^{'(n)} exp(+\beta_1^{'(n)}x) & \cdots & \chi_{N_d,(N_d/2)}^{'(n)} exp(-\beta_{N_d}^{'(n)}x) \\ \beta_1^{'(n)}\chi_{1,1}^{'(n)} exp(+\beta_1^{'(n)}x) & \cdots & -\beta_{N_d}^{'(n)}\chi_{N_d,1}^{'(n)} exp(-\beta_{N_d}^{'(n)}x) \\ \vdots & & \vdots \\ \beta_1^{'(n)}\chi_{1,(N_d/2)}^{'(n)} exp(+\beta_1^{'(n)}x) & \cdots & -\beta_{N_d}^{'(n)}\chi_{N_d,(N_d/2)}^{'(n)} exp(-\beta_{N_d}^{'(n)}x) \end{bmatrix}$$

where $\underline{\chi}_{m,p} \mid m = 1,\ldots,N_d \; ; \; p = 1,\ldots,N_d/2$ are eigenvector elements of the zero-energy solutions to the Hamiltonian under $-V_0$ and $\underline{\chi}_{m,p}^{'}$ are Hamiltonian eigenvectors under $+V_0$; β are wavenumbers that we calculate under $-V_0$ and $\beta^{'}$ are wavenumbers under $+V_0$. We calculate the matrices in the middle of the n^{th} unit cell where the electrostatic potential changes its sign at $x = n(a+b)+a$ as $\underline{\underline{\mathcal{M}}}_3(x)\Big|_{x\to(n(a+b)+a)_-}\underline{\mathbf{c}}^{(n)}\Big|_{x\to(n(a+b)+a)_-} = \underline{\underline{\mathcal{M}}}_4(x)\Big|_{x\to(n(a+b)+a)_+}\underline{\mathbf{c}}^{(n)}\Big|_{x\to(n(a+b)+a)_+}$ where

$$\underline{\underline{\mathcal{M}}}_3(x)\Big|_{x\to(n(a+b)+a)_-} =$$

$$\begin{bmatrix} \chi_{1,1}^{'(n)} exp(+\beta_1^{'(n)}x) & \cdots & \chi_{N_d,1}^{'(n)} exp(-\beta_{N_d}^{'(n)}x) \\ \vdots & & \vdots \\ \chi_{1,(N_d/2)}^{'(n)} exp(+\beta_1^{'(n)}x) & \cdots & \chi_{N_d,(N_d/2)}^{'(n)} exp(-\beta_{N_d}^{'(n)}x) \\ \beta_1^{'(n)}\chi_{1,1}^{'(n)} exp(+\beta_1^{'(n)}x) & \cdots & -\beta_{N_d}^{'(n)}\chi_{N_d,1}^{'(n)} exp(-\beta_{N_d}^{'(n)}x) \\ \vdots & & \vdots \\ \beta_1^{'(n)}\chi_{1,(N_d/2)}^{'(n)} exp(+\beta_1^{'(n)}x) & \cdots & -\beta_{N_d}^{'(n)}\chi_{N_d,(N_d/2)}^{'(n)} exp(-\beta_{N_d}^{'(n)}x) \end{bmatrix}$$

$$\underline{\underline{\mathcal{M}}}_4(x)\Big|_{x\to(n(a+b)+a)_+} =$$
$$\begin{bmatrix} \chi^{(n)}_{1,1}exp(+\beta^{(n)}_1 x) & \cdots & \chi^{(n)}_{N_d,1}exp(-\beta^{(n)}_{N_d} x) \\ \vdots & & \vdots \\ \chi^{(n)}_{1,(N_d/2)}exp(+\beta^{(n)}_1 x) & \cdots & \chi^{(n)}_{N_d,(N_d/2)}exp(-\beta^{(n)}_{N_d} x) \\ \beta^{(n)}_1\chi^{(n)}_{1,1}exp(+\beta^{(n)}_1 x) & \cdots & -\beta^{(n)}_{N_d}\chi^{(n)}_{N_d,1}exp(-\beta^{(n)}_{N_d} x) \\ \vdots & & \vdots \\ \beta^{(n)}_1\chi^{(n)}_{1,(N_d/2)}exp(+\beta^{(n)}_1 x) & \cdots & -\beta^{(n)}_{N_d}\chi^{(n)}_{N_d,(N_d/2)}exp(-\beta^{(n)}_{N_d} x) \end{bmatrix}.$$

Next, we write the transfer equation of the n^{th} cell as $\underline{\mathbf{c}}^{(n)} = \underline{\underline{\mathcal{R}}}^{(n)}((n-1)d)\cdot\underline{\mathbf{c}}^{(n-1)}$ where $\underline{\underline{\mathcal{R}}}^{(n)}((n-1)d) = \underline{\underline{\mathcal{T}}}(b)\cdot\underline{\underline{\mathcal{M}}}_4^{-1}(x=(n(a+b)+a))\cdot\underline{\underline{\mathcal{M}}}_3(x=(n(a+b)+a))\cdot\underline{\underline{\mathcal{T}}}(a)\cdot\underline{\underline{\mathcal{M}}}_2^{-1}(x=(n(a+b)))\cdot\underline{\underline{\mathcal{M}}}_1(x=(n(a+b)))$ where $\underline{\underline{\mathcal{T}}}(d^*)$ is the diagonal translation matrix that corresponds to a $x=d^*$ translation along $+x$-direction where $\underline{\underline{\mathcal{T}}}(d^*) = \text{Diag}\left[\cdots \quad exp\left(+\beta^{(n)}_{N_d/2}d^*\right) \quad exp\left(-\beta^{(n)}_{N_d/2+1}d^*\right) \quad \cdots\right]$. In the transfer matrix, $\underline{\underline{\mathcal{T}}}(a)$ translates amplitude vectors $\underline{\mathbf{c}}^{(n)}\Big|_{x\to(n(a+b))}$ to $\underline{\mathbf{c}}^{(n)}\Big|_{x\to(n(a+b)+a)}$ and $\underline{\underline{\mathcal{T}}}(b)$ translates amplitude vectors $\underline{\mathbf{c}}^{(n)}\Big|_{x\to(n(a+b)+a)}$ to the end of the unit cell $\underline{\mathbf{c}}^{(n)}\Big|_{x\to(n(a+b)+a+b)}$.

We now set $a=b=d/2$ and call $\underline{\underline{\mathcal{R}}}^{(n)}((n-1)d)$ the *recursion matrix*, which is the transfer matrix of the n^{th} unit cell that starts at $x=(n-1)d$. Assuming there are N unit cells; we calculate the complete transfer matrix that connects the amplitude vector at the beginning of the superlattice $\underline{\mathbf{c}}^{(0)}$ to the amplitude vector at the end of the superlattice $\underline{\mathbf{c}}^{(N)}$ as

$$\underline{\mathbf{c}}^{(N)} \propto \prod_{s=1}^{N}\underline{\underline{\mathcal{R}}}^{(s)}(x=(s-1)d)\cdot\underline{\mathbf{c}}^{(0)}. \tag{4.6}$$

Making use of the symmetry of the superlattice; we calculate the transfer matrix of n^{th} cell is related to that of $n-1^{\text{th}}$ as $\underline{\underline{\mathcal{R}}}^{(n)} = \underline{\underline{\mathcal{T}}}(-d)\cdot\underline{\underline{\mathcal{R}}}^{(n-1)}\cdot\underline{\underline{\mathcal{T}}}(d)$. Since we can write unit cell transfer matrices of different cells in terms of each other; we rewrite Eq. 4.6 in terms of the unit cell transfer matrix at the origin $\left(\underline{\underline{\mathcal{R}}}^{(1)}(x=0)\right)$ as

$$\underline{\mathbf{c}}^{(N)} = \underline{\underline{\mathcal{T}}}(-Nd)\cdot\left(\underline{\underline{\mathcal{R}}}^{(1)}(x=0)\right)^N\cdot\underline{\mathbf{c}}^{(0)} \tag{4.7}$$

After dropping the unit cell superscript (1); we show that N^{th} cell amplitude vector is

proportional to the amplitude vector at the beginning of the superlattice at $x = 0$ as

$$\underline{\mathbf{c}}^{(N)} \propto \left(\underline{\underline{\mathcal{R}}}\right)^{N} \cdot \underline{\mathbf{c}}^{(0)} \tag{4.8}$$

where $\underline{\underline{\mathcal{R}}} = \underline{\underline{\mathcal{R}}}^{(1)}(x = 0)$ is the recursion-matrix and it is the transfer matrix of the 1^{st} unit cell that starts at the origin $x = 0$. After calculating the superlattice transfer matrix using the recursion matrix $\underline{\underline{\mathcal{R}}}$, we continue to construct the zero-energy wavefunction.

4.1.2. Zero-energy wavefunction construction

In this section, we construct zero-energy modes that ensure the asymptotic decay because of the repetitive nature of the superlattice. This method differs from the one previously calculated in Section 3 because we do not explicitly solve the Hamiltonians in Eqs. 3.1 and 3.5 to construct zero-energy modes as the meta-topological wire extends; rather, we leave the asymptotic decay to the recursive nature of the superlattice. Our intention is to show that there exists Majorana modes if the exponential decay of the zero-energy solution is guaranteed as $x \to \infty$. Here, we use Hamiltonians Eqs. 3.1 and 3.5 to show the existence of the zero-energy modes. Also; we extend our argument to the off-diagonalized version of these Hamiltonians as shown in Eqs. 3.2 and 3.6 in the next section.

We first write the most general wavefunction in a unit cell that uses the eigenvectors of Eqs. 3.1 and 3.5 $\left(\text{defined by } \underline{\underline{H}}\underline{\psi}_j = \epsilon\underline{\psi}_j \mid (j = 1, \ldots, N_d)\right)$ with amplitude vectors $\underline{\mathbf{c}}$ as

$$\Psi(x) = \begin{bmatrix} \underline{\psi}_1 & \ldots & \underline{\psi}_{N_d} \end{bmatrix} \cdot \underline{\mathbf{c}}. \tag{4.9}$$

This construction does not need to at zero-energy, it is the most general local solution of the system –Eq. 4.9 is a wavefunction with a set of amplitude vectors $\underline{\mathbf{c}} = \begin{bmatrix} c_1 & \cdots & c_{N_d} \end{bmatrix}^T$ at the start of a unit cell. The j index has an upper bound N_d that is twice the dimension of the Hamiltonians $\underline{\underline{H}}$ *–i.e.* $N_d = 4$ for p-wave topological superconductor and $N_d = 8$ s-wave topological superconductor. In order to have a complete solution; note that the amplitude vector $\mathbf{c}$ has dimensions $\dim(\mathbf{c}) = N_d \times 1$ that multiply individual N_d Hamiltonian eigenvectors for the most general wavefunction. So if we want to calculate the most general wavefunction we need to determine N_d-many c_j amplitudes by imposing two boundary conditions to write the most general wavefunction.

Next we write down the zero-energy wavefunction at the start of the N^{th} unit cell as

$$\begin{aligned}\Psi_{\epsilon=0}(x=Nd) &= \left(\begin{bmatrix}\underline{\psi}_1 & \dots & \underline{\psi}_{N_d}\end{bmatrix}\Big|_{x=Nd}\right)\cdot\underline{\mathbf{c}}^{(N)}\\ \Psi^{(N)}_{\epsilon=0} &= \left(\begin{bmatrix}\underline{\psi}_1 & \dots & \underline{\psi}_{N_d}\end{bmatrix}\Big|_{x=Nd}\right)\cdot\underline{\underline{\mathcal{T}}}(-Nd)\cdot\left(\underline{\underline{\mathcal{R}}}\right)^N\cdot\underline{\mathbf{c}}^{(0)}\end{aligned} \tag{4.10}$$

where, we have used the superlattice transfer matrix equation in Eq. 4.7 to carry the N^{th} unit cell amplitudes to the start of the superlattice and the $\underline{\underline{\mathcal{R}}}$ is the recursion matrix of the first cell with which the superlattice starts. We then make a similarity transformation as $\underline{\underline{\mathcal{R}}} = \underline{\underline{\mathcal{P}}}\cdot\underline{\underline{\tau}}\cdot\underline{\underline{\mathcal{P}}}^{-1}$ with similarity transformation matrices $\underline{\underline{\mathcal{P}}} = \begin{bmatrix}\underline{\zeta}_1\cdots\underline{\zeta}_{N_d}\end{bmatrix}$ that uses the normalized eigenvectors of the recursion matrix $\underline{\underline{\mathcal{R}}}\underline{\zeta}_j = \tau_j\underline{\zeta}_j \mid j = 1\cdots N_d$. The diagonal matrix in the similarity transformation has elements of the recursion matrix eigenvalues as $\underline{\underline{\tau}} = \text{Diag}\begin{bmatrix}\tau_1\cdots\tau_{N_d}\end{bmatrix}$. So we rewrite the zero-energy wavefunction at the N^{th} unit cell as

$$\begin{aligned}\Psi^{(N)}_{\epsilon=0} &= \left(\begin{bmatrix}\underline{\psi}_1 & \dots & \underline{\psi}_{N_d}\end{bmatrix}\Big|_{x=Nd}\right)\cdot\underline{\underline{\mathcal{T}}}(-Nd)\cdot\left(\underline{\underline{\mathcal{P}}}\cdot\underline{\underline{\tau}}\cdot\underline{\underline{\mathcal{P}}}^{-1}\right)^N\cdot\underline{\mathbf{c}}^{(0)}\\ &= \left(\begin{bmatrix}\underline{\psi}_1 & \dots & \underline{\psi}_{N_d}\end{bmatrix}\Big|_{x=Nd}\right)\cdot\underline{\underline{\mathcal{T}}}(-Nd)\cdot\underline{\underline{\mathcal{P}}}\cdot\underline{\underline{\tau}}^N\cdot\underline{\underline{\mathcal{P}}}^{-1}\cdot\underline{\mathbf{c}}^{(0)},\end{aligned} \tag{4.11}$$

where in the second equation, we calculate the product of $\left(\underline{\underline{\mathcal{P}}}\cdot\underline{\underline{\tau}}\cdot\underline{\underline{\mathcal{P}}}^{-1}\right)^N$ explicitly. Since translation matrix $\underline{\underline{\mathcal{T}}}$ and unitary transformation matrix $\underline{\underline{\mathcal{P}}}$ are normalized vectors, the asymptotic nature of the zero-energy wavefunction only depends on the amplitude of the eigenvalues of the recursion matrix $|\tau_j|$. If there are modes with recursion matrix eigenvalue smaller than unit moduli, $\underline{\underline{\tau}}^N$ term ensures their decay along the wire as it extends to infinity. Here, it is important to talk about the recursion matrix eigenvalues: As we construct explicitly in the previous section, our recursion matrix is the transfer matrix of the first unit cell at the beginning of the superlattice. Transfer matrices are pseudounitary matrices; as a consequence of pseudounitary half the eigenvalue moduli of the recursion matrix are inverses of the other half [85]. So the diagonal matrix that has recursion matrix eigenvalues have the form $\underline{\underline{\tau}} = \text{Diag}\begin{bmatrix}\tau_1\cdots\tau_{N_d/2}, 1/\tau_1\cdots 1/\tau_{N_d/2}\end{bmatrix}$ where the ordering of recursion matrix eigenvalues in the diagonal matrix is arbitrary. So, recursion matrix has $N_d/2$ eigenvalues that have smaller than unit moduli, the other recursion matrix $N_d/2$ eigenvalues have bigger than unit moduli. The Hamiltonian eigenvectors that are connected to recursion matrix eigenvalues with smaller than unit moduli decay as the wire extends to infinity since $\Psi^{(N)}_{\epsilon=0} \propto \underline{\underline{\tau}}^N\cdot\underline{\underline{\mathcal{P}}}^{-1}\cdot\underline{\mathbf{c}}^{(0)}$. Imposing the boundary condition at origin gives us $N_d/2$ equations to determine N_d-many amplitude vectors c_j since the di-

mensions of the Hamiltonian eigenvectors ψ_j is $\dim(\psi_j) = N_d/2 \times 1$ Next; we consider Hamiltonian eigenvectors that are connected to recursion matrix eigenvalues with bigger than unit moduli. Since we want asymptotic decay of the zero-energy wavefunction we impose a second boundary condition $\Psi^{(N)}_{\epsilon=0}(x \to \infty) = 0$ for zero-energy wavefunction decay. The second boundary condition then cancels the diverging terms in the zero-energy wavefunction and gives us $N_d/2$ equations where $\Psi^{(N)}_{\epsilon=0} \propto \underline{\underline{\tau}}^N \cdot \underline{\underline{\mathcal{P}}}^{-1} \cdot \underline{\mathbf{c}}^{(0)}$. The elements of the unitary transformation matrix are recursion matrix eigenvectors where $\underline{\underline{\mathcal{P}}}^{-1} = \left[\underline{\zeta}_1 \cdots \underline{\zeta}_{N_d}\right]^{-1} = \left[\underline{\zeta}_1 \cdots \underline{\zeta}_{N_d}\right]^T$ so the second boundary condition gives us $N_d/2$-many equations as $\underline{\zeta_k}\, c^{(0)} = 0$. Hence, we can determine the wavefunction since we have N_d-many amplitudes c_j and get N_d equations after imposing boundary conditions. Our zero-energy wavefunction construction decays along the wire as $x \to \infty$ and we can write the complete solution of it since we can determine the amplitudes that connect Hamiltonian eigenvectors.

Up to this point we show that we can construct a zero-energy wavefunction that could exhibit Majorana mode characteristics in a sense that it is a zero-energy solution localized at the beginning of the superlattice. We now continue to apply our wavefunction construction to p-wave and s-wave meta-topological insulators in order to derive topological indices that show topological triviality.

4.2. Topological Index Calculation Using Transfer-Matrix Eigenvalues

In this section; we calculate new topological indices for both p-wave and s-wave one-dimensional meta-topological insulator wires to detect Majorana modes using recursion matrix eigenvalues. After showing that the superlattice allows construction of zero-energy wavefunctions; we now show that recursion matrix eigenvalues τ's can be used to pinpoint configurations where Majorana modes exist. In the previous section we constructed a zero-energy wavefunction that exhibits two important Majorana wavefunction characteristics: Our solutions are normalizable, hence they asymptotically decay as they extend into the superlattice and they are at zero-energy. We prove the existence of a Majorana mode at the origin by checking whether we can construct a zero-energy wavefunction using the boundary conditions; however, zero-energy wavefunctions are not necessarily Majorana wavefunctions –in amongst the zero-energy solutions some are not topologically protected. Such solutions accidentally satisfy the boundary condition at the origin; and a perturbation drives them away from zero-energy in pairs. In order to distinguish zero-

energy modes from Majorana modes, we use the off-diagonalized Hamiltonian eigenvectors that we explain in the Chapter 3. Off-diagonalized eigenvectors of the Hamiltonian allow us to take into account the asymptotic behavior of zero-energy solutions in both blocks so that we can distinguish accidental Andreev bound state solutions from genuine Majorana soltions. We start by explaining how a Majorana state wavefunction can be constructed, we proceed to derive new topological indices that depend on the recursive nature of the superlattice. We compare our analytical results for the topological indices numerical simulations by plotting the topological phase space. We find a good agreement between analytics and numerics.

4.2.1. Topological Index Calculation for p-wave Wires

We start by rewriting zero-energy wavefunction in Eq. 4.11 for a p-wave meta-topological wire as

$$\Psi_{\epsilon=0}^{(N)} = \left(\begin{bmatrix} \underline{\psi}_1 & \dots & \underline{\psi}_4 \end{bmatrix} \Big|_{x=Nd} \right) \cdot \underline{\underline{\mathcal{T}}}(-Nd) \cdot \underline{\underline{\mathcal{P}}} \cdot \underline{\underline{\tau}}^N \cdot \underline{\underline{\mathcal{P}}}^{-1} \cdot \underline{\mathbf{c}}^{(0)} \tag{4.12}$$

where we substitute $N_d = 4$ which is the number of Hamiltonian eigenvectors that we can construct our zero-energy wavefunction. We show that 4 amplitudes can be determined by imposing two boundary conditions on the wire and the zero-energy wavefunction decays along the wire as $x \to \infty$. We now proceed to construct p-wave zero-energy wavefunction in Eq. 4.12 using eigenvectors of the off-diagonalized Hamiltonian. We do this in order to account for the Majorana wavefunction which has a diverging and converging block Hamiltonian eigenvectors in both upper and lower blocks. Up to this point, we do not consider the ordering of the Hamiltonian eigenvectors $\underline{\psi}_j$ during our calculations since the wavefunction decays along the wire and 4 constants can be determined by imposing boundary conditions. However; we specify the ordering of Hamiltonian eigenvectors when using block Hamiltonian eigenvectors since this ordering directly affects the nature of the recursion matrix since we use Hamiltonian eigenvectors to construct it. So we put upper Hamiltonian block eigenvectors as $\underline{\psi}_1$ and $\underline{\psi}_2$ and lower Hamiltonian eigenvectors as $\underline{\psi}_3$ and $\underline{\psi}_4$. This choice puts the recursion matrix into a block form as $\underline{\underline{\mathcal{R}}} = \begin{bmatrix} \underline{\underline{R}}^{(\mathrm{u})} & 0 \\ 0 & \underline{\underline{R}}^{(\mathrm{l})} \end{bmatrix}$ where $\underline{\underline{R}}^{(\mathrm{u})}$ and $\underline{\underline{R}}^{(\mathrm{l})}$ are upper and lower recursion matrix blocks. The block recursion matrix also orders the diagonal eigenvalue matrix $\underline{\tau}$ so that we can write it in terms of upper and lower block recursion matrix eigenvalues as $\underline{\tau}^{(\mathrm{u})} = \mathrm{Diag} \begin{bmatrix} t_1^{(\mathrm{u})} & t_2^{(\mathrm{u})} \end{bmatrix}$

and $\underline{\underline{\tau}}^{(\mathrm{l})} = \mathrm{Diag}\begin{bmatrix} t_1^{(\mathrm{l})} & t_2^{(\mathrm{l})} \end{bmatrix}$. The upper and lower recursion matrix eigenvalues are calculated as $\underline{\underline{R}}^{(\mathrm{u})}\underline{s}_i^{(\mathrm{u})} = t_i^{(\mathrm{u})}\underline{s}_i^{(\mathrm{u})}$ and $\underline{\underline{R}}^{(\mathrm{l})}\underline{s}_i^{(\mathrm{l})} = t_i^{(\mathrm{l})}\underline{s}_i^{(\mathrm{l})} \mid i = 1, 2$. As we show in previous chapter, we should have a diverging and decaying block Hamiltonian solution in each block in order to have a Majorana mode. The asymptotic behavior of block eigenvectors are connected to recursion matrix eigenvalues as $t_i^N \propto e^{2Nd/A}$ as t_i is a recursion matrix eigenvalue, Nd is the extent of the wire which extends to infinity $Nd \to \infty$ [85] and A is a constant that is a function of the Lyapunov exponent and superconductor coherence length. The block diagonal eigenvalue moduli take the form $|t_1^{(\mathrm{u})}| > 1, |t_2^{(\mathrm{u})}| < 1$ and $|t_1^{(\mathrm{l})}| < 1, |t_2^{(\mathrm{l})}| > 1$. We thus derive the topological index

$$\mathbb{Q}_{\mathrm{D}}^{(\mathrm{p,MTI})} = \prod_{i=1}^{2} \mathrm{sgn}\left(|t_i^{(\mathrm{u})}| - 1\right) \tag{4.13}$$

Our formula checks for the existence of Majorana mode by looking at the asymptotic nature of block solutions of the Hamiltonian and gives a topological index that is calculated using the block recursion matrix eigenvalues by yielding -1 when a topologicallay protected Majorana mode is present.

In Fig. 4.2a; we plot the topological phase space of a p-wave topological superconductor wire as a function of chemical potential μ and electrostatic potential $V(x) = V_0$ that is constant along the wire. The blue area of the density plot show topologically nontrivial phases ($\mu > V_0$) and the red area signify topologically trivial phases ($\mu < V_0$) of the topological superconductor wire. The green dashed line is the phase transition line plotted at $\mu = V_0$. In Fig. 4.2b; we calculate the topological phase space of a p-wave meta-topological wire as a function of chemical potential μ and piecewise continuous electrostatic potential of amplitude $V_0 = \max(V_{\mathrm{SL}})$. Density plots are the results of numerical calculations for Eq. 3.3 for $V(x) = V_{\mathrm{SL}}(x)$ and white lines are calculated using Eq. 4.13 for a piecewise continuous electrostatic potential with amplitude V_0. The superlattice potential $V_{\mathrm{SL}}(x)$ changes the asymptotic behavior of the Lyapunov exponent in Eq. 3.3 as well as the existence of the Majorana mode. We keep the dashed green topological phase transition line of a p-wave topological superconductor wire to show different phase spaces of both types of topological wires. The density plot and white lines that are calculated for the same potential with our two different formulations of the topological index fits very well so that we say that Eqs. 4.13 and 3.3 show significant agreement. We plot Figs. 4.2a and 4.2b for a single superlattice unit cell with an effective spin orbit

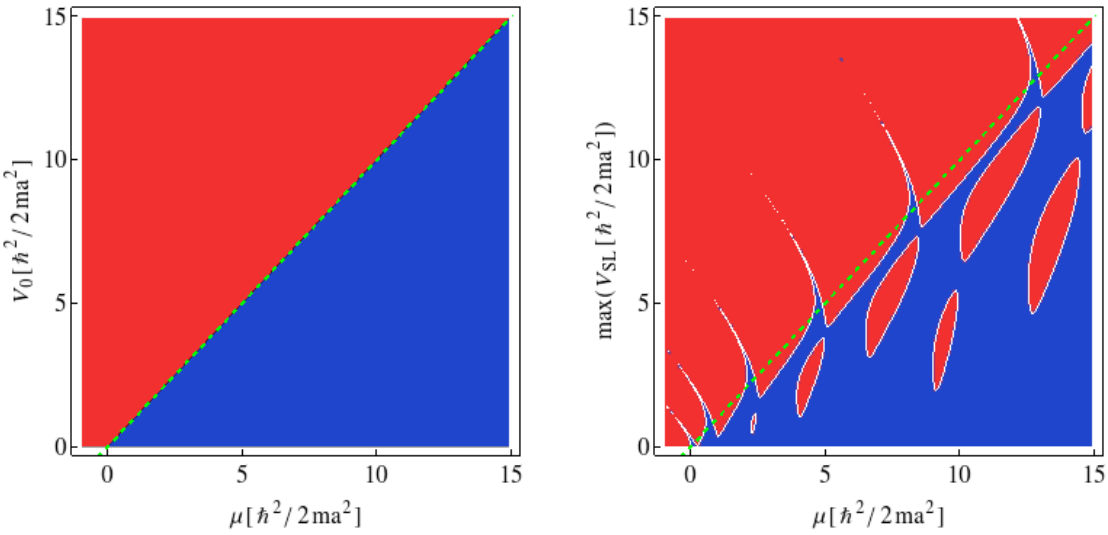

Figure 4.2: Topological phase space of a p-wave topological superconductor wire as a function of chemical potential μ and an applied constant electrostatic gate potential along wire is plotted in (a). Topological phase space of a p-wave meta-topological insulator as a function of chemical potential μ and electrostatic potential amplitude $\max(V_{\text{SL}})$ is plotted in (b). Density plot is calculated using Eq. 4.13 where red areas signify topologically trivial configurations and blue areas signify topologically nontrivial configurations. White lines are calculated using Eq. 3.3 where they converge to p-wave topological superconductor phase transition line $\mu = V_0$ when the electrostatic potential is absent. Calculations are done for a p-wave topological superconductor and meta-topological insulator wire with an effective spin-orbit coupling $\Delta_{\text{eff}} = 0.03\hbar^2/2ma^2$ unit cell length $d = 2a$. Phase transition boundary in the density is excellently covered by white lines so both formulations of the topological indices show strong agreement. The red specks below the p-wave topological superconductor phase transition line $\mu > V_0$ show that a topologically nontrivial wire can be tuned into its trivial phase by the application of an electrostatic potential. The topological order also flips from trivial to nontrivial for s-wave topological superconductor wires that are the tails of blue spikes that are above the green dashed topological superconductor wire phase transition line $\mu < V_0$.

coupling strength $\Delta_{\text{eff}} = 0.03\hbar^2/2ma^2$ where the length of the superlattice unit cell is $d = 2a$. The effect of the electrostatic superlattice on topological phase space can be seen in Fig. 4.2b as it leads to topologically nontrivial to trivial phase transitions that we see in red patches which are below the yellow topological superconductor wire phase transition line. We also see topologically trivial to nontrivial phase transitions as parts of spikes that are above the phase transition line. Our analytical formula fits the numerical solution well.

We continue to analyze s-wave meta-topological wires.

4.2.2. Topological Index Calculation for s-wave Wires

We start by rewriting zero-energy wavefunction in Eq. 4.11 for an s-wave meta-topological wire as

$$\Psi_{\epsilon=0}^{(N)} = \left(\left[\underline{\psi}_1 \quad \dots \quad \underline{\psi}_8 \right] \Big|_{x=Nd} \right) \cdot \underline{\underline{\mathcal{T}}}(-Nd) \cdot \underline{\underline{\mathcal{P}}} \cdot \underline{\underline{\tau}}^N \cdot \underline{\underline{\mathcal{P}}}^{-1} \cdot \underline{\mathbf{c}}^{(0)} \tag{4.14}$$

where we now have $N_d = 8$ Hamiltonian eigenvectors to construct a zero-energy solution. The amplitude vector $\underline{\mathbf{c}}^{(0)}$ has 8 components that can be determined by imposing two boundary conditions on the wire as we explain in Section 4.1.2. We order the first 4 Hamiltonian eigenvectors as solutions of the upper Hamiltonian block and the remaining 4 local solutions are the general solutions to the lower Hamiltonian block. The ordering of block Hamiltonian puts the recursion matrix into a block form as $\underline{\underline{\mathcal{R}}} = \begin{bmatrix} \underline{\underline{R}}^{(\text{u})} & 0 \\ 0 & \underline{\underline{R}}^{(\text{l})} \end{bmatrix}$ where $\underline{\underline{R}}^{(\text{u})}$ and $\underline{\underline{R}}^{(\text{l})}$ are upper and lower recursion matrix blocks. Then, the block recursion matrix puts the diagonal eigenvalue matrix vector into two segments that have eigenvalues of upper and lower block as $\underline{\tau}^{(\text{u})} = \text{Diag}\left[t_1^{(\text{u})} \quad \cdots \quad t_4^{(\text{u})} \right]$ and $\underline{\tau}^{(\text{l})} = \text{Diag}\left[t_1^{(\text{l})} \quad \cdots \quad t_4^{(\text{l})} \right]$ The upper and lower recursion matrix eigenvalues are calculated as $\underline{\underline{R}}^{(\text{u})} \underline{s}_i^{(\text{u})} = t_i^{(\text{u})} \underline{s}_i^{(\text{u})}$ and $\underline{\underline{R}}^{(\text{l})} \underline{s}_i^{(\text{l})} = t_i^{(\text{l})} \underline{s}_i^{(\text{l})} \mid i = 1, \dots, 4$. In the previous chapter we show that the asymptotic behavior of Majorana modes solutions has three diverging and one decaying modes in one block and three converging and one diverging modes in the other block. Since the zero-energy wavefunction construction in Eq. 4.14 in the N^{th} unit cell has $\underline{\underline{\tau}}^N$ which affects its asymptotic behavior as the wire extends, we again relate the asymptotic behavior of the zero-energy wavefunction to the eigenvalues of the recursion matrix. The asymptotic behavior of block eigenvectors are connected to recursion matrix eigenvalues as $t_i \propto e^{2L/A}$ as $t_i > 1$ is a recursion matrix eigenvalue, L is the extent of the wire

which extends to infinity $L \to \infty$ and A is a constant that is a function of the Lyapunov exponent and superconductor coherence length [85]. Since we have three decaying solutions and one diverging solutions in each block, eigenvalue moduli now have the form $|t_1^{(\mathrm{u})}| > 1, |t_2^{(\mathrm{u})}| > 1, |t_3^{(\mathrm{u})}| > 1, |t_4^{(\mathrm{u})}| < 1$ and $|t_1^{(\mathrm{l})}| < 1, |t_2^{(\mathrm{l})}| < 1, |t_3^{(\mathrm{l})}| < 1, |t_4^{(\mathrm{l})}| > 1$; the indices and the ordering of the eigenvalues are irrelevant we only use them to count number of eigenvectors with moduli smaller than unity. With this form of diagonal recursion matrix eigenvalue matrices, we exclude accidental solutions since they have two diverging and two increasing solutions in each block. So we derive a topological index that check the recursion matrix eigenvalue moduli with respect to unity for upper and lower block recursion matrices. Hence, our topological index for s-wave meta-topological wire reads

$$\mathbb{Q}_{\mathrm{D}}^{(\mathrm{s,MTI})} = \prod_{i=1}^{4} \mathrm{sgn}\left(|t_i^{(\mathrm{u})}| - 1\right). \tag{4.15}$$

The formula indicates the existence of Majorana mode is determined by the asymptotic nature of block Hamiltonian solutions and relates it to block recursion matrix eigenvalues.

We plot the topological phase space of a s-wave topological superconductor wire as a function of chemical potential μ and Zeeman field B in Fig. 4.3a. Using Eq. 3.8 with no electrostatic potential along the wire $V(x) = 0$; red regions are topologically nontrivial part of the phase space and blue regions signify topologically trivial phase space. The phase transition line is plotted with a green dashed line that is at $B^2 = \mu^2 + \Delta^2$ and our calculations using Eq. 4.15 with a zero electrostatic potential along the wire exactly fits the dashed green phase transition line. Fig. 4.3b shows the phase space of an s-wave meta-topological wire where again red indicates topologically nontrivial phases and blue indicates topological trivial phases. The density plot is calculated using Eq. 3.8 when an electrostatic superlattice is applied on the wire as $V(x) = V_{\mathrm{SL}}$ with an amplitude $V_0 = \hbar^2/2ma^2$ where the calculations are done for a unit cell of length $d = 2a$. White lines are calculated using Eq. 4.15 with the same superlattice potential and we also keep dashed green phase transition line of the s-wave topological superconductor wire in Fig. 4.3b. Our plots fit together very well. The plots are made for a wire with spin orbit coupling strength $\alpha = 0.03\hbar^2/2ma^2$, superconductor pair potential $\Delta = 0.81\hbar^2/2ma^2$ for a unit cell of length $d = 2a$.

The effect of the electrostatic superlattice on the s-wave topological superconductor

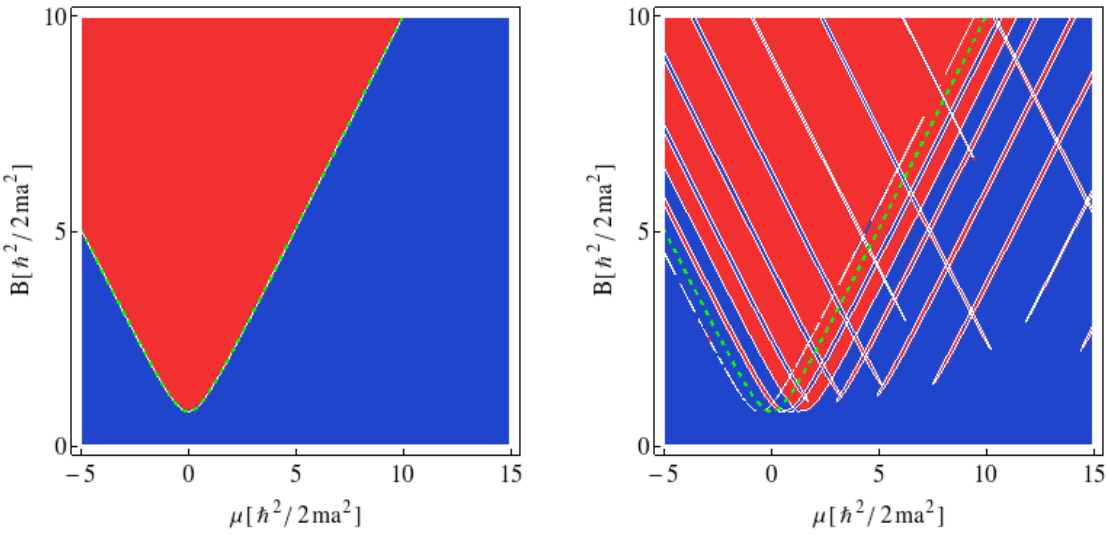

Figure 4.3: Topological phase space diagrams calculated from Eqs. 3.8 and 4.15 for a (a) clean s-wave topological superconductor wire with no superlattice and (b) meta-topological insulator wire, as a function of chemical potential μ and Zeeman field strength B. Red and blue parts of the density plot signify topologically nontrivial and trivial configurations that are calculated using 3.8 and white lines are calculated using Eq. 4.15. Both topological phase spaces are calculated with spin orbit coupling strength $\alpha = 0.03\hbar^2/2ma^2$ and superconductor pair potential $\Delta = 0.81\hbar^2/2ma^2$ for a unit cell of length $d = 2a$. The white lines exactly covers the density plot transition boundary so we say that our topological indices formulae show strong agreement. The s-wave topological superconductor wire has no electrostatic potential applied onto it; whereas, an electrostatic superlattice potential is applied on the meta-topological insulator wire with an amplitude $V_0 = \hbar^2/2ma^2$. The application of electrostatic potential flips topological order in s-wave topological superconductor wires as it can be seen by comparing the dashed yellow phase transition line of s-wave topological superconducting wire $B^2 = \mu^2 + \Delta^2$. Flipping of topological order at $B^2 < \mu^2 + \Delta^2$ turns a topologically trivial s-wave wire into a nontrivial one so that a Majorana mode exists in s-wave meta-topological insulator wires at configurations at which s-wave topological superconductor wire is topologically trivial.

can be seen by looking at the phase space of meta-topological wire: Superlattice flips the topological order of s-wave topological superconductors as topological order is induced in topologically trivial wires.

4.3. Conclusion

In this chapter, we show that the application of a weak electrostatic superlattice potential on topological superconductor wires changes their topological order and thus drive them into or out of their topological phases. Specifically, we show that we can drive p- and s-wave topological superconductors out of their topologically nontrivial phases with the application of a weak electrostatic superlattice. To show this, we use the presence of Majorana modes as a sign to determine topological order by analyzing whether a Majorana mode wavefunction can be constructed. Our method uses weak superlattices does not lead to local changes in topological order so we call them *meta-topological insulators*. We derive topological indices that use the recursion nature of the superlattice and our topological indices are compliant with the topological classification of meta-topological insulators as they also belong the class D since no symmetries are broken. We numerically compare our results for meta-topological superconductors in Eqs. 4.13 and 4.15 to our earlier results given in Eqs. 3.3 and 3.8 in presence of a superlattice, and find they show very good agreement. In the next section we generalize our formulae to thin wires that also have a transverse degree of freedom along y-direction.

Chapter 5

MULTICHANNEL TOPOLOGICAL AND META-TOPOLOGICAL WIRES

In this chapter; we extend our results of Chapters 3 and 4 to multichannel topological superconductor and meta-topological thin-wires. Owing to the transverse degree of freedom, our topologically nontrivial zero-energy calculation needs to account for the possibiliy of multiple Majorana modes. We construct multichannel Majorana mode wavefunctions using our wavefunction analysis and define topological indices that are consistent with their corresponding topological classification shown in Table 2.2. We present our analytical and numerical results for both p-wave and s-wave topological superconductor and meta-topological thin-wires and compare them using our tight binding simulations.

We concentrate on thin wires whose superconducting coherence length is much larger than the transverse length of the wire. As we explain in Chapter 2; the thin-wire constraint ($\xi \gg W$) makes the chiral symmetry breaking p_y contribution to the Hamiltonian [83] subdominant so that we can off-diagonalize the Hamiltonians and include these perturbatively. Also; without the p_y contribution; there is a special time-reversal symmetry since the Hamiltonians become real. Hence the Hamiltonians now has three symmetries including the intrinsic particle hole symmetry of superconductors. The topological class that has of all three symmetries with $+1$ eigenvalues is Altland Zirnbauer class-BDI with $\mathbb{Z}$ topological indices [72]; so thin wires belong to this class [91]. In light of this; we calculate a class-BDI topological index $\mathbb{Q}_{\text{BDI}}$ in $\mathbb{Z}$ and also calculate class-D topological index $\mathbb{Q}_{\text{D}}$ in $\mathbb{Z}_2$ which are connected to each other as $\mathbb{Q}_{\text{D}} = -1^{\mathbb{Q}_{\text{BDI}}}$ [19].

5.1. Multichannel p-wave Wires

In this section we calculate topological index for multichannel p-wave topological superconductor and meta-topological wires in thin-wire limit to derive class-BDI and class-D topological indices. Thus we generalize our results from Chapter 4 on meta-topological

insulators to multichannel wires. We also perform tight binding simulations and compare our results.

5.1.1. Topological Superconducting Wires

Starting with the Bogoliubov-de Gennes Hamiltonian for 2D wires, we first investigate the Hamiltonian in the thin-wire limit and define a topological index $\mathbb{Q}^{(\mathrm{p})}_{\mathrm{BDI}}$. This allows us to generalize our topological index result of Eq. 3.3 to multichannel wires. The Hamiltonian reads as

$$H = h(\mathbf{p}; x, y)\tau_z + \Delta_{\mathrm{eff}}\mathbf{p}\cdot\tau, \tag{5.1}$$

where $h(\mathbf{p}; x, y) = \mathbf{p}^2/2m - \mu$ is the kinetic term, Δ_{eff} is the effective spin-orbit coupling strength and Pauli matrices $\tau_i \mid (i = 1, 2, 3)$ define the electron-hole space [4, 5]. Unlike the single channel wire the Hamiltonian now has a chiral symmetry breaking contribution that does not allow us to off-diagonalize the Hamiltonian and analyze the asymptotic behavior of the block wavefunctions. Nevertheless for thin-wires with a superconducting coherence length much larger than the transverse coordinate of the system ($\xi_{\mathrm{p}} \gg W$) we may ignore this contribution since $\langle \Delta_{\mathrm{eff}} p_y \rangle \propto W/\xi_{\mathrm{p}}$ [86]. However, different from an actual stacking of 1D wires, our 2D thin-wire approximation has contributions coming from transverse confinement channels as $\langle p_y^2 \rangle \propto n_y^2\pi^2/W^2$ where $n_y = 0, \ldots, N_y$ is the transverse channel index [81]. Now the wire approximately belongs to class-BDI with topological indices in $\mathbb{Z}$ so we focus on the corresponding topological index. Later on we treat the chiral symmetric Hamiltonian perturbatively. The restoration of chiral symmetry allows us to off-diagonalize Hamiltonian in Eq.5.1 as

$$H \simeq \left(\frac{p_x^2}{2m} - \mu_{n_y}\right)\tau_z + \Delta_{\mathrm{eff}} p_x \tau_x \tag{5.2}$$

with a renormalized chemical potential $\mu_{n_y} = \mu - \hbar^2 n_y^2 \pi^2/W^2$ that contains transverse channel contribution. The off-diagonalization process of this Hamiltonian is the same we make in Chapter 3 but with a chemical potential μ_{n_y} with transverse channel energies. Zero-energy solutions are asymptotically of the form $\chi_{n_y\pm} \sim e^{\pm\kappa x} e^{\Lambda_{n_y} x} a(x, y)$ where κ is the inverse coherence length $\kappa \equiv \xi_{\mathrm{p}} = m\Delta_{\mathrm{eff}}/\hbar$ and $a(x, y)$ is a $\mathcal{O}(1)$ nondivergent function. Now, Lyapunov exponent along x-direction also depends on the index of transverse channels so we write them to include this contribution as Λ_{n_y}. Similar to the 1D p-wave topological superconductor wire, Majorana solutions exist when $|\Lambda_{n_y}| < \kappa$ where each

Hamiltonian block have an asymptotically decaying and diverging zero-energy solution as the wire extends to infinity. However; we formulate the exponential factors of Majorana wavefunctions differently from the way we do for the p-wave wire since a 2D p-wave wire belongs to class D with a $\mathbb{Z}_2$ topological index, but the thin-wire approximately belongs class BDI with a $\mathbb{Z}$ topological index rather than to class D with a topological index $\mathbb{Z}_2$ as the p-wave chain belongs. We use subscript BDI to derive the quantum number of thin-wires as

$$\mathbb{Q}_{\text{BDI}}^{(\text{p})} = \sum_{n_y=1}^{N_y} \Theta\left(|\Lambda_{n_y}| - \frac{1}{\xi_{\text{p}}}\right), \tag{5.3}$$

where there are N_y-many longitudinal channels and Heaviside theta function gives 0 for a topologically trivial wire and adds $+1$ for each Majorana mode in the transverse channels.

Next, we construct a multichannel p-wave topological superconductor topological index using the wavefunction decay argument but with transverse confinement channels along the y-direction. Zero-energy solutions of block Hamiltonians has the form $\chi_{n_y\pm} \sim e^{\pm\kappa x} e^{\Lambda_{n_y} x} a(x,y)$ where $a(x,y)$ is a nondivergent function; whereas, we take into account Lyapunov exponents along x-direction that has different longitudinal channel contributions while constructing the topological formula. Also; we derive the topological index respecting the topological classification of the chain as it belongs to the class D with a $\mathbb{Z}_2$ topological quantum number. Similar to the discussion leading up to Eq. 3.3, we find the topological index as

$$\mathbb{Q}_{\text{D}}^{(\text{p})} = \prod_{n_y}^{N_y} sgn\left(|\Lambda_{n_y}| - \frac{1}{\xi_{\text{p}}}\right), \tag{5.4}$$

where this equation gives -1 if a Majorana mode is present and $+1$ when the wire is topologically trivial. We stress that Eqs. 5.3 and 5.4 depend only on the coherence length and normal state properties. In the above formula we take into account multiple crossings over the inverse superconducting coherence length of N_y-many Lyapunov exponents along the x-direction.

We now continue to generalize our topological index formulae for multichannel meta-topological thin-wires.

5.1.2. Meta-Topological Insulators

In this section, we derive exact formulas for the topological indices.ï£ijï£ijï£ijï£ij In Section 4, we showed that we can construct a zero-energy wavefunction that depends on the elements of recursion matrix eigenvectors whose eigenvalues are less than unit moduli. Then, we imposed boundary conditions and showed that we can construct a topologically protected Majorana mode wavefunction since we exclude accidental zero-mode wavefunctions from topologically protected modes while we construct the meta-topological wire index in Eq. 4.13. We apply the same method to multichannel meta-topological wires as follows: We start by rewriting a zero-energy wavefunction at the start of the N^{th} unit cell like in Eq. 4.12 but for a transverse channel with an n_y index as follows

$$\Psi^{(N)}_{n_y,\epsilon=0} = \left(\left[\underline{\psi}_{n_y,1} \quad \dots \quad \underline{\psi}_{n_y,4} \right] \Big|_{x=Nd} \right) \cdot \underline{\underline{\mathcal{T}}}(-Nd) \cdot \underline{\underline{\mathcal{P}}} \cdot \underline{\underline{\tau}}^{N} \cdot \underline{\underline{\mathcal{P}}}^{-1} \cdot \underline{\mathbf{c}}^{(0)} \tag{5.5}$$

where $\underline{\psi}_{n_y,j}$ are zero-energy block Hamiltonian eigenvectors with a renormalized chemical potential $\mu_{n_y} = \mu - \hbar^2 n_y^2 \pi^2 / W^2$ since we omit the chiral symmetry breaking p_y contribution. For a channel with chemical potential μ_{n_y}; we calculate the matrices in Eq. 5.5 same way we did in Section 4.2.1 but at different n_y channels since the dimensions of the translation matrix $\underline{\underline{\mathcal{T}}}$, similarity transformation matrix $\underline{\underline{\mathcal{P}}}$ and diagonal recursion matrix eigenvalue matrix $\underline{\underline{\tau}}$ do not change.

To construct the zero-energy wavefunction, we use upper Hamiltonian block eigenvectors as $\underline{\psi}_{n_y,1}$, $\underline{\psi}_{n_y,2}$ and lower block eigenvectors as $\underline{\psi}_{n_y,3}$, $\underline{\psi}_{n_y,4}$ so that the recursion matrix eigenvalues get into a block diagonal form as $\underline{\underline{\tau}}^{(\text{u})} = \text{Diag}\left[t^{(\text{u})}_{n_y,1} \quad t^{(\text{u})}_{n_y,2} \right]$ and $\underline{\underline{\tau}}^{(\text{l})} = \text{Diag}\left[t^{(\text{l})}_{n_y,1} \quad t^{(\text{l})}_{n_y,2} \right]$. We calculate upper and lower block diagonal eigenvalue matrices for each channel as $\underline{\underline{R}}^{(\text{u})} \underline{s}^{(\text{u})}_{n_y,i} = t^{(\text{u})}_{n_y,i} \underline{s}^{(\text{u})}_{n_y,i}$ and $\underline{\underline{R}}^{(\text{l})} \underline{s}^{(\text{l})}_{n_y,i} = t^{(\text{l})}_{n_y,i} \underline{s}^{(\text{l})}_{n_y,i} \mid i = 1, 2$. The zero-energy wavefunction in Eq. 5.5 should have one asymptotically decaying and diverging wavefunction in each block to be topologically nontrivial; so we determine the asymptotic behavior of the recursion matrix eigenvalues using $t_i^N \propto e^{2Nd/A_{n_y}}$ where t_i is a recursion matrix eigenvalue, Nd is the extent of the wire which extends to infinity $Nd \to \infty$ and A_{n_y} is a constant for a channel which is a function of the Lyapunov exponent and the coherence length [85]. So the block diagonal eigenvalue moduli take the form of $|t^{(\text{u})}_{n_y,1}| > 1, |t^{(\text{u})}_{n_y,1}| < 1$ and $|t^{(\text{l})}_{n_y,1}| < 1, |t^{(\text{l})}_{n_y,1}| > 1$ where the subscripts do not correspond to an ordering of the eigenvalues but we use them to count the eigenvalues with smaller than unit moduli. Therefore we derive the multichannel meta-topological

thin wire topological index as

$$\mathbb{Q}_{\mathrm{D}}^{(\mathrm{p,MTI})} = \prod_{n_y,i=1}^{N_y,2} \mathrm{sgn}\left(|t_{n_y,i}^{(\mathrm{u})}| - 1\right), \tag{5.6}$$

where the above equation takes into account multiple transverse channels with index $n_y = 1, 2, \cdots$. This formula can also be derived by using the lower diagonal block of recursion matrix eigenvalues since the total number of decaying and diverging modes remains the same because of the pseudounitarity of the recursion matrix.

In Fig. 5.1a we plot the topological phase space for a 3-channel p-wave topological superconducting wire as a function chemical energy μ and electrostatic potential $V(x) = V_0$ that is constant along the wire. Blue areas in the phase space are calculated using $\mu_{n_1} > V_0 > \mu_{n_2}$ and $\mu_{n_3} > V_0$ where the wire is topologically nontrivial since there are odd numbers of channels. In red areas, the wire is in its topologically trivial phase since there are no Majorana modes for $\mu_{n_1} < V_0$ and two Majorana modes that hybridize due to the chiral symmetry-breaking terms, when $\mu_{n_2} > V_0 > \mu_{n_3}$. The dashed green lines are topological phase transitions that are at $\mu_{n_1} = V_0$, $\mu_{n_2} = V_0$ and $\mu_{n_3} = V_0$. Fig. 5.1b is the phase space plot for a meta-topological wire as a function of chemical energy μ and amplitude of piecewise continuous electrostatic potential $V_0 = \max(V_{\mathrm{SL}})$. The density plots are calculated with Eq. 5.4 and $\mathbb{Q}_{\mathrm{D}}^{(\mathrm{p})} = (-1)^{\mathbb{Q}_{\mathrm{BDI}}^{(\mathrm{p})}}$ in presence of the superlattice and red and blue areas are topologically trivial and nontrivial configurations of the meta-topological wire, as we calculated from Eq. 5.3 [19]. The white lines are calculated using Eq. 5.6 in presence of a superlattice potential with amplitude V_0. Density plots and contour plots that we calculate with two different formulations of the topological index fit perfectly. Therefore we conclude that our analytical formula Eq. 5.3 which uses normal state data and the coherence length is a good approximation to the exact formulation of Eq. 5.6. In both plots we plot the phase space of a single superlattice unit cell with effective spin orbit coupling strength $\Delta_{\mathrm{eff}} = 0.03\hbar^2/2ma^2$ where the length of the superlattice unit cell is $d = 2a$. We again see that electrostatic superlattice can flip the topological order in a multichannel meta-topological wire and comparing plots in Figs. 5.1a and 5.1b we say that multiple number of channels directly affects the changes in topological order. Next; we present our tight binding simulations that we calculate using the
$\mathbb{Q}_{\mathrm{D}}^{(\mathrm{p})} = \mathrm{sgn}(\mathrm{Det}(r))$ topological index formula where r is the reflection matrix part of the scattering matrix and we compare it to our topological index formula in Eq. 5.3 with

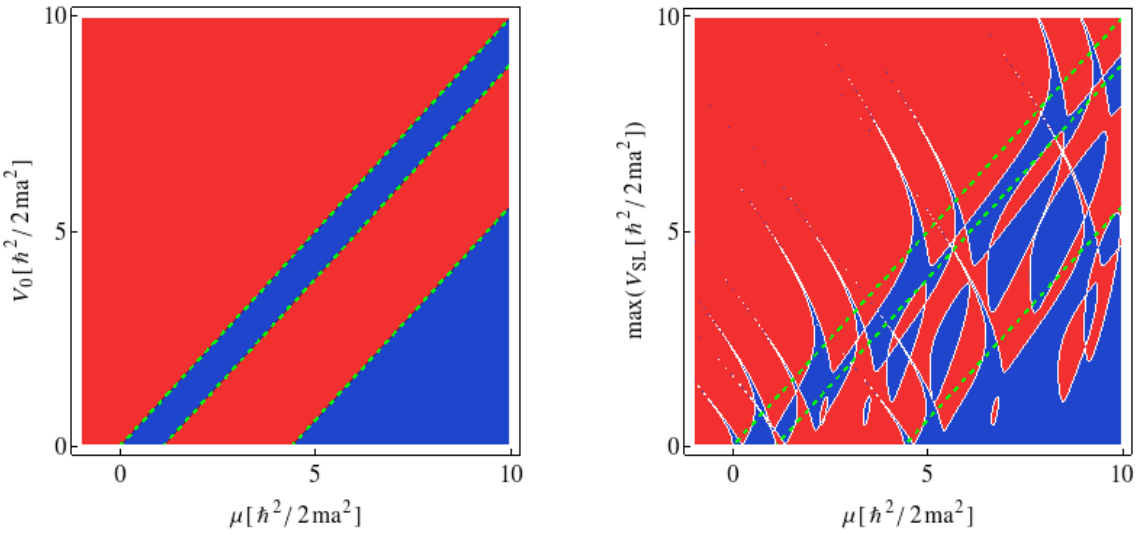

Figure 5.1: Topological phase space of a 3 channel p-wave topological superconducting wire as a function of chemical potential μ and a constant potential V_0 along the wire is plotted in (a). Topological phase space of a 3 channel p-wave meta-topological insulator wire as a function of chemical potential μ and electrostatic superlattice potential amplitude $\max(V_{\text{SL}})$ is plotted in (b). The density plots are calculated using topological index in Eq. 5.6 where red areas signify topologically trivial phases and blue areas signify the nontrivial topological phases of the wire. Dashed green lines are p-wave topological superconductor boundaries at $\mu_{n_y} = V_0 \mid n_y = 1, 2, 3$. The white lines are plotted using Eq. 5.3 where dashed green lines and white lines converge when the superlattice is absent. The plots are for a thin wire with a unit cell length $d = 6a$, effective spin-orbit coupling $\Delta_{\text{SL}} = 0.03\hbar^2/2ma^2$ with a superlattice unit cell length $d = 2a$. In p-wave meta-topological insulator wire, the phase transition boundary in the density plot is perfectly covered by the white lines showing that our topological indices formulae show significant agreement. Compared to the single channel phase space plots, there exists more topologically trivial phase space area that transitions into their topological phases with the application of an electrostatic superlattice.

$\mathbb{Q}_{\mathrm{D}}^{(\mathrm{p})} = (-1)^{\mathbb{Q}_{\mathrm{BDI}}^{(\mathrm{p})}}$ [1, 78].

We calculate our numerical results for a wire of length $L = 15000a$ that is attached to metallic leads at both ends with an effective spin orbit coupling strength $\Delta_{\text{eff}} = 0.3t$ where $t = \hbar^2/2ma^2$ and a is the lattice constant. Fig. 5.2a is the tight binding calculating of the topological phase space of a 3 channel p-wave topological superconductor as a function of chemical potential μ and electrostatic potential $V(x) = V_0$ that is constant along the wire. Figs. 5.2b- 5.2f are phase spaces of 3 channel meta-topological wire that we calculate as a function of chemical potential μ and electrostatic superlattice potential with amplitude $V_0 = \max(V_{\mathrm{SL}})$ superlattice unit cell lengths $d = 10a$, $d = 20a$, $d = 30a$, $d = 40a$, $d = 50a$, respectively. The black lines are obtained by calculating $\mathbb{Q}_{\mathrm{D}}^{(\mathrm{p})} = (-1)^{\mathbb{Q}_{\mathrm{BDI}}^{(\mathrm{p})}}$ using Eq. 5.3 and tight binding dispersion relation. Our tight binding calculations and analytical results show a significant agreement since Eq. 5.3 accounts for the asymptotic behavior of the Majorana wavefunction since we have a very long meta-topological wire of length $L = 15000a$. We see that superlattice flips the topological order of topological superconductor wires and drives them in and out of their topological phases.

5.2. Multichannel s-wave Wires

In this section we focus on multichannel s-wave topological superconductor and meta-topological insulator wires.

5.2.1. Topological Superconductor Wires

We start by calculating multichannel topological index $\mathbb{Q}_{\mathrm{BDI}}^{(\mathrm{s})}$ for a 2D Bogoliubov-de Gennes Hamiltonian Eq. 5.1 for narrow wires. The Hamiltonian reads

$$H = h(\mathbf{p}; x, y)\tau_z + \alpha(\mathbf{p} \times \sigma)\tau_z + B\sigma_x + \Delta\tau_x, \tag{5.7}$$

where $h(\mathbf{p}; x, y) = \mathbf{p}^2/2m - \mu$ is the single particle kinetic term, α is the spin-orbit coupling strength, B is the Zeeman field strength, and Δ is the superconducting pair potential constant [17, 19, 92]. Pauli matrices σ_i $(i = x, y, z)$ and τ_i $(i = x, y, z)$ represent the spin- and particle-hole spaces. In thin-wire limit $\xi_{\mathrm{s}} \gg W$, we omit the chiral symmetry breaking contribution the the Hamiltonian coming from p_y since its expectation value becomes negligible as $\langle \Delta p_y \rangle \propto W/\xi_{\mathrm{s}}$ [42]. We absorb the remaining p_y contribution to the Hamiltonian $\langle p_y^2 \rangle$ by renormalizing the chemical potential to include the transverse quantization

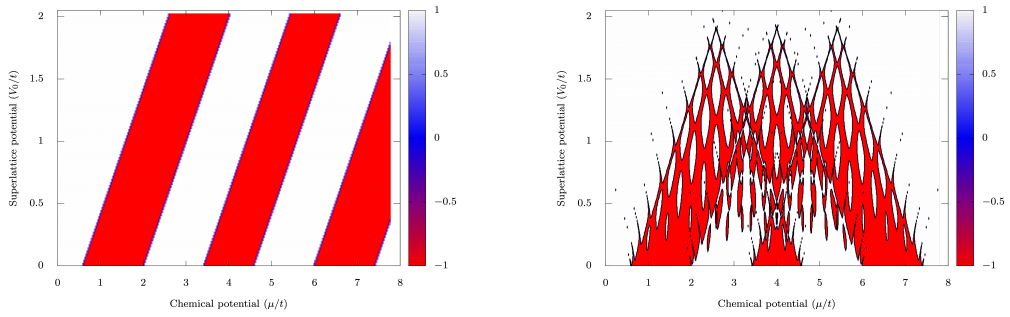

(a) **(b)**

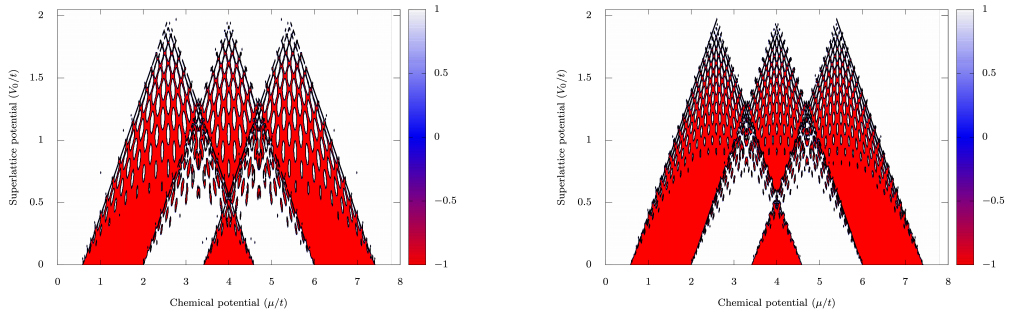

(c) **(d)**

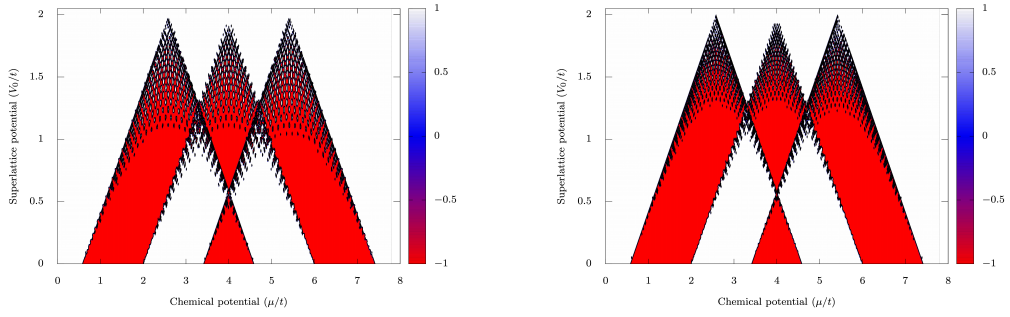

(e) **(f)**

Figure 5.2: Topological phase space of a 3 channel p-wave topological superconductor as a function of chemical energy μ and constant potential along the wire is plotted in Fig. 5.2a. Topological phase space of a 3 channel p-wave meta-topological insulator wire as a function of chemical energy μ and electrostatic superlattice amplitude $\max(V_{\text{SL}})$ is plotted in Figs. 5.2b-5.2f for different lengths of electrostatic superlattice unit cell lengths $d = 10a$, $d = 20a$, $d = 30a$, $d = 40a$, $d = 50a$; respectively. Red and white density plots are results of tight binding calculations where we detect topological phases using $\text{sgn}(\text{Det}(r))$ [1]. The numerical tight binding calculations are made for a 3 channel wire of length $L = 10000a$ for an effective pair potential $\Delta_{\text{eff}} = 0.3t$ where $t = \hbar^2/2ma^2$and a is the lattice constant. The black lines are calculated using Eq. 5.3 and they fit nicely to our numerical calculations.

as $\mu \to \mu_{n_y} = \mu - \hbar^2 n_y^2 \pi^2 / W^2$ [81]. Later we treat chiral symmetry breaking term in perturbation theory. We then off-diagonalize the Hamiltonian with the method we explain in Section 3 and write the zero-energy block solutions for a channel with index n_y with as

$$\phi_{n_y\pm} = \eta_\pm(\epsilon) e^{\pm\kappa_\alpha x} \left(A f_{n_y}(x;\epsilon) + B g_{n_y}(x;-\epsilon) \right) \tag{5.8}$$

$$+ \eta_\pm(-\epsilon) e^{\mp\kappa_\alpha x} \left(C f_{n_y}(x;-\epsilon) + D g_{n_y}(x;\epsilon) \right) \quad , \tag{5.9}$$

where spinors $\eta_\pm(\epsilon)$ are eigenvectors of $\epsilon\sigma_x + \Delta\sigma_z$ with positive and negative eigenvalues for channels n_y, κ_α is the inverse coherence length with $\kappa_\alpha \equiv \xi_{\rm s}^{-1} = m\alpha\Delta/\sqrt{B^2 - \Delta^2}$ [3, 91]. Here; $f_{n_y}(x;\pm\epsilon)$ and $g_{n_y}(x;\pm\epsilon)$ are linearly independent decaying and diverging solutions of the single particle Hamiltonian with $\underline{\underline{h}}(p)\underline{\psi}_{n_y} = \pm\epsilon\underline{\psi}_{n_y}$ whose exponential behavior we write down using Lyapunov exponents along x-direction as $f_{n_y}(x;\pm\epsilon) \propto e^{\Lambda_{n_y}(\pm\epsilon)x}$ and $g_{n_y}(x;\pm\epsilon) \propto e^{\Lambda_{n_y}(\pm\epsilon)x}$ at chemical potential μ_{n_y}. We do not consider the $B < \Delta$ case because it leads to divergent solutions, so we analyze the asymptotic behavior of the block-wavefunctions when $B > \Delta$. Zero-energy block solutions $\phi_{n_y\pm}$ have exponential factors $e^{\pm(|\kappa_\alpha| - \Lambda_{n_y}(+\epsilon))x}$, $e^{\pm(|\kappa_\alpha| + \Lambda_{n_y}(+\epsilon))x}$, $e^{\pm(-|\kappa_\alpha| - \Lambda_{n_y}(-\epsilon))x}$ and $e^{\pm(-|\kappa_\alpha| + \Lambda_{n_y}(-\epsilon))x}$ which gives two decaying and two diverging block-solutions when $\Lambda_{n_y}(-\epsilon) < |\kappa_\alpha| < \Lambda_{n_y}(+\epsilon)$ and three decaying and one diverging block-solutions when $\Lambda_{n_y}(-\epsilon) > |\kappa_\alpha| > \Lambda_{n_y}(+\epsilon)$ for each Hamiltonian block. As we already show in Section 3, when we have two decaying and two diverging solutions in the same Hamiltonian block we have accidental solutions so we must count them out. Therefore we derive the multichannel topological index for s-wave topological superconductor wires with a $\mathbb{Z}$ topological index as

$$\mathbb{Q}_{\rm BDI}^{\rm (s)} = \sum_{n_y=1}^{N_y} \Theta\left(\frac{1}{\xi_{\rm s}} - \Lambda_{n_y}(+\epsilon) \right) \Theta\left(\Lambda_{n_y}(-\epsilon) - \frac{1}{\xi_{\rm s}} \right)$$

$$- \sum_{n_y=1}^{N_y} \Theta\left(\frac{1}{\xi_{\rm s}} - \Lambda_{n_y}(-\epsilon) \right) \Theta\left(\Lambda_{n_y}(+\epsilon) - \frac{1}{\xi_{\rm s}} \right) \tag{5.10}$$

where this equation accounts for Majorana modes at the wire's ends for a multichannel s-wave topological superconductor [91]. In Eq. 5.10, the first term accounts for all zero-energy solutions and the second term subtracts the number of accidental solutions. We

also derive the topological index for each channel with n_y index as

$$Q_{\text{BDI}}^{(\text{s},n_y)} = \begin{cases} +1, & \text{if } \Lambda_{n_y}(-\epsilon) > \xi_{\text{s}}^{-1} > \Lambda_{n_y}(\epsilon) \\ -1, & \text{if } \Lambda_{n_y}(-\epsilon) < \xi_{\text{s}}^{-1} < \Lambda_{n_y}(\epsilon) \\ 0, & \text{otherwise} \end{cases}$$

where the first condition accounts for the Majorana modes and we set the second condition to exclude accidental solutions. We count topologically protected states using a summation over all channels as $\mathbb{Q}_{\text{BDI}}^{(\text{s})} = \sum_{n_y} Q_{\text{BDI}}^{(\text{s},n_y)}$ [91].

We now construct multichannel s-wave topological superconductor wire topological index in class D. We use Hamiltonian block solutions whose exponential behaviors are $e^{\pm(|\kappa_\alpha|-\Lambda_{n_y}(+\epsilon))x}$, $e^{\pm(|\kappa_\alpha|+\Lambda_{n_y}(+\epsilon))x}$, $e^{\pm(-|\kappa_\alpha|-\Lambda_{n_y}(-\epsilon))x}$ and $e^{\pm(-|\kappa_\alpha|+\Lambda_{n_y}(-\epsilon))x}$. Since we are in topological class D, topological index should be in $\mathbb{Z}_2$. Using similar arguments of asymptotic decay along the wire, we derive multichannel s-wave topological index by counting the crossings of the Lyapunov exponents of different channels over the superconducting coherence length as

$$\mathbb{Q}_{\text{D}}^{(\text{s})} = \prod_{n_y=1}^{N_y} sgn\left(|\Lambda_{n_y}(-\epsilon)| - \frac{1}{\xi_{\text{s}}}\right) sgn\left(|\Lambda_{n_y}(+\epsilon)| - \frac{1}{\xi_{\text{s}}}\right), \tag{5.11}$$

where we calculate the topological index using the condition $\Lambda_{n_y}(-\epsilon) > |\kappa_\alpha| > \Lambda_{n_y}(-\epsilon)$ which gives three decaying and one diverging block functions so that a zero-energy solutions are Majorana wavefunctions.

5.2.2. Meta-Topological Insulators

In this section we extend our exact treatment of the meta-topological wire index formula in Eq. 4.15 to multichannel thin wires and show that zero-energy wavefunction for each channel along y-direction with indices n_y can be calculated. We first rewrite the zero-energy wavefunction for a single transverse channel as

$$\Psi_{n_y,\epsilon=0}^{(N)} = \left(\left[\underline{\psi}_{n_y,1} \quad \cdots \quad \underline{\psi}_{n_y,8}\right]\Big|_{x=Nd}\right) \cdot \underline{\underline{\mathcal{T}}}(-Nd) \cdot \underline{\underline{\mathcal{P}}} \cdot \underline{\underline{\tau}}^N \cdot \underline{\underline{\mathcal{P}}}^{-1} \cdot \underline{\mathbf{c}}^{(0)}, \tag{5.12}$$

where $\underline{\psi}_{n_y,j}$ are the zero energy Hamiltonian eigenvectors for each of the n_y channels. Translation matrix $\underline{\underline{\mathcal{T}}}$, similarity transformation matrix $\underline{\underline{\mathcal{P}}}$ and diagonal recursion matrix eigenvalue matrix $\underline{\underline{\tau}}$ are calculated at the chemical potential μ_{n_y} for a single channel so the

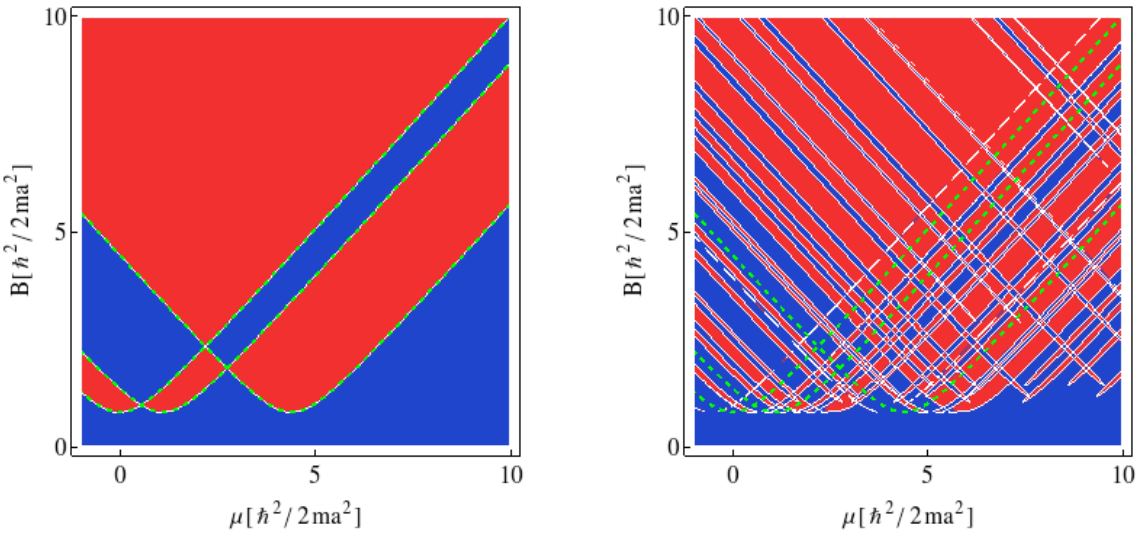

Figure 5.3: Topological phase space calculations of a 3 channel s-wave topological superconductor in (a) and meta-topological insulator wire in (b) as a function of chemical potential μ and Zeeman field strength B. The density plots are calculated using Eq. 5.10 where red areas are topologically nontrivial phases and blue areas are topologically trivial phases. White lines are plotted using Eq. 5.13 and dashed green lines are s-wave topological superconductor phase transition boundaries at $B^2 = \mu_{n_y}^2 + \Delta^2 \mid n_y = 1, 2, 3$. Both topological phase spaces are calculated with spin orbit coupling strength $\alpha = 0.03\hbar^2/2ma^2$, superconductor pair potential $\Delta = 0.81\hbar^2/2ma^2$ for a unit cell of length $d = 2a$. The white lines cover the phase transitions boundaries in the density plot showing that our formulations of the topological index are in strong agreement. Topological order flips with the application of the electrostatic superlattice. The s-wave meta-topological insulator wire phase space strong topological reentrant behavior as the phase spaces of each three channels mix into each other.

dimensions of these matrices do not change. We now calculate the zero-energy wavefunction after the imposition of boundary conditions. To construct the wavefunctions we again use upper Hamiltonian block eigenvectors as $\underline{\psi}_{n_y,1}$, $\underline{\psi}_{n_y,2}$, $\underline{\psi}_{n_y,3}$, $\underline{\psi}_{n_y,4}$ and lower block eigenvectors as $\underline{\psi}_{n_y,5}$, $\underline{\psi}_{n_y,6}$, $\underline{\psi}_{n_y,7}$, $\underline{\psi}_{n_y,8}$. Then the recursion matrix gets into a block diagonal form as $\underline{\underline{\tau}}^{(\mathrm{u})} = \mathrm{Diag}\begin{bmatrix} t^{(\mathrm{u})}_{n_y,1} & \cdots & t^{(\mathrm{u})}_{n_y,4} \end{bmatrix}$ and $\underline{\underline{\tau}}^{(\mathrm{l})} = \mathrm{Diag}\begin{bmatrix} t^{(\mathrm{l})}_{n_y,1} & \cdots & t^{(\mathrm{l})}_{n_y,4} \end{bmatrix}$, where we calculate upper and lower recursion matrix eigenvalues for each channel as $\underline{\underline{R}}^{(\mathrm{u})}\underline{s}^{(\mathrm{u})}_{n_y,i} = t^{(\mathrm{u})}_{n_y,i}\underline{s}^{(\mathrm{u})}_{n_y,i}$ and $\underline{\underline{R}}^{(\mathrm{l})}\underline{s}^{(\mathrm{l})}_{n_y,i} = t^{(\mathrm{l})}_{n_y,i}\underline{s}^{(\mathrm{l})}_{n_y,i} \mid i = 1, \cdots, 4$. The wavefunction in Eq. 5.12 should have three asymptotically decaying and one diverging wavefunction in one block for a topologically protected solution, so we determine the asymptotic behavior of the recursion matrix eigenvalues with $t_i^N \propto e^{2Nd/A_{n_y}}$ where t_i is a recursion matrix eigenvalue [85]. So the upper and lower block diagonal eigenvalue moduli take the form $|t^{(\mathrm{u})}_{n_y,1}| > 1, |t^{(\mathrm{u})}_{n_y,2}| > 1, |t^{(\mathrm{u})}_{n_y,3}| > 1, |t^{(\mathrm{u})}_{n_y,1}| < 1$ and $|t^{(\mathrm{l})}_{n_y,1}| > 1, |t^{(\mathrm{l})}_{n_y,2}| < 1, |t^{(\mathrm{l})}_{n_y,3}| < 1, |t^{(\mathrm{l})}_{n_y,4}| < 1$, where the subscripts of recursion matrix eigenvalues does not order the eigenvalues but we use them to count the number of eigenvalues with moduli less than unity. Therefore we obtain the multichannel meta-topological thin wire topological index as

$$\mathbb{Q}_{\mathrm{D}}^{(\mathrm{s,MTI})} = \prod_{n_y,i=1}^{N_y,4} \mathrm{sgn}\left(|t^{(\mathrm{u})}_{n_y,i}| - 1\right), \tag{5.13}$$

where our formulation also includes contributions coming from different channels. Topological index in Eq. 5.13 can also be derived using the lower block diagonal eigenvalue matrix since the total number of decaying and diverging solutions are constant. Next we present our numerical results.

We plot the topological phase space of a 3 channel s-wave topological superconductor wire in Fig. 5.3a. We obtain density plots using the topological index formula in Eq. 5.13 as a function of chemical potential μ and Zeeman field strength B. The red and blue segments in the phase space signify topologically nontrivial and trivial areas respectively and there is no electrostatic potential $V(x) = 0$ along the wire. The dashed green lines are phase space boundaries that we calculate using topological index in Eq. 5.10 by using the relation $\mathbb{Q}_{\mathrm{D}}^{(\mathrm{p})} = (-1)^{\mathbb{Q}_{\mathrm{BDI}}^{(\mathrm{p})}}$ [19] with Lyapunov exponents calculated for a constant potential. The calculations done using Eq. 5.10 excellently fits the three parabolas that come from the topologically nontrivial phase space conditions $B^2 > \mu_{n_y}^2 + \Delta^2 \mid \mu_{n_y} = \mu - \hbar^2 n_y^2 \pi^2 / W^2$ for a three channel s-wave wire $n_y = 1, 2, 3$.

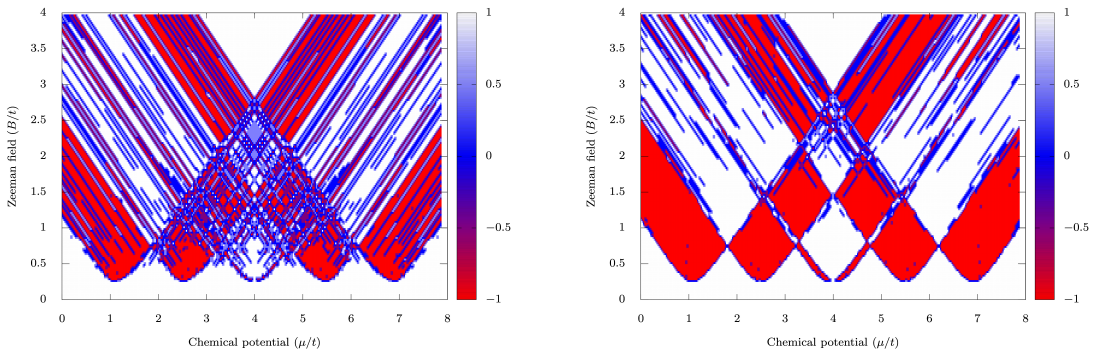

(a) **(b)**

Figure 5.4: Tight binding calculations of topological phase spaces of two 3 channel s-wave meta-topological insulator wires as a function of chemical potential μ and Zeeman field strength B with a spin orbit coupling constant $\alpha = 0.05t$, superconducting pair potential $\Delta = 0.25t$ where $t = \hbar^2/2ma^2$ and a is the lattice constant. Both wires in the plots have the length $L = 20000a$ and they are under an electrostatic superlattice potential with an amplitude $\max(V_{\text{SL}}) = t$. Numerical tight binding calculations are made using the topological index $\mathbb{Q}_{\text{D}}^{(\text{p})} = \text{sgn}(\text{Det}(r))$ [1]. Two wires only differ from each other by the electrostatic superlattice unit cell lengths; in (a) the unit cell length is $d = 25a$ and in (b) the unit length is $d = 100a$. The geometry of the electrostatic superlattice affects the topological phase space strongly. With a smaller unit cell length we see a more severe reentrant behavior of the topological phase compared to the wire. As the superlattice unit cell length gets larger; we get a clearer phase space which can be useful in physical realizations of s-wave meta-topological insulator wires.

Topologically trivial blue patches for $B^2 > \mu_{n_y}^2 + \Delta^2$ arise from the hybridization of Majorana modes, when two bands have Majorana modes at some point in the phase space, the wire becomes topologically trivial. Fig. 5.3b is the topological phase space of an s-wave meta-topological wire when the superlattice potential $V(x) = V_{\text{SL}}$ is turned on with an amplitude $V_0 = \hbar^2/2ma^2$ where b is half the length of the superlattice unit cell $d = 2a$. The dashed green s-wave topological superconductor wire phase transition lines are kept to compare the phase spaces of both type of wires. The white lines are calculated using Eq. 5.10 with $\mathbb{Q}_{\text{D}}^{(\text{p})} = (-1)^{\mathbb{Q}_{\text{BDI}}^{(\text{p})}}$ and they fit the density plot results that we calculate using Eq. 5.13. Figs. 5.3a and 5.3b are calculated with spin orbit coupling strength $\alpha = 0.03\hbar^2/2ma^2$, superconductor pair potential $\Delta = 0.81\hbar^2/2ma^2$ for a unit cell of length $d = 2a$.

In Figs. 5.4a and 5.4b we present the topological phase space of two 3 channel s-wave meta-topological insulator wires as a function of chemical potential μ and Zeeman field strength B with a spin orbit coupling constant $\alpha = 0.05t$, superconducting pair potential $\Delta = 0.25t$ with $t = \hbar^2/2ma^2$ and a is the lattice constant. Both wires in the plots have the length $L = 20000a$ and it is under an electrostatic superlattice potential with an amplitude $\max(V_{\text{SL}}) = t$. Red and white areas in the phase space signify topologically nontrivial and trivial phases, respectively and the density plots are made calculating the topological index with $\mathbb{Q}_{\text{D}}^{(\text{p})} = \text{sgn}(\text{Det}(r))$ [1]. We compare numerical density plots to our analytical topological formula by calculating the topological phase using topological index formula Eq. 5.10 with $\mathbb{Q}_{\text{D}}^{(\text{p})} = (-1)^{\mathbb{Q}_{\text{BDI}}^{(\text{p})}}$. The difference in topological phase spaces is caused by the superlattice unit cell length where we plot in Fig. 5.4a for a superlattice unit cell length $d = 25a$ and in Fig. 5.4b for $d = 100a$. Different unit cell lengths lead to different topological phase spaces as we see a strong topological reentrant behavior because of the number of times that the Majorans wavefunction gets backscattered to the end of the wire. The meta-topological wire in 5.4a has four times less superlattice unit cells in it which affects the phase space significantly as the topological reentrant behavior does not dominate the phase space.

Therefore we extend the superlattice unit cell length to $d = 800a$ for a 3 channel wire and plot our tight binding results using $\mathbb{Q}_{\text{D}}^{(\text{p})} = \text{sgn}(\text{Det}(r))$ as the red and white density plots and compare them to our numerical calculations using topological index formula

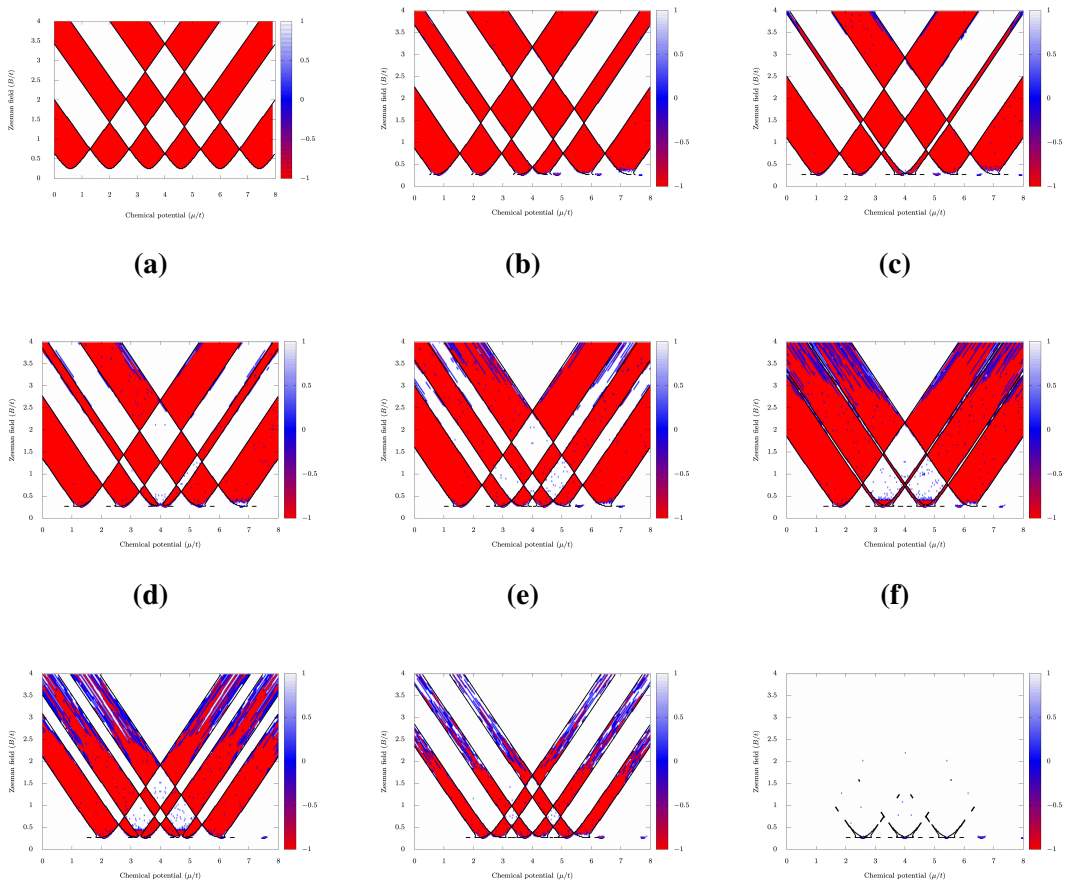

Figure 5.5: Topological phase tight binding plots as a function of chemical potential μ and Zeeman field strength B of a 3 channel s-wave topological superconductor wire is plotted in Fig. 5.5a and of a 3 channel s-wave meta-topological insulator wires are plotted in Figs. 5.5b-5.5i under different electrostatic superlattice amplitudes $\max(V_{\text{SL}}) = 0.25t$, $\max(V_{\text{SL}}) = 0.5t$, $\max(V_{\text{SL}}) = 0.75t$, $\max(V_{\text{SL}}) = 1.0t$, $\max(V_{\text{SL}}) = 1.25t$, $\max(V_{\text{SL}}) = 1.5t$, $\max(V_{\text{SL}}) = 1.75t$, $\max(V_{\text{SL}}) = 2.0t$; respectively. The tight binding calculations are done with $\mathbb{Q}_{\text{D}}^{(\text{p})} = \text{sgn}(\text{Det}(r))$ [1] with spin orbit coupling constant $\alpha = 0.05t$, superconducting pair potential $\Delta = 0.25t$ where $t = \hbar^2/2ma^2$ and a is the lattice constant. The superlattice unit cell length of the wires is $d = 800a$ with a length $L = 60000a$. The topological phase space changes as the amplitude of the electrostatic superlattice increases and we show that topologically nontrivial configurations become more experimentally accessible since nontrivial segments of the phase space move towards each other. So the electrostatic potential can be used to observe Majorana modes in s-wave topological superconductor wires by driving a topologically trivial wire into its nontrivial phase.

Eq. 5.10 with $\mathbb{Q}_{\mathrm{D}}^{(\mathrm{p})} = (-1)^{\mathbb{Q}_{\mathrm{BDI}}^{(\mathrm{p})}}$ that we show as the solid black lines. In Fig. 5.5 we use a very long wire of length $L = 60000a$ in order to increase the number of reflections which directly effects the nature of the Majorana mode due to backscattering to wire end. In our tight binding plots in Fig. 5.5 we use a wire with the same material parameters as the wires in Figs. 5.4. Fig. 5.5a is the phase space of a 3 channel topological superconductor wire which has no electrostatic potential applied onto it. In Figs. 5.5b- 5.5i we plot topological phase space of a 3 channel meta-topological wire as a density plot using our tight binding results where the superlattice potential amplitudes of each realization are $\max(V_{\mathrm{SL}}) = 0.25t$, $\max(V_{\mathrm{SL}}) = 0.5t$, $\max(V_{\mathrm{SL}}) = 0.75t$, $\max(V_{\mathrm{SL}}) = 1.0t$, $\max(V_{\mathrm{SL}}) = 1.25t$, $\max(V_{\mathrm{SL}}) = 1.5t$, $\max(V_{\mathrm{SL}}) = 1.75t$, $\max(V_{\mathrm{SL}}) = 2.0t$; respectively. As we increase the superlattice potential amplitudes the bands gets closer to each other around $\mu = 4t$ because of the tight binding dispersion relation and display a more experimentally accessible phase space as we see in Fig. 5.5f. We also see that as the superlattice potential gets stronger we start seeing topological reentrant behavior at higher Zeeman field strengths as in Figs. 5.5g and 5.5h. The reentrant behavior starts to dominate topologically nontrivial phase space and after a certain superlattice strength the topologically nontrivial phase almost completely disappears as in Fig. 5.5i. The reason for the nontrivial phases disappearance is that by applying a very strong superlattice we violate our weak superlattice potential condition so the wire completely loses its nontrivial phase.

5.3. Conclusion

In this chapter we derived topological indices for multichannel p-wave and s-wave topological superconductor and meta-topological wires. Considering the thin wire limit; we derive topological indices for p-wave and s-wave topological superconductors in class D as Eqs. 5.4 and 5.11, in class BDI as Eqs. 5.3 and 5.10. Also; we calculate topological indices of p-wave and s-wave meta-topological insulators that use block recursion matrix eigenvalues in Eqs. 5.6 and 5.13. We also performed simulations that show an excellent agreement with the analytical formulae that we derive using two different methods. We also compare our formulae to our tight binding calculations that we numerically calculate with a different topological index formula and we see that our analytical results also show a good agreement with tight binding calculations. In topological superconductor wires, the application of an electrostatic superlattice flips the topological order so meta-topological insulator wires have a different topological phase space than that of

topological insulator wires. The electrostatic potential we use is a weak electrostatic potential that does not lead to local topological phase transitions that can turn the wire into a collection of trivial and nontrivial segments. Specifically, we find that p-wave and s-wave wires can be driven out of their topologically nontrivial phases to enter their trivial phase with the application of a weak electrostatic superlattice. The reverse statement also holds for topological wires so an electrostatic superlattice can drive a topologically trivial wire into its nontrivial phase that harbors Majorana modes. After analysing the geometry of the electrostatic superlattice we see that applying of an electrostatic potential on a very long s-wave meta-topological wire with considerably larger superlattice unit cells we can alter the topological phase space which makes it experimentally more accesible to create Majorana modes in configurations where an s-wave topological superconductor wire is its trivial phase. We published some of the results of this chapter in Ref. [91].

Chapter 6

MODULATING CONDUCTANCE IN QUANTUM ANOMALOUS HALL EFFECT

In quantum Hall effect; externally applied magnetic field breaks time reversal symmetry and leads to the creation of edge states, as discussed in Chapter 2 [55–58]. While the magnetic field seems essential to the existence of a topologically nontrivial phase, it turns out substituting it with an internal magnetization on topological insulators and still have a quantized Hall effect. First proposed by Qi *et al.* in 2006 [93] this phase is called the Quantum Anomalous Hall effect. In this proposal, the effective system with magnetization M_0 that harbors edge states is specified with Hamiltonian [94]

$$H_{\text{QAH}} = h(\mathbf{p}; M_0)\sigma_z + \alpha \mathbf{p} \cdot \sigma, \tag{6.1}$$

where $\sigma_i (i = x, y, z)$ are Pauli spinors in spin-space, α is the spin orbit constant. Different from p-wave realizations of topological superconductors which have Hamiltonian in the particle-hole space, the quantum anomalous Hall Hamiltonian is written in a spin space. So, the kinetic term now has a magnetization term $h(\mathbf{p}; M_0) = M_0 + A\mathbf{p}^2$ where M_0 is the magnetization. In the kinetic term the constant factor A determines the topologically nontrivial phase (see Chung *et al.* [94]). The quantum anomalous Hall Hamiltonian in Eq. 6.1 does not posses chiral symmetry so we cannot use our method of off-diagonalization to explicitly calculate topologically nontrivial states. We therefore capture essential features of the edge state by considering its asymptotic nature. This step is similar to our calculations in Chapter 5, so we do not repeat it here.

The quantum anomalous Hall system whose Hamiltonian is given by Eq. 6.1 has gapless states [93]. We apply a magnetic superlattice to cause the opening and closing of the band gap. Similar to the case of the electrostatic superlattice of Chapters 4 and 5, we

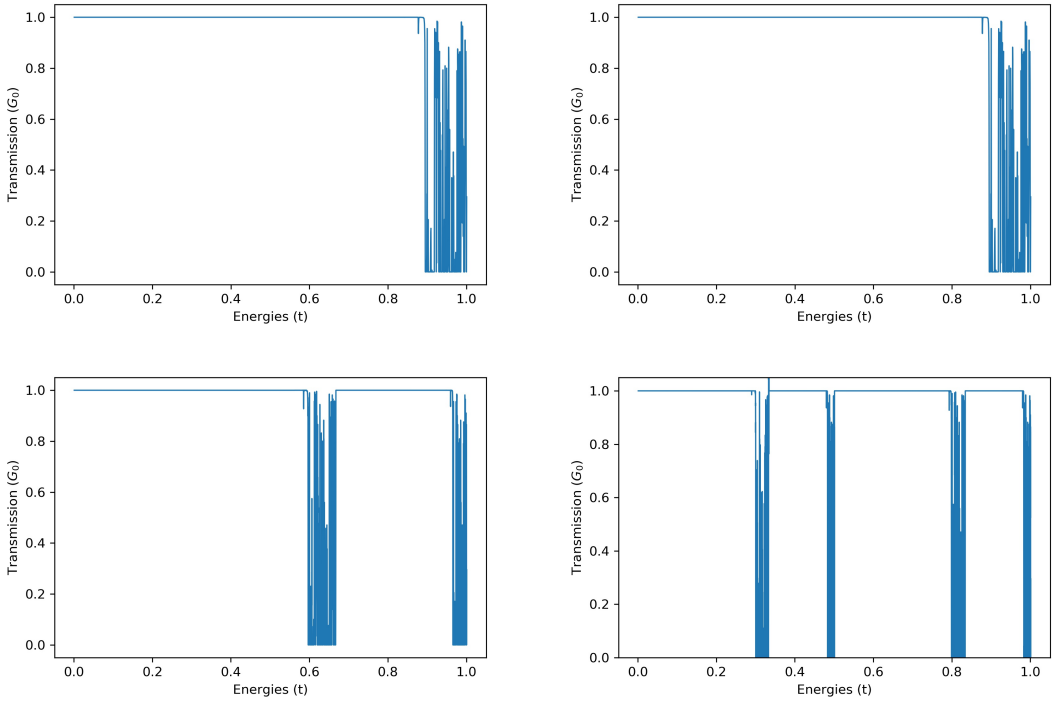

Figure 6.1: Intermittent closings in the insulating band-gap in a quantum anomalous Hall insulator caused by the application of magnetic superlattice with an amplitude $0.6t$ with an average magnetization $\langle M(x)\rangle = -1.0t$ where $t = \hbar^2/2ma^2$ where a is the lattice constant.

apply a weak magnetic superlattice that is not powerful enough to change the topological order of a quantum anomalous Hall system $\langle M_{\text{SL}}\rangle = M_0$ and observe that we can open mini-gaps in the energy spectrum that harbor topologically nontrivial edge states. We define the magnetic superlattice as

$$M_{\text{SL}}(x) = \begin{cases} M_0 + M, & \text{for } 0 \leq x \,(\text{mod}\, d) < \frac{d}{2} \\ M_0 - M, & \text{for } \frac{d}{2} \leq x \,(\text{mod}\, d) < d \end{cases}$$

where the amplitude of modulation M is not strong enough to open minigaps without the magnetic superlattice. We see the effect of the weak magnetic superlattice opening mini-gaps as the transmission switches to zero in Fig. 6.1. We propose a potential experimental setup hat can be constructed using weak magnetic superlattices that control transmission via the edge states by changing the superlattice parameters and the energy of the incoming particle.

Chapter 7

CONCLUSION

In this Thesis, we investigate the effects of irregular and regular scattering on topological order for topological superconducting wires. Work done in this Thesis is partially published in Refs. [3, 91]. The results of Chapter 6 will be published in a separate manuscript (in preparation).

In Chapter 2; we give a brief introduction to the topological properties of materials. After we explain important developments, we concentrate on topological superconductors. We explain the existence of topologically protected Majorana modes and properties of topological superconducting thin wires. We also explain our numerical methods that we use for tight binding simulations and detection of the Majorana mode.

In Chapter 3; we investigate effects of disorder on the topological index of single channel p-wave and s-wave topological superconducting wires. We start by calculating zero-energy wavefunction solutions and look at their asymptotic limit as the topological superconductor wire extends into infinity. By investigating the asymptotic behavior and imposing boundary conditions, we derive new topological indices that show whether topological superconductor wires harbor Majorana modes at their ends. We compare our analytical formulae with numerical tight binding calculations that show significant agreement. We conclude that irregular scattering caused by the disorder leads to a flip topological order.

In Chapter 4; we apply an electrostatic superlattice on topological superconductor wires that we name as *meta-topological insulators* due to their different topological phase spaces compared to that of topological superconductor wires. We start by analyzing the transfer matrix of the electrostatic superlattice and then construct a zero-energy wavefunc-

tion that we use to show topologically protected Majorana wavefunctions exists. We also derive new topological indices that solely depend on the transfer matrix eigenvalues and we compare them to our topological indices from the previous chapter using numerical methods where they show significant agreement.

In Chapter 5; we extend our topological indices formulae to multichannel topological superconductor and meta-topological thin wires. Different from our earlier topological indices for single channel wires, we derive two topological indices for each type of multi-channel topological superconductor and meta-topological thin wires since the topological classification of superconductors requires a $\mathbb{Z}$ topological index in 2D. We numerically compare our analytical formulae to our tight binding simulations and they show significant agreement. Especially, we show that topological order of meta-topological thin wires can be flipped depending on the electrostatic superlattice modulation amplitude and unit cell length. We show that the electrostatic superlattice opens and closes the insulating band gap at configurations where the wire should be topologically trivial, making potential applications with s-wave topological superconductor wires more easy to attain.

In Chapter 6; we demonstrate the opening and closing of the band gap using a magnetic superlattice in a quantum anomalous Hall sample. We show that the quantum anomalous Hall sample exhibits topologically protected edge states in configurations where they band gap should be open without the application of the magnetic superlattice.

Bibliography

[1] I. C. Fulga, F. Hassler, A. R. Akhmerov, and C. W. J. Beenakker, "Scattering formula for the topological quantum number of a disordered multimode wire," *Phys. Rev. B*, vol. 83, p. 155429, Apr 2011.

[2] A. Kitaev, "Fault-tolerant quantum computation by anyons," *Annals of Physics*, vol. 303, no. 1, pp. 2 – 30, 2003.

[3] I. Adagideli, M. Wimmer, and A. Teker, "Effects of electron scattering on the topological properties of nanowires: Majorana fermions from disorder and superlattices," *Phys. Rev. B*, vol. 89, p. 144506, Apr 2014.

[4] M. Z. Hasan and C. L. Kane, "Colloquium: Topological insulators," *Rev. Mod. Phys.*, vol. 82, pp. 3045–3067, Nov 2010.

[5] X.-L. Qi and S.-C. Zhang, "Topological insulators and superconductors," *Rev. Mod. Phys.*, vol. 83, pp. 1057–1110, Oct 2011.

[6] J. Alicea, "New directions in the pursuit of majorana fermions in solid state systems," *Reports on Progress in Physics*, vol. 75, p. 076501, jun 2012.

[7] M. Leijnse and K. Flensberg, "Introduction to topological superconductivity and majorana fermions," *Semiconductor Science and Technology*, vol. 27, p. 124003, nov 2012.

[8] C. Beenakker, "Search for majorana fermions in superconductors," *Annual Review of Condensed Matter Physics*, vol. 4, no. 1, pp. 113–136, 2013.

[9] C. Nayak, S. H. Simon, A. Stern, M. Freedman, and S. Das Sarma, "Non-abelian anyons and topological quantum computation," *Rev. Mod. Phys.*, vol. 80, pp. 1083–1159, Sep 2008.

[10] R. Jackiw and P. Rossi, "Zero modes of the vortex-fermion system," *Nuclear Physics B*, vol. 190, no. 4, pp. 681 – 691, 1981.

[11] M. M. Salomaa and G. E. Volovik, "Cosmiclike domain walls in superfluid ^3B: Instantons and diabolical points in (k,r) space," *Phys. Rev. B*, vol. 37, pp. 9298–9311, Jun 1988.

[12] G. Moore and N. Read, "Nonabelions in the fractional quantum hall effect," *Nuclear Physics B*, vol. 360, no. 2, pp. 362 – 396, 1991.

[13] N. Read and D. Green, "Paired states of fermions in two dimensions with breaking of parity and time-reversal symmetries and the fractional quantum hall effect," *Phys. Rev. B*, vol. 61, pp. 10267–10297, Apr 2000.

[14] D. A. Ivanov, "Non-abelian statistics of half-quantum vortices in p-wave superconductors," *Phys. Rev. Lett.*, vol. 86, pp. 268–271, Jan 2001.

[15] A. Y. Kitaev, "Unpaired majorana fermions in quantum wires," *Physics-Uspekhi*, vol. 44, pp. 131–136, oct 2001.

[16] J. Alicea, "Majorana fermions in a tunable semiconductor device," *Phys. Rev. B*, vol. 81, p. 125318, Mar 2010.

[17] R. M. Lutchyn, J. D. Sau, and S. Das Sarma, "Majorana fermions and a topological phase transition in semiconductor-superconductor heterostructures," *Phys. Rev. Lett.*, vol. 105, p. 077001, Aug 2010.

[18] J. D. Sau, S. Tewari, R. M. Lutchyn, T. D. Stanescu, and S. Das Sarma, "Non-abelian quantum order in spin-orbit-coupled semiconductors: Search for topological majorana particles in solid-state systems," *Phys. Rev. B*, vol. 82, p. 214509, Dec 2010.

[19] Y. Oreg, G. Refael, and F. von Oppen, "Helical liquids and majorana bound states in quantum wires," *Phys. Rev. Lett.*, vol. 105, p. 177002, Oct 2010.

[20] T.-P. Choy, J. M. Edge, A. R. Akhmerov, and C. W. J. Beenakker, "Majorana fermions emerging from magnetic nanoparticles on a superconductor without spin-orbit coupling," *Phys. Rev. B*, vol. 84, p. 195442, Nov 2011.

[21] M. Kjaergaard, K. Wölms, and K. Flensberg, "Majorana fermions in superconducting nanowires without spin-orbit coupling," *Phys. Rev. B*, vol. 85, p. 020503, Jan 2012.

[22] I. Martin and A. F. Morpurgo, "Majorana fermions in superconducting helical magnets," *Phys. Rev. B*, vol. 85, p. 144505, Apr 2012.

[23] S. Nadj-Perge, I. K. Drozdov, B. A. Bernevig, and A. Yazdani, "Proposal for realizing majorana fermions in chains of magnetic atoms on a superconductor," *Phys. Rev. B*, vol. 88, p. 020407, Jul 2013.

[24] B. Braunecker and P. Simon, "Interplay between classical magnetic moments and superconductivity in quantum one-dimensional conductors: Toward a self-sustained topological majorana phase," *Phys. Rev. Lett.*, vol. 111, p. 147202, Oct 2013.

[25] F. Pientka, L. I. Glazman, and F. von Oppen, "Topological superconducting phase in helical shiba chains," *Phys. Rev. B*, vol. 88, p. 155420, Oct 2013.

[26] J. Klinovaja, P. Stano, A. Yazdani, and D. Loss, "Topological superconductivity and majorana fermions in rkky systems," *Phys. Rev. Lett.*, vol. 111, p. 186805, Nov 2013.

[27] S. Nakosai, Y. Tanaka, and N. Nagaosa, "Two-dimensional p-wave superconducting states with magnetic moments on a conventional s-wave superconductor," *Phys. Rev. B*, vol. 88, p. 180503, Nov 2013.

[28] M. M. Vazifeh and M. Franz, "Self-organized topological state with majorana fermions," *Phys. Rev. Lett.*, vol. 111, p. 206802, Nov 2013.

[29] Y. Kim, M. Cheng, B. Bauer, R. M. Lutchyn, and S. Das Sarma, "Helical order in one-dimensional magnetic atom chains and possible emergence of majorana bound states," *Phys. Rev. B*, vol. 90, p. 060401, Aug 2014.

[30] J. Röntynen and T. Ojanen, "Topological superconductivity and high chern numbers in 2d ferromagnetic shiba lattices," *Phys. Rev. Lett.*, vol. 114, p. 236803, Jun 2015.

[31] V. Mourik, K. Zuo, S. M. Frolov, S. R. Plissard, E. P. A. M. Bakkers, and L. P. Kouwenhoven, "Signatures of majorana fermions in hybrid superconductor-semiconductor nanowire devices," *Science*, vol. 336, no. 6084, pp. 1003–1007, 2012.

[32] M. T. Deng, C. L. Yu, G. Y. Huang, M. Larsson, P. Caroff, and H. Q. Xu, "Anomalous zero-bias conductance peak in a nbâĂŞinsb nanowireâĂŞnb hybrid device," *Nano Letters*, vol. 12, no. 12, pp. 6414–6419, 2012. PMID: 23181691.

[33] A. D. K. Finck, D. J. Van Harlingen, P. K. Mohseni, K. Jung, and X. Li, "Anomalous modulation of a zero-bias peak in a hybrid nanowire-superconductor device," *Phys. Rev. Lett.*, vol. 110, p. 126406, Mar 2013.

[34] H. O. H. Churchill, V. Fatemi, K. Grove-Rasmussen, M. T. Deng, P. Caroff, H. Q. Xu, and C. M. Marcus, "Superconductor-nanowire devices from tunneling to the multichannel regime: Zero-bias oscillations and magnetoconductance crossover," *Phys. Rev. B*, vol. 87, p. 241401, Jun 2013.

[35] I. Adagideli, P. M. Goldbart, A. Shnirman, and A. Yazdani, "Low-energy quasiparticle states near extended scatterers in d-wave superconductors and their connection with susy quantum mechanics," *Phys. Rev. Lett.*, vol. 83, pp. 5571–5574, Dec 1999.

[36] P. Neven, D. Bagrets, and A. Altland, "Quasiclassical theory of disordered multichannel majorana quantum wires," *New Journal of Physics*, vol. 15, p. 055019, may 2013.

[37] O. Motrunich, K. Damle, and D. A. Huse, "Griffiths effects and quantum critical points in dirty superconductors without spin-rotation invariance: One-dimensional examples," *Phys. Rev. B*, vol. 63, p. 224204, May 2001.

[38] P. W. Brouwer, M. Duckheim, A. Romito, and F. von Oppen, "Topological superconducting phases in disordered quantum wires with strong spin-orbit coupling," *Phys. Rev. B*, vol. 84, p. 144526, Oct 2011.

[39] J. D. Sau and S. Das Sarma, "Density of states of disordered topological superconductor-semiconductor hybrid nanowires," *Phys. Rev. B*, vol. 88, p. 064506, Aug 2013.

[40] H.-Y. Hui, J. D. Sau, and S. Das Sarma, "Generalized eilenberger theory for majorana zero-mode-carrying disordered p-wave superconductors," *Phys. Rev. B*, vol. 90, p. 064516, Aug 2014.

[41] A. R. Akhmerov, J. P. Dahlhaus, F. Hassler, M. Wimmer, and C. W. J. Beenakker, "Quantized conductance at the majorana phase transition in a disordered superconducting wire," *Phys. Rev. Lett.*, vol. 106, p. 057001, Jan 2011.

[42] A. C. Potter and P. A. Lee, "Engineering a $p + ip$ superconductor: Comparison of topological insulator and rashba spin-orbit-coupled materials," *Phys. Rev. B*, vol. 83, p. 184520, May 2011.

[43] T. D. Stanescu, R. M. Lutchyn, and S. Das Sarma, "Majorana fermions in semiconductor nanowires," *Phys. Rev. B*, vol. 84, p. 144522, Oct 2011.

[44] M.-T. Rieder, P. W. Brouwer, and i. d. I. m. c. Adagideli, "Reentrant topological phase transitions in a disordered spinless superconducting wire," *Phys. Rev. B*, vol. 88, p. 060509, Aug 2013.

[45] P. W. Brouwer, M. Duckheim, A. Romito, and F. von Oppen, "Probability distribution of majorana end-state energies in disordered wires," *Phys. Rev. Lett.*, vol. 107, p. 196804, Nov 2011.

[46] J. D. Sau, S. Tewari, and S. Das Sarma, "Experimental and materials considerations for the topological superconducting state in electron- and hole-doped semiconductors: Searching for non-abelian majorana modes in 1d nanowires and 2d heterostructures," *Phys. Rev. B*, vol. 85, p. 064512, Feb 2012.

[47] A. M. Lobos, R. M. Lutchyn, and S. Das Sarma, "Interplay of disorder and interaction in majorana quantum wires," *Phys. Rev. Lett.*, vol. 109, p. 146403, Oct 2012.

[48] F. Pientka, A. Romito, M. Duckheim, Y. Oreg, and F. von Oppen, "Signatures of topological phase transitions in mesoscopic superconducting rings," *New Journal of Physics*, vol. 15, p. 025001, feb 2013.

[49] W. DeGottardi, D. Sen, and S. Vishveshwara, "Majorana fermions in superconducting 1d systems having periodic, quasiperiodic, and disordered potentials," *Phys. Rev. Lett.*, vol. 110, p. 146404, Apr 2013.

[50] D. Chevallier, P. Simon, and C. Bena, "From andreev bound states to majorana fermions in topological wires on superconducting substrates: A story of mutation," *Phys. Rev. B*, vol. 88, p. 165401, Oct 2013.

[51] W. DeGottardi, M. Thakurathi, S. Vishveshwara, and D. Sen, "Majorana fermions in superconducting wires: Effects of long-range hopping, broken time-reversal symmetry, and potential landscapes," *Phys. Rev. B*, vol. 88, p. 165111, Oct 2013.

[52] P. Jacquod and M. Büttiker, "Signatures of majorana fermions in hybrid normal-superconducting rings," *Phys. Rev. B*, vol. 88, p. 241409, Dec 2013.

[53] I. A. Gruzberg, N. Read, and S. Vishveshwara, "Localization in disordered superconducting wires with broken spin-rotation symmetry," *Phys. Rev. B*, vol. 71, p. 245124, Jun 2005.

[54] F. Pientka, G. Kells, A. Romito, P. W. Brouwer, and F. von Oppen, "Enhanced zero-bias majorana peak in the differential tunneling conductance of disordered multisubband quantum-wire/superconductor junctions," *Phys. Rev. Lett.*, vol. 109, p. 227006, Nov 2012.

[55] K. v. Klitzing, G. Dorda, and M. Pepper, "New method for high-accuracy determination of the fine-structure constant based on quantized hall resistance," *Phys. Rev. Lett.*, vol. 45, pp. 494–497, Aug 1980.

[56] R. B. Laughlin, "Quantized hall conductivity in two dimensions," *Phys. Rev. B*, vol. 23, pp. 5632–5633, May 1981.

[57] D. J. Thouless, M. Kohmoto, M. P. Nightingale, and M. den Nijs, "Quantized hall conductance in a two-dimensional periodic potential," *Phys. Rev. Lett.*, vol. 49, pp. 405–408, Aug 1982.

[58] M. Kohmoto, "Topological invariant and the quantization of the Hall conductance," *Annals of Physics*, vol. 160, pp. 343–354, Apr. 1985.

[59] F. D. M. Haldane, "Model for a quantum hall effect without landau levels: Condensed-matter realization of the "parity anomaly"," *Phys. Rev. Lett.*, vol. 61, pp. 2015–2018, Oct 1988.

[60] Y. Ando and L. Fu, "Topological crystalline insulators and topological superconductors: From concepts to materials," *Annual Review of Condensed Matter Physics*, vol. 6, no. 1, pp. 361–381, 2015.

[61] D. Tong, "Lectures on the Quantum Hall Effect," *arXiv 1606.06687*, 2016.

[62] R. Resta, "Geometry and topology in electronic structure theory." Lecture notes obtained from webpage at http://www-dft.ts.infn.it/~resta/, Accessed 26.06.2017, 2016.

[63] D. Thouless, *Topological Quantum Numbers in Nonrelativistic Physics*. World Scientific Publishing Company Pte Limited, 1998.

[64] M. Franz and L. Molenkamp, eds., *Topological Insulators*, vol. 6 of *Contemporary Concepts of Condensed Matter Science*. Elsevier, 2013.

[65] B. A. Bernevig and T. Hughes, *Topological Insulators and Topological Superconductors*. Princeton University Press, 41 William Street, Princeton, New Jersey 08540: Princeton University Press, 2013.

[66] M. Nakahara, *Geometry, Topology and Physics, Second Edition*. Graduate student series in physics, Taylor & Francis, 2003.

[67] C. L. Kane and E. J. Mele, "Quantum spin hall effect in graphene," *Phys. Rev. Lett.*, vol. 95, p. 226801, Nov 2005.

[68] M. Gmitra, S. Konschuh, C. Ertler, C. Ambrosch-Draxl, and J. Fabian, "Band-structure topologies of graphene: Spin-orbit coupling effects from first principles," *Phys. Rev. B*, vol. 80, p. 235431, Dec 2009.

[69] L. Fu and C. L. Kane, "Topological insulators with inversion symmetry," *Phys. Rev. B*, vol. 76, p. 045302, Jul 2007.

[70] J. Sakurai and J. Napolitano, *Modern quantum mechanics*. Addison-Wesley, 2010.

[71] S. Ryu, A. P. Schnyder, A. Furusaki, and A. W. W. Ludwig, "Topological insulators and superconductors: Tenfold way and dimensional hierarchy," *New Journal of Physics*, vol. 12, no. 6, p. 065010, 2010.

[72] A. Altland and M. R. Zirnbauer, "Nonstandard symmetry classes in mesoscopic normal-superconducting hybrid structures," *Phys. Rev. B*, vol. 55, pp. 1142–1161, Jan 1997.

[73] A. Kitaev, "Periodic table for topological insulators and superconductors," *AIP Conference Proceedings*, vol. 1134, no. 1, p. 22, 2009.

[74] A. P. Schnyder, S. Ryu, A. Furusaki, and A. W. W. Ludwig, "Classification of topological insulators and superconductors," *AIP Conference Proceedings*, vol. 1134, no. 1, p. 10, 2009.

[75] L. Fu and C. L. Kane, "Superconducting proximity effect and majorana fermions at the surface of a topological insulator," *Phys. Rev. Lett.*, vol. 100, p. 096407, Mar 2008.

[76] J. R. Williams, A. J. Bestwick, P. Gallagher, S. S. Hong, Y. Cui, A. S. Bleich, J. G. Analytis, I. R. Fisher, and D. Goldhaber-Gordon, "Unconventional josephson effect in hybrid superconductor-topological insulator devices," *Phys. Rev. Lett.*, vol. 109, p. 056803, Jul 2012.

[77] G. Kells, D. Meidan, and P. W. Brouwer, "Low-energy subgap states in multichannel p-wave superconducting wires," *Phys. Rev. B*, vol. 85, p. 060507, Feb 2012.

[78] C. W. Groth, M. Wimmer, A. R. Akhmerov, and X. Waintal, "Kwant: A software package for quantum transport," *New Journal of Physics*, vol. 16, no. 6, p. 063065, 2014.

[79] P. De Gennes, *Superconductivity Of Metals And Alloys*. Advanced Books Classics, Westview Press, 1999.

[80] S. Datta, *Electronic Transport in Mesoscopic Systems*. Cambridge Studies in Semiconductor Physi, Cambridge University Press, 1997.

[81] M.-T. Rieder, G. Kells, M. Duckheim, D. Meidan, and P. W. Brouwer, "Endstates in multichannel spinless p-wave superconducting wires," *Phys. Rev. B*, vol. 86, p. 125423, Sep 2012.

[82] M. Wimmer, A. R. Akhmerov, M. V. Medvedyeva, J. Tworzydło, and C. W. J. Beenakker, "Majorana bound states without vortices in topological superconductors with electrostatic defects," *Phys. Rev. Lett.*, vol. 105, p. 046803, Jul 2010.

[83] A. C. Potter and P. A. Lee, "Multichannel generalization of kitaev's majorana end states and a practical route to realize them in thin films," *Phys. Rev. Lett.*, vol. 105, p. 227003, Nov 2010.

[84] L.-J. Lang and S. Chen, "Majorana fermions in density-modulated p-wave superconducting wires," *Phys. Rev. B*, vol. 86, p. 205135, Nov 2012.

[85] C. W. J. Beenakker, "Random-matrix theory of quantum transport," *Rev. Mod. Phys.*, vol. 69, pp. 731–808, Jul 1997.

[86] A. C. Potter and P. A. Lee, "Topological superconductivity and majorana fermions in metallic surface states," *Phys. Rev. B*, vol. 85, p. 094516, Mar 2012.

[87] F. Domínguez, F. Hassler, and G. Platero, "Dynamical detection of majorana fermions in current-biased nanowires," *Phys. Rev. B*, vol. 86, p. 140503, Oct 2012.

[88] L. Jiang, D. Pekker, J. Alicea, G. Refael, Y. Oreg, and F. von Oppen, "Unconventional josephson signatures of majorana bound states," *Phys. Rev. Lett.*, vol. 107, p. 236401, Nov 2011.

[89] P. San-Jose, E. Prada, and R. Aguado, "ac josephson effect in finite-length nanowire junctions with majorana modes," *Phys. Rev. Lett.*, vol. 108, p. 257001, Jun 2012.

[90] D. I. Pikulin, J. P. Dahlhaus, M. Wimmer, H. Schomerus, and C. W. J. Beenakker, "A zero-voltage conductance peak from weak antilocalization in a majorana nanowire," *New Journal of Physics*, vol. 14, p. 125011, dec 2012.

[91] B. Pekerten, A. Teker, O. Bozat, M. Wimmer, and i. d. I. Adagideli, "Disorder-induced topological transitions in multichannel majorana wires," *Phys. Rev. B*, vol. 95, p. 064507, Feb 2017.

[92] J. Kammhuber, M. C. Cassidy, H. Zhang, Ã. GÃijl, F. Pei, M. W. A. de Moor, B. Nijholt, K. Watanabe, T. Taniguchi, D. Car, S. R. Plissard, E. P. A. M. Bakkers, and L. P. Kouwenhoven, "Conductance quantization at zero magnetic field in insb nanowires," *Nano Letters*, vol. 16, no. 6, pp. 3482–3486, 2016. PMID: 27121534.

[93] X.-L. Qi, Y.-S. Wu, and S.-C. Zhang, "Topological quantization of the spin hall effect in two-dimensional paramagnetic semiconductors," *Phys. Rev. B*, vol. 74, p. 085308, Aug 2006.

[94] S. B. Chung, X.-L. Qi, J. Maciejko, and S.-C. Zhang, "Conductance and noise signatures of majorana backscattering," *Phys. Rev. B*, vol. 83, p. 100512, Mar 2011.